NASA Contractor Report 174700

3-D INELASTIC ANALYSIS METHODS FOR HOT SECTION COMPONENTS (BASE PROGRAM)

First Annual Status Report
For the Period
February 14, 1983 to February 14, 1984

R.B. Wilson, M.J. Bak,
S. Nakazawa, and P.K. Banerjee

Contract NAS3-23697
February 1984

NASA

ENTER:

9 1 1 RN/NASA-CR-174700
DISPLAY 09/6/1
85N21686*# ISSUE 12 PAGE 1863 CATEGORY 39 RPT#: NASA-CR-174700 NAS 1.26:174700 PWA-5940-19 ASR-1 CNT#: NAS3-23697 84/02/00 167 PAGES
UNCLASSIFIED DOCUMENT
UTTL: 3-D inelastic analysis methods for hot section components (base program) --- turbine blades, turbine vanes, and combustor liners TLSP: Annual Status Report, 14 Feb. 1983 - 14 Feb. 1984
AUTH: A/WILSON, R. B.; B/BAK, M. J.; C/NAKAZAWA, S.; D/BANERJEE, P. K.
CORP: Pratt and Whitney Aircraft, East Hartford, Conn. CSS: (Engineering Div.)
AVAIL.NTIS SAP: HC A08/MF A01
MAJS: /*COMPUTER PROGRAMS/*FINITE ELEMENT METHOD/*HIGH TEMPERATURE/*INELASTIC STRESS/*STRESS ANALYSIS/*STRUCTURAL ANALYSIS
MINS: / BUCKLING/ CREEP ANALYSIS/ LINEARITY/ MATHEMATICAL MODELS/ NONLINEARITY/ STRUCTURAL VIBRATION/ TIME DEPENDENCE
ABA: Author

NASA Contractor Report 174700

3-D INELASTIC ANALYSIS METHODS FOR HOT SECTION COMPONENTS (BASE PROGRAM)

First Annual Status Report

R.B. Wilson, M.J. Bak,
S. Nakazawa, and P.K. Banerjee

Prepared for
NASA-Lewis Research Center
Under Contract NAS3-23697

NASA

1.REPORT NO. NASA CR-174700	2. GOVERNMENT AGENCY	3.RECIPIENT'S CATALOG NO.
4.TITLE AND SUBTITLE 3-D INELASTIC ANALYSIS METHODS FOR HOT SECTION COMPONENTS (BASE PROGRAM)		5. REPORT DATE February, 1984 6. PERFORMING ORG. CODE
7.AUTHOR(S) R. B. Wilson, M. J. Bak, S. Nakazawa and P. K. Banerjee		8. PERFORMING ORG. REPT. NO. PWA-5940-19
9.PERFORMING ORG. NAME AND ADDRESS UNITED TECHNOLOGIES CORPORATION Pratt & Whitney, Engineering Division 400 Main St., East Hartford, CT 06108		10. WORK UNIT NO. 11. CONTRACT OR GRANT NO. NAS3-23697
12. SPONSORING AGENCY NAME AND ADDRESS National Aeronautics and Space Administration Lewis Research Center Project Manager, C. C. Chamis, MS 49-6 21000 Brookpark Road, Cleveland, OH 44135		13. TYPE REPT./PERIOD COVERED First Annual Status Report 14. SPONSORING AGENCY CODE RTOP 533-04-1A
15. SUPPLEMENTARY NOTES		

16. ABSTRACT

A 3-D Inelastic Analysis Methods program is described. This program consists of a series of new computer codes embodying a progression of mathematical models (mechanics of materials, special finite element, boundary element) for streamlined analysis of: (1) combustor liners, (2) turbine blades, and (3) turbine vanes. These models address the effects of high temperatures and thermal/mechanical loadings on the local (stress/strain) and global (dynamics, buckling) structural behavior of the three selected components. These models are used to solve 3-D inelastic problems using linear approximations in the sense that: (1) stresses/strains and temperatures in generic modeling regions are linear functions of the spatial coordinates, and (2) solution increments for load, temperature and/or time are extrapolated linearly from previous information. Three linear formulation computer codes, referred to as MOMM (Mechanics of Materials Model), MHOST (MARC-Hot Section Technology), and BEST (Boundary Element Stress Technology), have been developed and are briefly described in this report.

17. KEY WORDS (SUGGESTED BY AUTHOR(S))	18. DISTRIBUTION STATEMENT
3-D Inelastic Analysis, Finite Elements, Boundary Elements, High Temperature, Creep, Vibration, Buckling, Solution Methods, Constitutive Modeling	Unclassified Unlimited

19. SECURITY CLASS THIS (REPT)	20. SECURITY CLASS THIS (PAGE)	21. NO. PGS	22. PRICE *
Unclassified	Unclassified		

* For sale by the National Technical Information Service, Springfield, VA 22161

PREFACE

This Annual Status Report describes the results of work performed during the first year of the NASA Hot Section Technology program, "3-D Inelastic Analysis Methods for Hot Section Components" (contract NAS3-23697). The goal of the program is to develop computer codes which permit more accurate and efficient structural analyses of gas turbine blades, vanes, and combustor liners. The program is being conducted under the direction of Dr. C. C. Chamis of the NASA-Lewis Research Center. Prime contractor activities at United Technologies Corporation are managed by Dr. E. S. Todd. Subcontractor efforts at the United Technologies Research Center, MARC Analysis Research Corporation, and the State University of New York at Buffalo are led by Dr. B. N. Cassenti, Dr. J. C. Nagtegaal, and Dr. P. K. Banerjee, respectively.

Table of Contents

Table of Contents (continued)

SECTION 1.0

INTRODUCTION

Aircraft powerplant fuel consumption and expenditures for repair/replacement of worn or damaged parts make up a significant portion of commercial aviation's direct operating costs. For modern gas turbines, both factors depend heavily on the degree to which elevated flowpath temperatures are sustained in the hot section modules of the engine. Higher temperatures reduce fuel consumption by raising the basic efficiency of the gas generator thermodynamic cycle. At the same time, these elevated temperatures work to degrade the durability of structural components (combustor liners, turbine blades and vanes, airseals, etc.) that must function adjacent to or within the hot gaspath itself, leading in turn to larger maintenance/material costs. Pursuit of the best compromise between performance and durability presents a challenge that will continue to tax the ingenuity of advanced gas turbine design analysts for years to come.

Hot section durability problems appear in a variety of forms, ranging from oxidation/corrosion, erosion, and distortion (creep deformations) to occurrence of fatigue cracking. Even modest changes in shape, from erosion or distortion of airfoils for example, can lead to measurable performance deterioration that must be accurately predicted during propulsion system design to insure that long-term efficiency guarantees can be met. Larger distortions introduce serious problems such as hot spots and profile shifts resulting from diversion of cooling air, high vibratory stresses associated with loose turbine blade shrouds, difficult disassembly/reassembly of mating parts at overhaul, etc. These problems must be considered and efforts made to eliminate their effects during the engine design/development process. Initiation and propagation of fatigue cracks represents a direct threat to component structural integrity and must be thoroughly understood and accurately predicted to insure continued safe and efficient engine operation.

Accurate prediction of component fatigue lives is strongly dependent on the success with which inelastic stress/strain states in the vicinity of holes, fillets, welds, and other discontinuities can be calculated. Stress/strain computations for hot section components are made particularly difficult by two factors - the high degree of geometrical irregularity which accompanies sophisticated cooling schemes, and complex nonlinear material behavior associated with high temperature creep/plasticity effects. Since cooling air extraction reduces engine cycle efficiency, concerted efforts are made to minimize its use with the result that elaborate internal passages and surface ports are employed to selectively bathe local regions (airfoil leading edges, louver liner lips, etc.) for which the high temperature environment is most severe. These cooling features frequently interrupt load paths and introduce complex temperature gradients to the extent that the basic assumptions of one- and two-dimensional stress analysis procedures are seriously compromised and the use of three-dimensional techniques becomes mandatory. Even in the presence of cooling, component temperature and stress levels remain high relative

to the material's melting point and yield strength values. The combinations of centrifugal, aerodynamic, thermal, and other mechanical loadings that typically occur in flight operation then serve to drive the underlying material response beyond accepted limits for linear elastic behavior and into the regime characterized by inelastic, time-dependent structural deformations. Thus, an ability to account for both complexities, three-dimensional and inelastic effects, becomes essential to the design of durable hot section components.

General purpose finite element computer codes containing a variety of three-dimensional (brick) elements and inelastic material models have been available for more than a decade. Incorporation of such codes into the hot section design process has been severely limited by high costs associated with the extensive labor/computer/time resources required to obtain reasonably detailed results. Geometric modeling systems and automated input/output data processing packages have received first attention from software developers in recent years and will soon mature to the point that previous over-riding manpower concerns will be alleviated. Prohibitive amounts of Central Processing Unit (CPU) time are still required for execution of even modest-size three-dimensional inelastic stress analyses, however, and is chief among the obstacles remaining to be remedied. With today's computers and solution algorithms, models described by a few hundred displacement degrees of freedom commonly consume one to three hours of mainframe CPU time during simulation of a single thermomechanical loading cycle. A sequence of many such cycles may, of course, be needed to reach the stabilized conditions of interest. Since accurate idealizations of components with only a few geometrical discontinuities can easily contain several thousand degrees of freedom, inelastic analysis of hot section hardware with existing codes falls outside the realm of practicality.

The Inelastic Methods program addresses the need to develop more efficient and accurate three-dimensional inelastic structural analysis procedures for gas turbine hot section components. A series of new, increasingly rigorous, stand-alone computer codes is being created for the comprehensive numerical analysis of combustor liners, turbine blades and vanes. Theoretical foundations for the codes feature mechanics of materials models, special finite element models, and boundary element models. Heavy attention will be given to evolution of novel modeling methods that permit non-burdensome yet accurate representations of geometrical discontinuities such as cooling holes and coating cracks. A selection of constitutive relations has been provided for economical or sophisticated description of inelastic material behavior as desired. Finally, advantages which accrue from application of the improved codes to actual components will be demonstrated by execution of benchmark analyses for which experimental data exist.

SECTION 2.0

SUMMARY

The 3-D Inelastic Analysis Methods program is divided into two 24-month segments: a base program, and an option program to be exercised at the discretion of the Government. During the base program, a series of new computer codes embodying a progression of mathematical models (mechanics of materials, special finite element, boundary element) is being developed for the streamlined analysis of combustor liners, turbine blades and turbine vanes. These models will address the effects of high temperatures and thermal/mechanical loadings on the local (stress/strain) and global (dynamics, buckling) structural behavior of the three selected components.

The first year (Task I) of the base program dealt with "linear" theory in the sense that stresses/strains and temperatures in generic modeling regions are linear functions of the spatial coordinates, and solution increments for load, temperature and/or time are extrapolated linearly from previous information. Three linear formulation computer codes, hereafter referred to as MOMM (Mechanics of Materials Model), MHOST (MARC-HOST), and BEST (Boundary Element Stress Technology), have been created and are described in more detail in Sections 3.2, 3.3, and 3.4, respectively.

The second half of the base program (Task II), as well as the option program (Tasks IV and V), will extend the models to include higher-order representations of deformations and loads in space and time to deal more effectively with collections of discontinuities such as cooling holes and coating cracks. Work on Task II (polynomial theory) has commenced and will be the subject of primary interest in the next Annual Status Report.

2.1 CONSTITUTIVE MODELS

Three increasingly rigorous constitutive relationships are employed by MOMM, MHOST, and BEST to account for nonlinear material behavior (creep/plasticity effects) in the elevated temperature regime. The simplified model assumes a bilinear approximation of stress-strain response and generally glosses over the complications associated with strain rate effects, etc. (Section 3.1.1). The state-of-the-art model partitions time-independent (plasticity) and time-dependent (creep) phenomena in the conventional way, invoking the Mises yield criterion and standard (isotropic, kinematic, combined) hardening rules for the former and a power law for the latter (Section 3.1.2). Walker's viscoplastic theory, which accounts for the interaction between creep and plasticity that occurs under cyclic loading conditions, has been adopted as the advanced constitutive model (Section 3.1.3).

2.2 MECHANICS OF MATERIALS MODEL

In essence, the Mechanics of Materials Model (MOMM) is a stiffness method finite element code that utilizes one-, two- and three-dimensional arrays of beam elements to characterize hot section component behavior. Limitations of such beam model representations are recognized, of course, but are fully acceptable in view of the benefits of having a fast, easy to use, computationally efficient tool available for application during the early phases of component design. The full complement of structural analysis types (static, buckling, vibration, dynamics) is provided by MOMM, in conjunction with the three constitutive models mentioned above. Capabilities of the code have been tested for a variety of relatively simple problem discretizations (examples are provided in Section 3.2.2). Work to establish modeling guidelines for simulation of two- and three-dimensional behavior is in progress.

2.3 SPECIAL FINITE ELEMENT MODEL

The MHOST (MARC-HOST) code employs both shell and solid (brick) elements in a mixed method framework to provide comprehensive capabilities for investigating local (stress/strain) and global (vibration, buckling) behavior of hot section components. Development of the code has taken full advantage of the wealth of technical expertise accumulated at the MARC Corporation over the last decade in support of their own commercially available software packages to create new/improved algorithms (Section 3.3.2) that promise to significantly reduce CPU (central processing unit) time requirements for three-dimensional analyses. First generation (Task I) MHOST code is operational and has been tested with a variety of academic as well as engine-related configurations (Section 3.3.4).

2.4 ADVANCED FORMULATION (BOUNDARY ELEMENT) MODEL

Successful assembly of the all-new BEST (Boundary Element Stress Technology) code constitutes perhaps the most important accomplishment of the Task I effort. The difficult challenge of extending the basic theory and algorithms to encompass inelastic and dynamic effects in three-space was effectively met by combining the special skills and efforts of the research and programming teams at SUNY-B and P&W. As with MOMM and MHOST, the initial version of BEST is executable and has been exercised with a number of small and large test cases (Section 3.4.5). While MHOST and BEST are currently viewed as mutually complementary, they are also competitors; and overall performance on large inelastic models will be watched with high interest as the codes mature.

SECTION 3.0

TECHNICAL PROGRESS

3.1 CONSTITUTIVE MODELS

Three material models are available for use with the mechanics of materials, special finite element, and boundary element models: 1) a simplified material model, 2) a state-of-the-art material model, and 3) an advanced material model. The simplified model uses secant moduli and assumes a bilinear stress-strain response which is currently neither strain-rate nor temperature dependent. Later versions of the simplified material model will include provisions for both temperature and strain-rate dependence. The state-of-the-art material model is a standard elastic-plastic-creep model (Reference 1). The advanced model is a modified form of Walker's viscoplastic material model (References 2 and 3). The following sections provide a detailed discussion of each of these models.

3.1.1 Simplified Secant Elastic Model

In the simplified elastic model, stress-strain curves for various strain rates are the basic input material properties. Tension response is assumed to be the same as compression response. The initial response is represented by an elastic material with modulus, E_o, and Poisson's ratio, ν_o. At the conclusion of the calculation for the response, an equivalent strain is predicted. At this strain, two equivalent stresses can be considered: 1) the calculated stress, and 2) the stress from the input stress-strain curves at the predicted strain. If the two stresses are sufficiently close in value, then the calculations can be terminated. If the two stresses are not sufficiently close, then the new modulus is taken to be the stress from the stress-strain curves divided by the strain, and the calculations are repeated.

This concept must now be expanded to multidimensional stress states. For this purpose, consider an elastic material, then:

$$\varepsilon_{ij} = \frac{1 + \nu}{E} \sigma_{ij} - \frac{\nu}{E} \sigma_{kk} \delta_{ij} \qquad (3.1\text{-}1)$$

where:

ε_{ij} is the mechanical strain tensor (i.e., total strain minus thermal strain),

σ_{ij} is the stress, and

δ_{ij} is the Kronecker delta.

The stress and strain can be partitioned into deviatoric and volumetric parts,

$$\varepsilon_{ij} = e_{ij} + 1/3\ \varepsilon_{kk}\ \delta_{ij} \tag{3.1-2}$$

$$\sigma_{ij} = S_{ij} + 1/3\ \sigma_{kk}\ \delta_{ij} \tag{3.1-3}$$

The volumetric components, from equation (3.1-1) are related by

$$\varepsilon_{kk} = \frac{1 - 2\nu}{E}\ \sigma_{kk} = \frac{1}{3K}\ \sigma_{kk} \tag{3.1-4}$$

where K is the bulk modulus.

The deviatoric parts can be shown to be related by

$$e_{ij} = \frac{1 + \nu}{E}\ S_{ij} \tag{3.1-5}$$

Let the equivalent stress be represented by

$$\bar{\sigma} = \sqrt{3J_2} = \sqrt{3/2\ S_{ij}\ S_{ij}} \tag{3.1-6}$$

where J_2 is the second invariant of the deviatoric stress tensor.

Then, from equations (3.1-5) and (3.1-6)

$$\bar{\sigma} = \frac{E}{1 + \nu}\ \sqrt{3/2\ e_{ij}\ e_{ij}} \tag{3.1-7}$$

Similarly, the equivalent strain can be taken to be

$$\bar{\varepsilon} = \sqrt{3j_2} = \sqrt{3/2\ e_{ij}\ e_{ij}} \tag{3.1-8}$$

where j_2 is the second invariant of the deviatoric strain tensor.

Equation (3.1-7) now becomes

$$\bar{\sigma} = \left(\frac{E}{1 + \nu}\right) \bar{\varepsilon} = 2G\bar{\varepsilon} \tag{3.1-9}$$

Since only the ratio $\bar{\sigma}/\bar{\varepsilon}$ will be used to represent the material response, an additional assumption is needed to obtain the second elastic constant. For this purpose, assume the bulk modulus is constant, and given by equation (3.1-4)

$$K = \frac{E}{3\,(1 - 2\nu)} = \frac{E_o}{3\,(1 - 2\nu_o)} = \frac{2\,(1 + \nu_o)\,G_o}{3\,(1 - 2\nu_o)} \qquad (3.1\text{-}10)$$

where G_o, E_o, ν_o are the moduli and Poisson's ratio at the origin (i.e., $\bar{\sigma}=\bar{\varepsilon}=0$). The current shear modulus is known from the slope $\bar{\sigma}/\bar{\varepsilon}$. Then from equation (3.1-9)

$$\frac{2\,(1 + \nu)\,G}{3\,(1 - 2\nu)} = \frac{2\,(1 + \nu_o)\,G_o}{3\,(1 - 2\nu_o)} \qquad (3.1\text{-}11)$$

Solving equation (3.1-11) for

$$\nu = \frac{1}{2}\left[1 - \frac{3\,(G/G_o)}{\dfrac{2\,(1 + \nu_o)}{1 - 2\nu_o} + \dfrac{G}{G_o}}\right] \qquad (3.1\text{-}12)$$

Figure 3.1-1 presents the variation in Poisson's ratio with modulus. The Young's modulus can be determined from

$$E = 2\,(1 + \nu)\,G = (1 + \nu)\,\bar{\sigma}/\bar{\varepsilon} \qquad (3.1\text{-}13)$$

As an example, consider a uniaxial stress state

$$\sigma_{ij} = \begin{cases} \sigma & i=j=1 \\ o & i\neq 1,\ j\neq 1 \end{cases} \qquad \text{and} \qquad \varepsilon_{ij} = \begin{cases} \varepsilon & i=j=1 \\ -\nu\varepsilon & i=j=2,3 \\ o & i\neq j \end{cases} \qquad (3.1\text{-}14)$$

Then

$$\bar{\sigma} = \sigma \quad \text{and} \quad \bar{\varepsilon} = (1 + \nu)\,\varepsilon = \varepsilon_{11} - \varepsilon_{22} \qquad (3.1\text{-}15)$$

The $\bar{\sigma}$, $\bar{\varepsilon}$ curve is now the input stress-strain curve.

To illustrate the convergence of the iterative procedure, consider three parallel bars supporting an equivalent total load. The bars are assumed to be elastic-plastic. Each has a Young's modulus of 10×10^6 psi and a hardening slope of 0.5×10^6 psi. The yield stresses are different. The central bar will be assumed to have a yield stress of 20 ksi while the two outer bars have a yield stress of 10 ksi. The area of each bar is 1/3 in^2, making a total area of 1.0 in^2. Figure 3.1-2 illustrates that convergence has occurred in six iterations for a total load of 30,000 lb and that each of the bars has yielded.

The material constants for the simplified model are input to the computer code through data input cards.

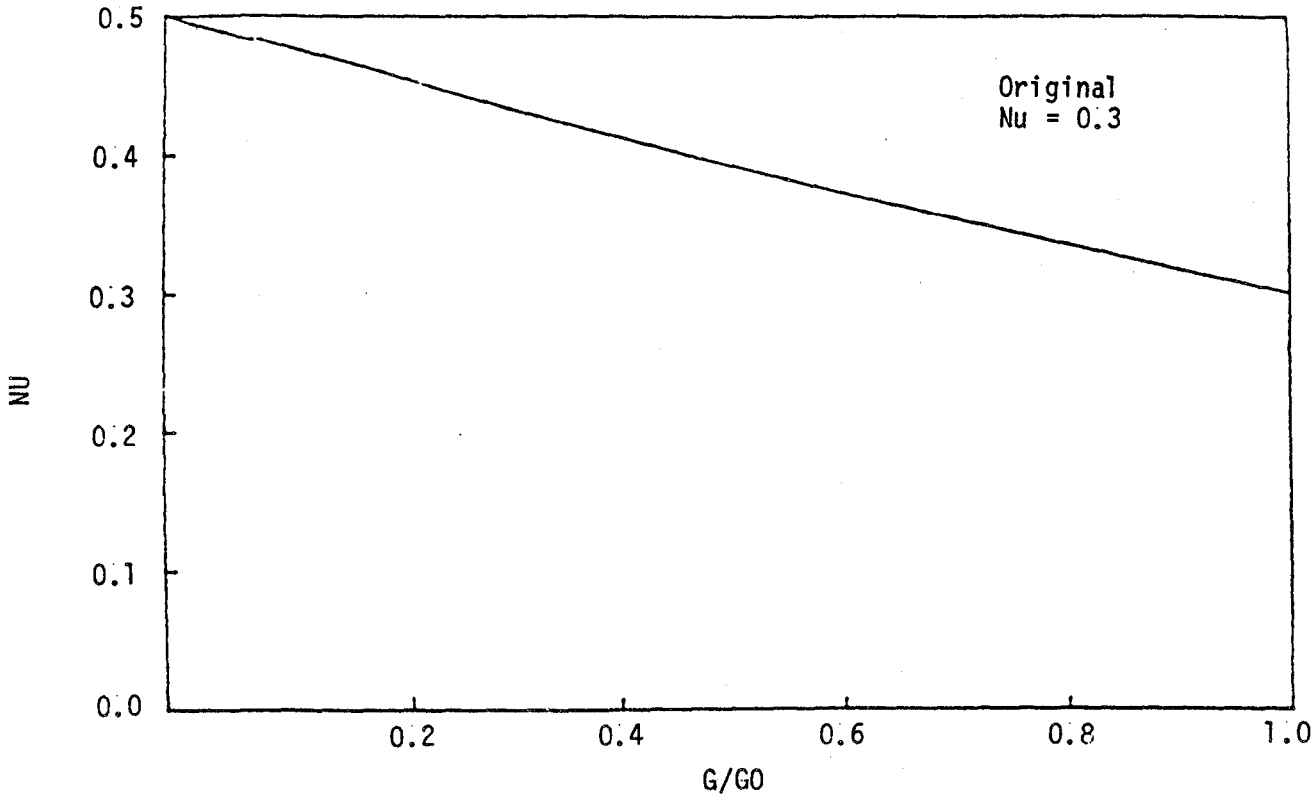

Figure 3.1-1 Variation in Nu

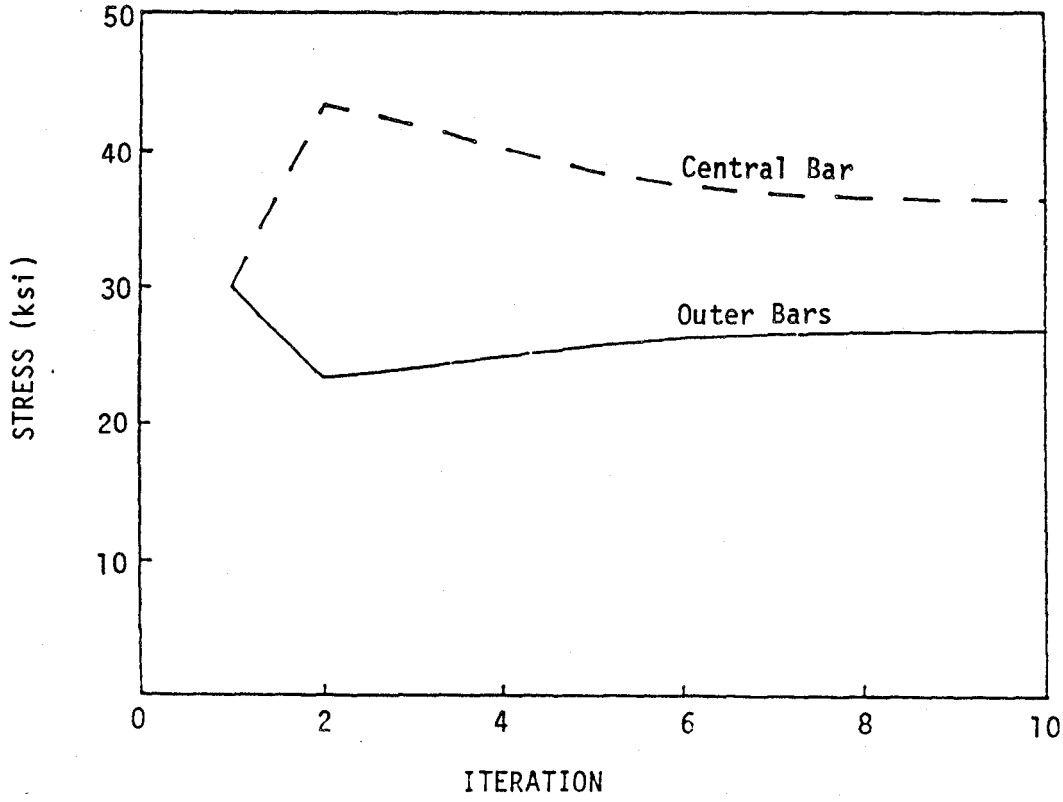

Figure 3.1-2 Three Bar Convergence Using Simplified Model

3.1.2 Current State-of-the-Art Model

The current state-of-the-art model has been taken to be the classical elastic-plastic-creep model that is available in the MARC code, and described in Reference 1. The creep model is essentially a steady state power law (stress) model. The plasticity model includes isotropic, kinematic, and a combined hardening law. Both the creep and plasticity models assume no permanent volumetric deformations. For the mechanics of materials computer code, the material properties for the state-of-the-art constitutive model are included in data statements in subroutine SOACON.

Plastic Iteration Procedure

Consider the case of a small strain elastic-plastic response of a typical structure. Sufficiently large applied loads will result in permanent or plastic deformation. A procedure for calculating the response of the structure undergoing plastic deformation is required.

To evaluate the response of the structure, the loading history is divided into a number of incrementally applied loading steps. Each of these load increments can then be applied sequentially to the structure. An iterative scheme is then required to calculate the response of the structure to each individual load increment.

At the beginning of a new load increment it may be assumed that the strain will change in a manner analogous to the previous increment. As an initial estimate all of the strain change is then assumed to be elastic. The change in the stresses can then be calculated using Hooke's Law or

$$\Delta\sigma_{ij} = L^{e}_{ijkl}\Delta\epsilon_{kl} \tag{3.1-16}$$

where: $\Delta\sigma_{ij}$ is the incremental stress vector,

$\Delta\epsilon_{kl}$ is the incremental total strain vector, and

L^{e}_{ijkl} is the matrix of elastic constants.

If the resulting total stress is within the yield surface, the matrix of material constants, L_{ijkl} is simply given by

$$L_{ijkl} = L^{e}_{ijkl} \tag{3.1-17}$$

If the resulting total stress is outside the yield surface, weighted material constants and stiffness matrices will have to be calculated. It should be noted at this point that if a load increment is exceedingly large and if there is a sudden change in the type of loading, care must be taken in order to iterate to the correct solution.

If the resulting total stress is outside the yield surface, the fraction of the stress increment that remains elastic must be determined. This corresponds to $\Delta\varepsilon^{el}_{ij}1$ in Figure 3.1-3. If the yield surface in stress space is considered to be given by

$$f(\sigma_{ij}) = 0,$$

then the appropriate m in

$$f(\sigma^{i-1}_{ij} + m\Delta\sigma_{ij}) = 0 \tag{3.1-18}$$

may be determined where σ^{i-1}_{ij} is the stress tensor from the previous increment.

The mean material matrix is calculated from

$$L_{ijkl} = mL^{e}_{ijkl} + (1-m)\, L^{e-p}_{ijkl} \tag{3.1-19}$$

where L^{e-p}_{ijkl} is the tensor relating $\dot{\sigma}_{ij}$ and $\dot{\varepsilon}_{kl}$.

Once the tensor L_{ijkl} has been determined, standard solutions can be applied to find the incremental changes in the displacements, strains and loads. For example, if the strains are given by

$$\{\Delta\varepsilon\} = [B]\,\{\Delta u\} \tag{3.1-20}$$

where $\{\Delta u\}$ is the vector of incremental nodal displacements, and $[B]$ is the matrix relating the vector of element strains $\{\Delta\varepsilon\}$ to the nodal displacements, the stiffness matrix can be found from

$$[K] = \int_V [B]^T\,[D]\,[B]\,dV \tag{3.1-21}$$

where [D] is the matrix representation of the tensor $L_{ijk\ell}$. The strain-displacement matrix $[B]$ depends on the formulation of the problem.

The incremental nodal displacements and strains can be evaluated by solving for Δu in

$$[K]\,\{\Delta u\} = \{\Delta P\} + \{\Delta G\} \tag{3.1-22}$$

and then applying equation (3.1-20).

In the mechanics of materials computer code the stiffness matrix K is held constant, and changes in the stiffness matrix are included in ΔG.

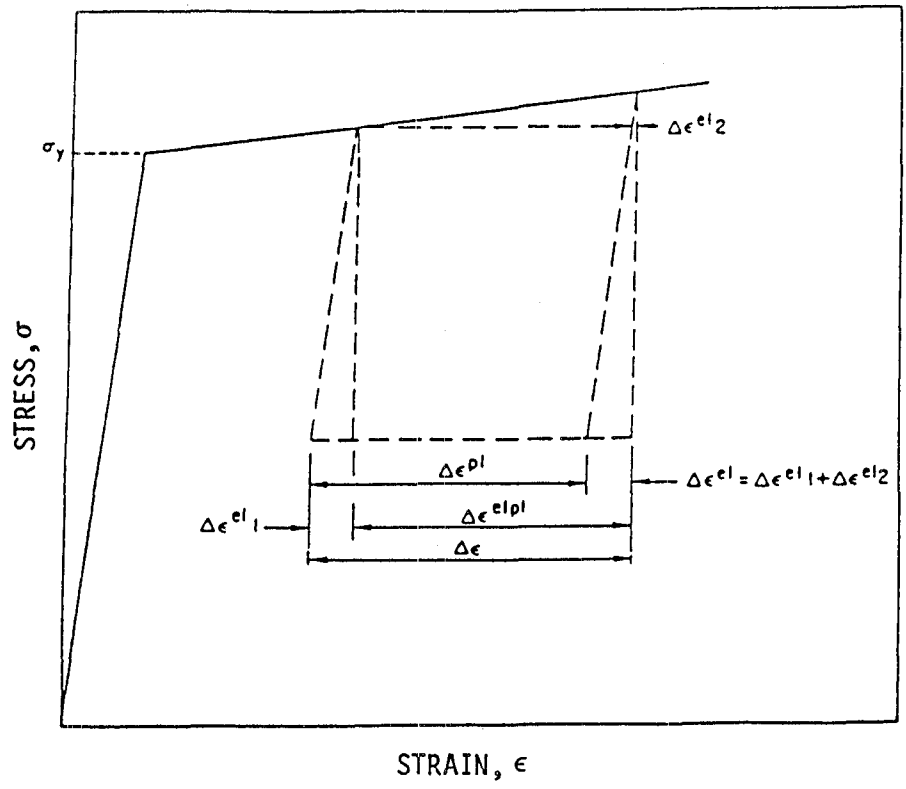

Figure 3.1-3 Elastic-Plastic Strain Decompositions for Bilinear Stress-Strain Law

The term ΔP in equation (3.1-22) is the applied incremental load. The term ΔG is defined as the pseudo-load correction to the stiffness matrix due to inelastic strains which is added to equation (3.1-22). The ΔG vector calculated from creep strain, for example, is shown in equation (3.1-34).

One iteration cycle is completed each time the stiffness matrix is formed and the resulting equations solved. At the end of each cycle the resulting solution must be tested for convergence. This is accomplished, by considering the change in energy,

$$r = \frac{E^N - E^{N-1}}{E^N} = \frac{E^N - E^{N-1}}{1/2\ (E^N + E^{N-1})} \qquad (3.1\text{-}23)$$

where E^{N-1} is the change in energy summed over all elements on the previous cycle and E^N is the energy including the present cycle.

An accurate solution will usually result if r is maintained less than 0.1 for elastic-plastic problems.

If the solution has satisfied the convergence, the stresses and strains can be updated and a new load increment added. If the solution has not converged, then a new guess for the strains, based on the latest cycle, must be input and the calculation procedure repeated. When the solution has not converged after a given number of cycles, the program should exit from the load incrementing loop.

Figure 3.1-4 is a flow chart illustrating the small strain elastic-plastic iteration procedure.

For isotropic materials the moduli in equation (3.1-19) are given by

$$L^{e}_{ijkl} = \frac{E}{1+\nu}\left\{\delta_{ik}\delta_{jl} + \frac{\nu}{1-2\nu}\,\delta_{ij}\,\delta_{kl}\right\} \tag{3.1-24}$$

and

$$L^{e-p}_{ijkl} = \frac{E}{1+\nu}\left\{\delta_{ik}\delta_{jl} + \frac{\nu}{1-2\nu}\,\delta_{ij}\delta_{kl} - \frac{3/2\,(S_{ij}-\Omega_{ij})\,(S_{kl}-\Omega_{kl})}{\left[1+\frac{2}{3}\left(\frac{1+\nu}{E}\right)H + \left(\frac{1+\nu}{E}\right)G\right]\sigma_o^2}\right\} \tag{3.1-25}$$

where E is Young's modulus

ν is Poisson's ratio

δ_{ij} is the Kronecker delta

$$\sigma_o = H\bar{\varepsilon}^{P} + \sigma_y \tag{3.1-26}$$

$$\dot{\Omega}_{ij} = G\,\dot{\varepsilon}^{P}_{ij} \tag{3.1-27}$$

$\dot{\varepsilon}^{P}_{ij}$ are the plastic strain rates

$$\bar{\varepsilon}^{P} = \sqrt{2/3\;\dot{\varepsilon}^{P}_{ij}\;\dot{\varepsilon}^{P}_{ij}} \tag{3.1-28}$$

G is the kinematic hardening slope

H is the isotropic hardening slope

σ_y is the initial yield stress, and

$S_{ij} = \sigma_{ij} - 1/3\;\sigma_{kk}\delta_{ij}$ is the deviatoric stress.

The strain rate has been decomposed into elastic (including thermal), plastic and creep components, or

$$\dot{\varepsilon} = \dot{\varepsilon}^{e} + \dot{\varepsilon}^{P} + \dot{\varepsilon}^{C} \tag{3.1-29}$$

The plastic yield surface was assumed to satisfy an equivalent Mises yield surface given by

$$1/2\ (S_{ij} - \Omega_{ij})\ (S_{ij} - \Omega_{ij}) = 1/3\ \sigma_o \qquad (3.1\text{-}30)$$

The method presented in Reference 4 is used to calculate the elastic-plastic moduli.

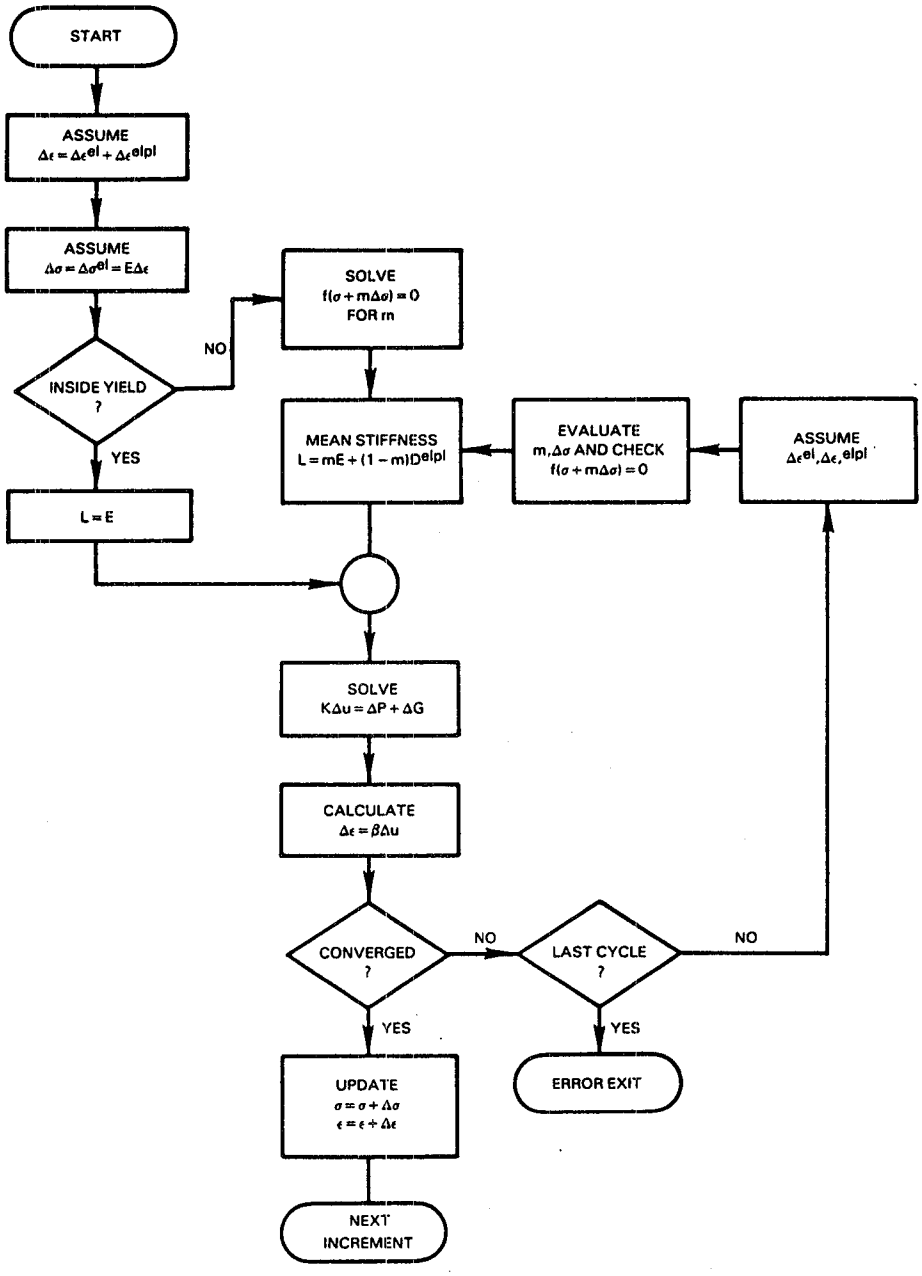

Figure 3.1-4 Elastic-Plastic Iteration Procedure

Time Effects Iteration Procedure

The creep strain rate will depend in general on the stress, the accumulated creep strain, the temperature and time. To illustrate the incrementing procedure, assume that the creep strain rate is normal to the Mises yield surface in stress space, then the creep strain rate is given by

$$\dot{\varepsilon}_{ij}^{cr} = \left[\frac{\sqrt{3/2\ S_{kl}\ S_{kl}}}{K}\right]^n \frac{3/2\ S_{ij}}{\sqrt{3/2\ S_{mn}\ S_{mn}}} \qquad (3.1\text{-}31)$$

For a specific time increment the incremental creep strains were approximated by

$$\Delta\varepsilon_{ij}^{cr} = \dot{\varepsilon}_{ij}^{cr}\ \Delta t. \qquad (3.1\text{-}32)$$

The incremental displacements are

$$[K]\ \{\Delta u\} = \{\Delta P\} + \{\Delta G\} \qquad (3.1\text{-}33)$$

where

$$\{\Delta G\} = \int [\beta]^T\ [E]\ \{\Delta\varepsilon^c\}\ dV \qquad (3.1\text{-}34)$$

is the pseudo-creep load, $\{\Delta\varepsilon^c\}$ is the vector of element creep strain, and [E] is the elasticity matrix. The strain increment can be calculated from equation (3.1-20) and the strains, creep strains, stresses and displacements can be updated.

A convergence test on the stresses should be performed. If the algorithm has not converged, a shorter time step should be used and the calculations repeated. If the criterion has been satisfied, then the time step can be increased. Figure 3.1-5 is a flow chart illustrating the small strain creep iteration procedure.

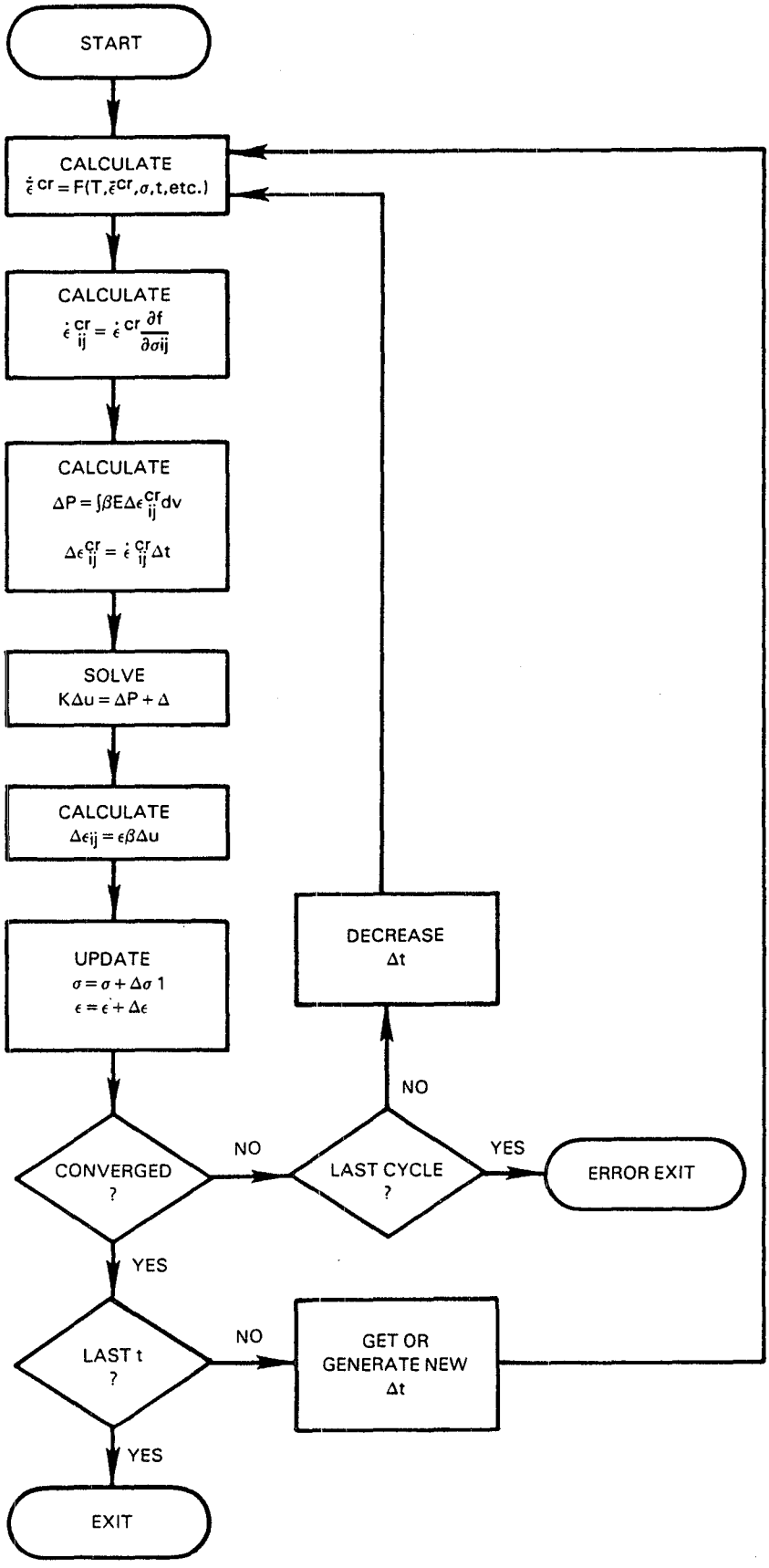

Figure 3.1-5 Creep Iteration Procedure

3.1.3 Advanced Viscoplastic Model

The viscoplastic model described in References 2 and 3 has been selected as the advanced constitutive model. Reference 2 describes the basic theory; while Reference 3 describes modifications to the form of the basic theory, and modifications to the material parameters for Hastelloy X. The modifications provide more accuracy at relatively low temperatures.

For uniaxial loading the viscoplastic material model (Figure 3.1-6) reduces to

$$\dot{c} = \left[\frac{|\sigma - \Omega|}{K}\right]^n \operatorname{sgn}(\sigma - \Omega) + \frac{(\sigma - \Omega)(1 - k)\langle\sigma\dot{\varepsilon}\rangle}{\sigma_\infty^2 - k\sigma^2} \tag{3.1-35}$$

$$\dot{\Omega} = n_2\dot{c} - n_3|\dot{c}|\Omega \tag{3.1-36}$$

$$c = \varepsilon - \frac{\sigma}{E} \tag{3.1-37}$$

where C is the inelastic strain,
Ω is the back stress,
σ is the stress,
ε is the strain, and
k, σ_∞, n, K, n_2, n_3 and E are material constants.

The absolute value and unit ramp functions are represented by

$$|x| = \begin{cases} -x & x<0 \\ x & x\geq 0 \end{cases} \tag{3.1-38}$$

and

$$\langle x\rangle = \begin{cases} 0 & x<0 \\ x & x\geq 0 \end{cases} \tag{3.1-39}$$

The inelastic strain in equation (3.1-35) consists of two components: 1) a time dependent power law creep component, containing the material constants n and k, and 2) a time independent plastic component, containing the material constants σ_∞ and k. The parameter σ_∞ becomes equivalent to the yield stress as: 1) k, in equation (3.1-35), approaches unity, and 2) the back stress, Ω, approaches zero. The back stress is a key variable in many viscoplastic material models. Its evolution is given by equation (3.1-36). Equation (3.1-37) represents the inelastic strain as the difference between the total strain and the elastic strain.

$$\dot{C}^{c}_{ij} = \left(\frac{\sqrt{3J_2'}}{K}\right)^{n}\left(\frac{\frac{3}{2}s_{ij}-\Omega_{ij}}{\sqrt{3J_2'}}\right)$$

$$\dot{C}^{p}_{ij} = \frac{\left(\frac{3}{2}s_{ij}-\Omega_{ij}\right)(1-\kappa)<\sigma_{ij}\dot{\epsilon}_{ij}>}{\sigma_{\infty}^{2}\left[1-\kappa(3J_2'/\sigma_{\infty}^{2})\right]}$$

$$\dot{\Omega}_{ij} = (n_1+n_2)\dot{C}_{ij} + C_{ij}\frac{\partial n_1}{\partial\Theta}\dot{\Theta} - (\Omega_{ij}-\overset{0}{\Omega}_{ij}-n_1C_{ij})\left(G-\frac{1}{n_2}\frac{\partial n_2}{\partial\Theta}\Theta\right)\cdot\overset{0}{\dot{\Omega}}_{ij}$$

$$\kappa = \kappa_1 - \kappa_2 e^{-n_7 R} = \beta\sigma_{\infty}$$

$$\dot{C}_{ij} = \dot{C}^{c}_{ij} + \dot{C}^{p}_{ij}$$

$$C_{ij} = (\delta_{ij}\lambda\epsilon_{kk} + 2\mu\epsilon_{ij} - \sigma_{ij} - \delta_{ij}(3\lambda+2\mu)\alpha\Theta)/2\mu$$

$$\dot{G} = (n_3 + n_4 e^{-n_5 R})\dot{R} + n_6\left(\frac{2}{3}\Omega_{ij}\Omega_{ij}\right)^{\frac{m-1}{2}},$$

$$\dot{R} = \sqrt{\frac{2}{3}\dot{C}_{ij}\dot{C}_{ij}},$$

$$\dot{\overset{\circ}{\Omega}}_{ij} = 3\overset{\circ}{\Omega}\left[\frac{\dot{C}_{ik}C_{kj}}{C_{pq}C_{pq}} + \frac{C_{ik}\dot{C}_{kj}}{C_{pq}C_{pq}} - \left(\frac{2C_{ik}C_{kj}}{C_{pq}C_{pq}}\right)\left(\frac{C_{rs}\dot{C}_{rs}}{C_{uv}C_{uv}}\right)\right] + \left[3\frac{C_{ik}C_{kj}}{C_{pq}C_{pq}} - \delta_{ij}\right]\frac{\partial\overset{\circ}{\Omega}}{\partial\Theta}\dot{\Theta}$$

$$s_{ij} = \sigma_{ij} - \frac{1}{3}\delta_{ij}\sigma_{kk}.$$

$$3J_2' = \frac{2}{3}\left(\frac{3}{2}s_{ij}-\Omega_{ij}\right)\left(\frac{3}{2}s_{ij}-\Omega_{ij}\right)$$

Material constants $\lambda, \mu, \overset{0}{\Omega}, n, m, n_1, n_2, n_3, n_4, n_5, n_6, n_7, K_1, K_2, \kappa, \sigma_{\infty}$ depend on temperature

Figure 3.1-6 Modified Walker's Theory

Subroutine HYPELA in the mechanics of materials computer code integrates Walker's viscoplastic equations and calls subroutine HYPCON to evaluate the material parameters. HYPCON contains the latest estimates for the parameters in the modified Walker's theory. Each load increment in the analysis is divided into NSPLIT subincrements. The integration of the constitutive equations is performed by using forward differences with a step size determined by dividing the load increment by NSPLIT. Subroutine HYPELA performs the integration in two ways: 1) a fixed step size, or 2) a variable step size. In the fixed step size, forward difference NSPLIT is the same for all load increments and subincrements.

In the variable step size, forward difference NSPLIT is determined by the magnitude of the change in a strain measure for every subincrement. The change in the strain measure is defined as

$$E = \Delta R + \frac{\sqrt{3\Delta J_2}}{2\mu} \tag{3.1-40}$$

where

$$\Delta R = \sqrt{2/3\ \Delta C_{ij}\ \Delta C_{ij}} \tag{3.1-41}$$

$$\Delta J_2 = 3/2\ \Delta S_{ij}\ \Delta S_{ij} \text{ and} \tag{3.1-42}$$

the quantity $\Delta\bar{\varepsilon}$ is calculated and is stored as variable ERRORO. There are three possible ways to determine NSPLIT. The method depends on the size of ERRORO. If

$$\text{ERROR2} < \text{ERRORO} < \text{ERROR1}, \tag{3.1-43}$$

then NSPLIT remains the same for the next subincrement (ERROR1 and ERROR2 are user-specified in HYPELA). If

$$\text{ERRORO} < \text{ERROR2}, \tag{3.1-44}$$

then NSPLIT is divided in two for the next subincrement and rounded (up) to the nearest integer. If

$$\text{ERRORO} > \text{ERROR1}, \tag{3.1-45}$$

then NSPLIT is doubled and the step is recomputed. The value of NSPLIT at the end of the increment is stored in the state variable TEMP(16). The initial value of NSPLIT is user-specified in HYPELA. The maximum value of NSPLIT is specified by MXSPLT. If NSPLIT exceeds MSXPLT, the message:

"UNABLE TO REDUCE ERROR IN LESS THAN MXSPLT SUBINCREMENTS"

is written where the value of MXSPLT is inserted in the WRITE statement. After this, the integration is performed using a constant step size.

3.1.4 List of Symbols

List of Symbols
Referenced Within Section 3.1

Symbol	Description	Page
ε_{ij}	Strain	3.1-1
σ_{ij}	Stress	3.1-1
δ_{ij}	Kronecker delta	3.1-1
ν	Poisson's ratio	3.1-1
E	Young's modulus	3.1-1
e_{ij}	Deviatoric strain	3.1-2
s_{ij}	Deviatoric stress	3.1-2
K	Bulk modulus	3.1-2
J_2	Second invariant of the deviatoric stress tensor	3.1-2
j_2	Second invariant of the deviatoric strain tensor	3.1-2
$\bar{\sigma}$	Equivalent stress	3.1-2
$\bar{\varepsilon}$	Equivalent strain	3.1-2
G	Shear modulus	3.1-2
$L_{ijk\ell}$	Matrix of material constants	3.1-5
$\{\Delta u\}$	Incremental nodal displacements	3.1-6
$\{\Delta\sigma\}$	Incremental stress	3.1-5
$[B]$	Strain-displacement matrix	3.1-6
[K]	Stiffness matrix	3.1-6

List of Symbols
Referenced Within Section 3.1

Symbol	Description	Page
$\{\Delta P\}$	Incremental applied load vector	3.1-6
$\{\Delta G\}$	Incremental pseudo-load vector	3.1-6
E^N	Energy in Nth cycle	3.1-7
r	Convergence parameter	3.1-7
$[E]$	Elasticity matrix	3.1-10
G	Kinematic hardening slope	3.1-8
H	Isotropic hardening slope	3.1-8
Ω	Back stress	3.1-12
c	Inelastic strain	3.1-12
λ, μ, $\mathring{\Omega}$, n, m, n_1, n_2, n_3, n_4, n_5, n_6, n_7, K_1, K_2, k, σ_∞	Material constants	3.1-12

3.1.5 References

1. "MARC General Purpose Finite Element Program," Volume A, B, C, D, E, Revision J2, MARC Analysis Research Corporation, Palo Alto, CA, 1981.

2. Walker, K. P.: "Research and Development Program for Nonlinear Structural Modeling with Advanced Time-Temperature Dependent Constitutive Relationships," NASA CR-165533, November 1981.

3. Cassenti, B. N. and R. L. Thompson: "Material Response Predictions for Hot Section Gas Turbine Engine Components," AIAA-83-2020, presented at the AIAA/SAE/ASME 19th Joint Propulsion Conference, Seattle, WA, June 27-29, 1983.

4. Rice, J. R. and D. M. Tracey: "Computational Fracture Mechanics," Numerical and Computer Methods in Structural Mechanics, edited by S. J. Fenves, N. Perrone, A. R. Robinson and W. C. Schnobrich, Academic Press, New York, 1973.

3.2 MECHANICS OF MATERIALS MODEL

3.2.1 Computer Program: Formulation/Description

The three-dimensional nonlinear mechanics of materials finite element computer program utilizes an intersecting network of beams to model a structural component. The program calculates the total strain as a linear function of position in cross section and along the length of the beam. Three material models are included in the code: the simplified material model, Walker's viscoplastic material model, and the state-of-the-art material model. Static and transient analyses can be performed with applied loads, thermal loads, and enforced displacements. The lowest frequency and mode shape using either initial or tangent stiffness is calculated; and buckling analysis is included in the static problem using initial or tangent stiffness. The program flow is summarized in Figure 3.2-1.

Input parameters to the computer code consist of information defining the model itself and information describing the method of solution desired. The model is defined by beams which are connected at grid points. The element coordinate system of a given beam is defined by an orientation grid point. The geometry of a beam is rectangular in cross section, with the dimensions of the cross section along the element coordinate axes specified. The material properties are specified for each beam, including Young's modulus, Poisson's ratio, mass density, coefficient of expansion, and yield stress. The initial temperature of the beam network is input, and the time at initial conditions is set to zero. A hardening slope for use with the simplified material model is entered, with a zero slope indicating perfectly-plastic behavior. Boundary conditions are specified by indicating at each node, excluding orientation grid points, a constrained or nonconstrained condition for the six degrees of freedom.

Input associated with the selection of the method of solution include the parameters that indicate:

1. the choice of constitutive model to be used,

2. the choice of a static or transient analysis,

3. the choice of initial or tangent stiffness in solving for the lowest frequency and mode shape, and

4. the choice of including buckling analysis with either initial or tangent stiffness.

The number of integration points in each beam is user-specified; stresses and strains are calculated at each integration point, and the user specifies between two and ten points along each element coordinate axis direction in each beam. The convergence value, defining the allowable energy change between two consecutive iterations in the static analysis or allowable range in internal energy for the adaptive time step calculation in the transient analysis, is entered by the user. The number and type of loading increments are also specified.

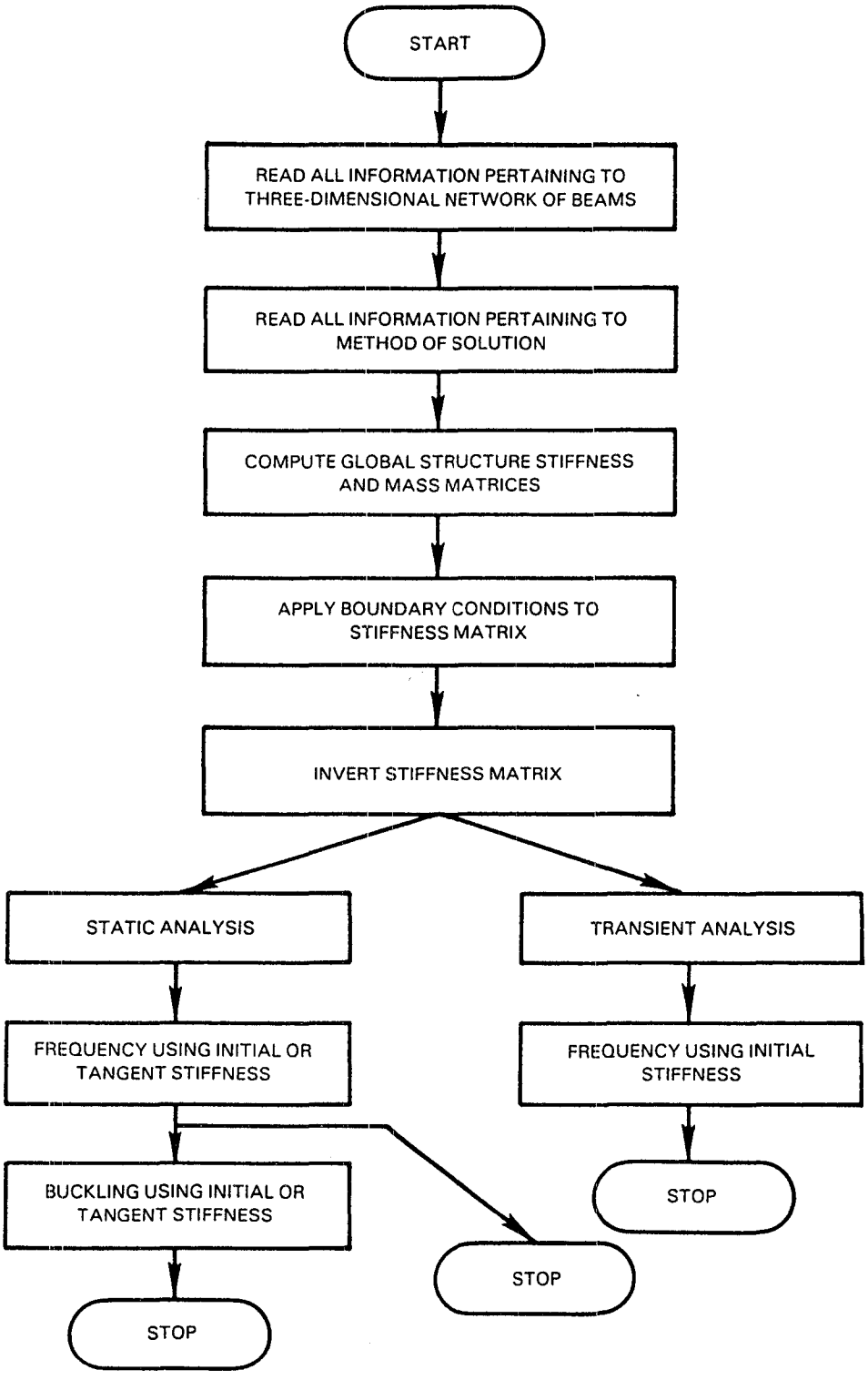

Figure 3.2-1 3-D Inelastic Mechanics of Materials Computer Program Flow Chart

The stiffness and mass matrices for each beam in the element coordinate system are computed and transformed to the global coordinate system. The stiffness and mass matrices are then assembled to form the global mass and stiffness matrices. The boundary conditions are applied to the stiffness matrix, and the matrix is then inverted. Any change in the stiffness due to nonlinear effects will be accounted for in the pseudo-load vector; therefore, the stiffness matrix is only inverted once.

Depending on user-input, the program now is directed to the appropriate branch of the program: static or transient analysis. For static analysis, the loading increment is read from the data input, including forces and moments or enforced displacements, specified at each degree of freedom of the structure. The temperature increment is also entered. An initial incremental displacement vector is set to zero and strain, stress and pseudo-load vectors are calculated from the incremental displacement vector using the mechanics of materials model selected by the user. The pseudo-load vector accounts for the effects of nonlinearity and allows the use of the original stiffness matrix throughout the calculations. The equations governing the system are as follows:

$$[K] \{\Delta u\} = \{\Delta P\} + \{\Delta G\} \qquad (3.2\text{-}1)$$

where $[K]$ = elastic stiffness matrix,

$\{\Delta u\}$ = incremental displacement vector,

$\{\Delta P\}$ = incremental applied load vector, and

$\{\Delta G\}$ = pseudo-load vector, due to inelastic strains.

$$\{\Delta G\} = \int [B]^T [E] \{\Delta \varepsilon\} \, dV \qquad (3.2\text{-}2)$$

where $[B]$ = strain-displacement matrix,
$[E]$ = elasticity matrix, and
$\{\Delta \varepsilon\}$ = inelastic strains.

Equation (3.2-1) is solved for the incremental displacement vector, Δu, which is substituted for the initial incremental displacement vector and used in the second iteration, continuing until the change in energy in two consecutive iterations is less than the convergence value input by the user. When convergence occurs, the incremental loading, displacements, strains and stresses for that loading increment are printed; the total load, displacement, strain and stress vectors, as well as temperature, are then updated. Each loading increment is read in and executed similarly, and the values of stress, strain and displacement for the total loading are calculated and printed upon conclusion of the last increment.

The transient analysis is based on a simple Euler integration and includes a self-adaptive time step scheme. Damping is not included directly in the transient analysis but is present in the viscoplastic material models. The loading for each increment is the total load at that given time, which is entered into the program by a user-supplied subroutine. The temperature increment and time

step are also entered. As in the static branch, the initial displacement vector is set to zero and the strains, stresses and pseudo-load vector are calculated using the designated mechanics of material model. An Euler integration is then used to calculate current displacements at the end of the present time step. The governing equations are as follows:

$$\{A\} = \{\Delta F\} - [K]\ \{\Delta U_o\} \tag{3.2-3}$$

$$\{\Delta V\} = [M]^{-1}\ \{A\} * DT \tag{3.2-4}$$

$$\{\Delta U_1\} = (\{V\} + 1/2\ \{\Delta V\}) * DT \tag{3.2-5}$$

where $\{A\}$ = acceleration vector,
$\{\Delta F\}$ = applied and pseudo-loads,
$[K]$ = elastic stiffness matrix,
$\{\Delta U_o\}$ = displacement vector at beginning of time step,
$\{\Delta V\}$ = change-in-velocity vector,
$[M]$ = mass matrix,
DT = time step,
$\{\Delta U_1\}$ = displacement vector at end of time step, and
$\{V\}$ = velocity vector.

A measure of the work done and the change in internal energy of the system during the time step is computed, and the time step is adapted accordingly. If the time step is accepted, the current displacements, strains and stresses are printed, and the current displacements are inserted for the initial displacements in the following time step. If the time step is unacceptable according to the adaptive scheme, the time step is changed, the load is recalculated, and the displacements are reset to the initial value at the beginning of that time step. The analysis continues until the user-designated number of increments is completed.

Following the static or transient analysis, the user has a choice between calculating the lowest frequency and mode shape or all frequencies and mode shapes. The method of solution for the calculation of the lowest frequency and mode shape is the inverse power method, which is represented by the following expression:

$$([K]^{-1}\ [M] - \lambda[I])\ \{x_{i+1}\} = \{x_i\} \tag{3.2-6}$$

where $[K]$ = stiffness matrix,
$[M]$ = mass matrix,
$[I]$ = identity matrix,
λ = eigenvalue, and
$\{x\}$ = eigenvector.

The method of solution in the calculation of all frequencies and mode shapes for a given problem is the Jacobi method, which is based on simple similarity transformations.

The procedure for determining the coefficients of the inverse stiffness matrix is one that can represent the original stiffness of the structure or the current stiffness including nonlinear effects. A small load is placed at one of the nonconstrained degrees of freedom of the structure, and the displacements are computed using the specified constitutive model. The coefficients of the appropriate row of the inverse stiffness matrix are calculated by dividing the calculated displacements by the applied force. This procedure is continued for each nonconstrained degree of freedom until an inverse stiffness matrix, with dimensions equal to the number of nonconstrained degrees of freedom of the structure, is formed. If the frequency is to be calculated using the initial stiffness of the structure, all variables used in the static or transient analysis are set to the original values. If the tangent stiffness is requested, all variables retain the current values for use in the frequency calculation. Only the initial stiffness option is available for use in a transient analysis since current stiffness cannot be readily calculated.

Buckling analysis can be executed in a static problem. The buckling analysis is based on a two step process similar to that in the NASTRAN finite element code. In the first step, the beam loads are determined. In the second step, a first order large displacement correction, proportional to the loads, is included in the stiffness matrix. Buckling occurs when the determinant of the new matrix vanishes. In the determination of the stiffness matrix used in the buckling calculation, the stiffness coefficients are calculated in the same fashion as was described in the frequency calculation, with the user choosing the initial or tangent stiffness. The beam loads are calculated using the initial stiffness matrix and then adding the pseudo-load vector. The actual buckling calculations are accomplished using the inverse power method to find the critical buckling factor and the buckled shape.

3.2.2 Program Validation/Verification

Some of the test cases (i.e., TEST1 - TEST5) which have been executed to validate the Mechanics of Materials Model (MOMM) computer code are summarized below. Each of these cases test various segments of the theory and computer code.

TEST1 - Cantilever Beam With Axial Load

A cantilever beam is loaded with a single static compressive loading increment. The beam (Figure 3.2-2) is made up of one member, with all degrees of freedom constrained at one end and all but two constrained at the end where the load is applied. The simple material model is used, and the loading causes only elastic displacements. The lowest frequency and buckling factor are obtained. The displacements, strains and stresses are found to be:

$$u_1 = P/K = -10^{-4}$$

$$\varepsilon_1 = u_1/L = -10^{-5}$$

$$\sigma_1 = E\varepsilon_1 = -100$$

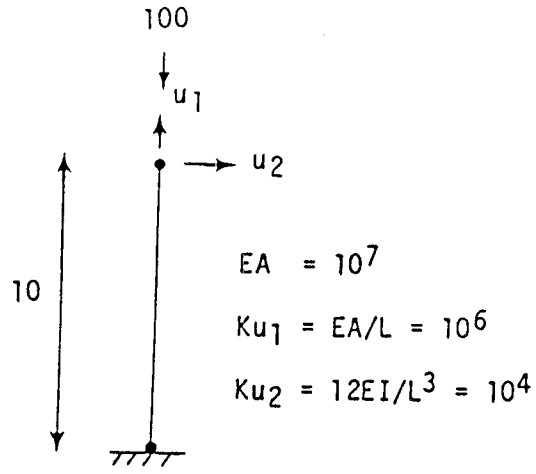

Figure 3.2-2 Schematic of TEST1 Beam

The resulting lowest frequency and buckling factor are:

$$f_{lowest} = \frac{w}{2\pi} = \frac{\sqrt{\frac{Ku_2}{m}}}{2\pi} = 22.5$$

$$\lambda_{cr} = \frac{Ku_2}{KG} = 833.3$$

Agreement between these computed values and independent closed-form solutions is exact.

TEST2 - Simply Supported, Centrally-Loaded Square Plate

A quarter of the square plate is modeled using symmetry boundary conditions (Figure 3.2-3). Four outside beams and four interior diagonal beams are used, with dimensions of the beams chosen so as to reproduce the stiffness and mass of the plate. One static loading increment is used with the simple constitutive model in the elastic range. The nonconstrained degrees of freedom are shown.

The theoretical central displacement is:

$$u_2 = .01160\ Pa^2/D$$

$$u_2 = -3.2428 \times 10^{-6}$$

The result from the MOMM computer run is:

$$u_2 = -3.4712 \times 10^{-6}$$

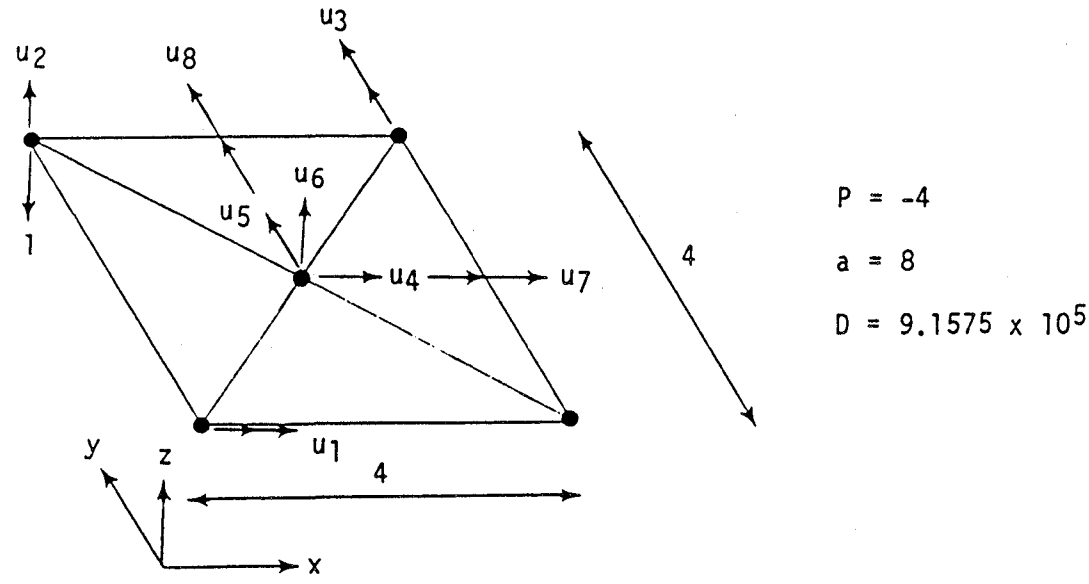

Figure 3.2-3 Square Plate Approximation Centrally Loaded

TEST3 - Beam With Axial Enforced Displacement (Static)

A static analysis (Figure 3.2-4) is performed using Walker's viscoplastic material model with twelve loading increments. The properties of Hastelloy X at a temperature of 871°C (1600°F) are used, and the tip displacement is enforced at a strain rate of 3.9×10^{-3} sec^{-1}. The computer program reproduces the experimental results. A plot of the stress-strain curve obtained from the output is shown in Figure 3.2-5.

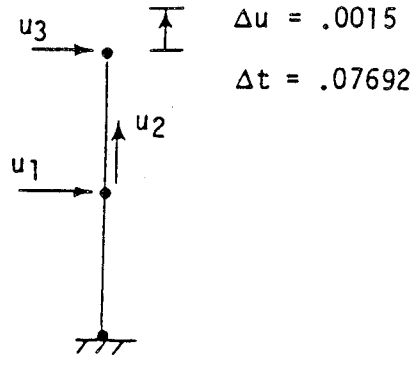

Figure 3.2-4 Schematic of TEST3

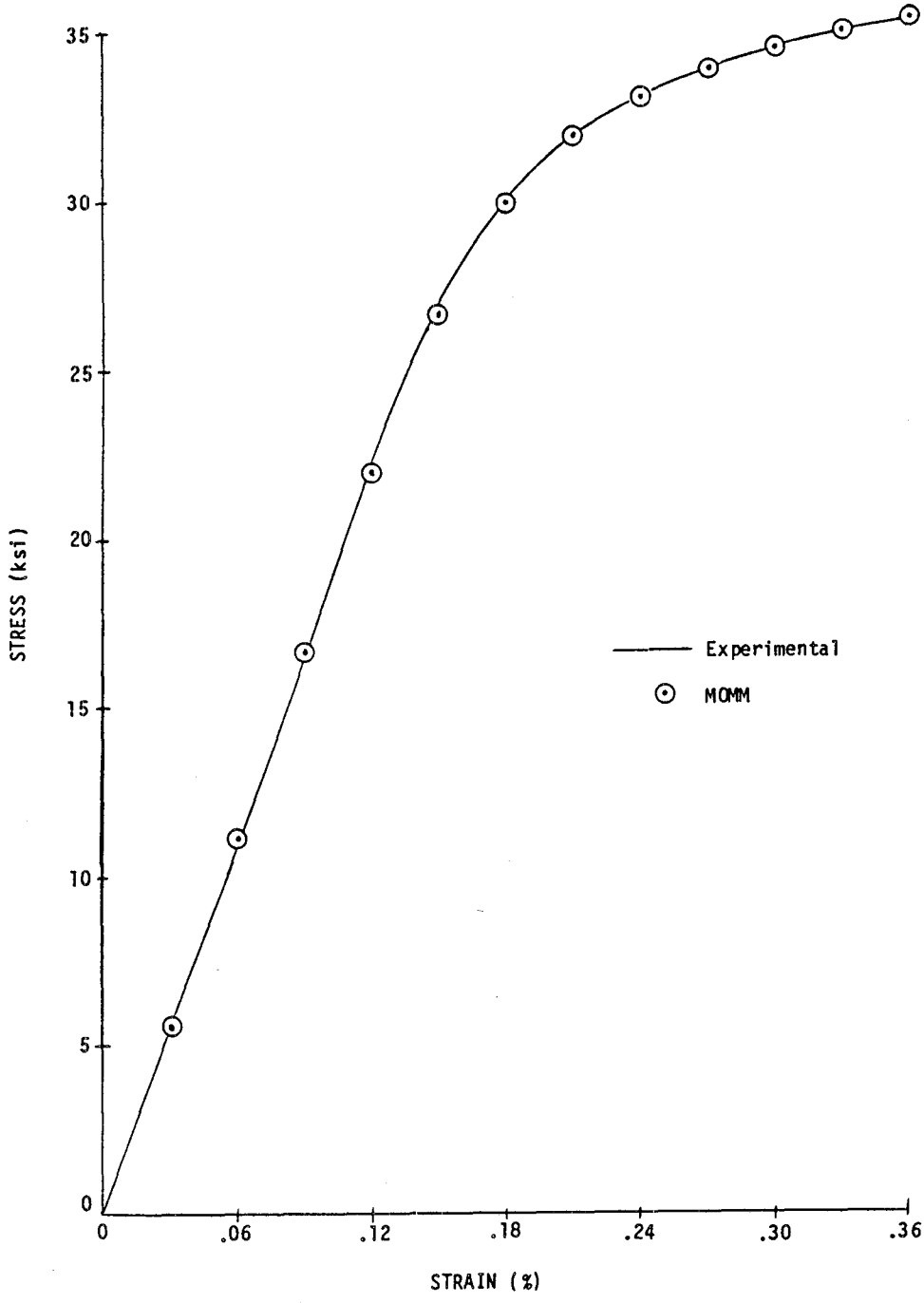

Figure 3.2-5 Stress-Strain Response for TEST3

TEST4 and TEST5 - Beam With Axial Enforced Displacements (Transient)

Both test cases contain a beam fixed at both ends with a node in the middle of the beam (Figure 3.2-6). One end is displaced so that the strain rate equals 3.9×10^{-3} sec^{-1}. A transient analysis is performed, with TEST4 containing Walker's viscoplastic material model and TEST5 containing the state-of-the-art material model. The viscoplastic material model uses the properties of Hastelloy X at a temperature of 871°C (1600°F). Figure 3.2-7 shows the displacement at the enforced displacement node, as well as the displacement at the center node versus time for each model. The results agree exactly with those obtained using a simple Euler integration.

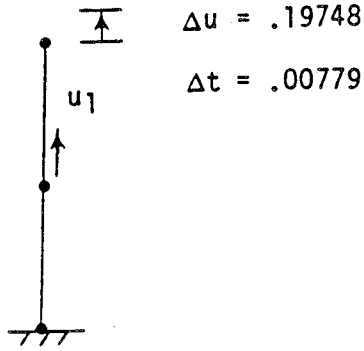

Figure 3.2-6 Schematic of TEST4 and TEST5

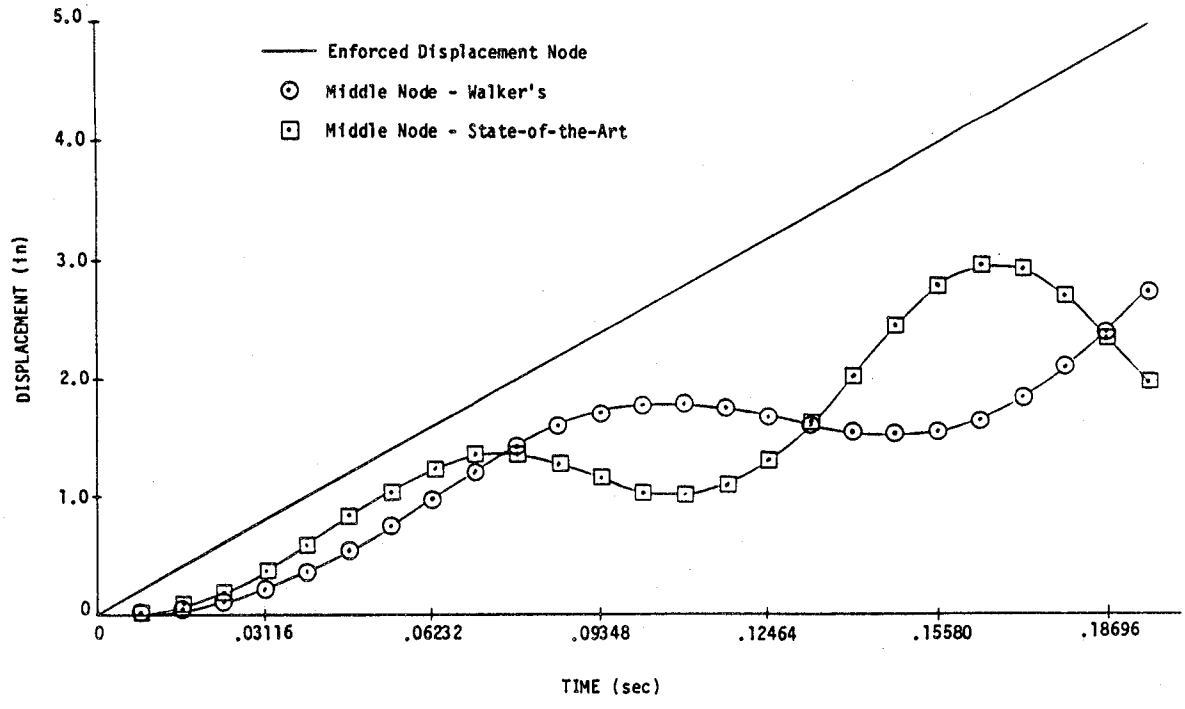

Figure 3.2-7 Displacement History for TEST4 and TEST5

3.2.3 List of Input Parameters

The following list contains the definitions of all variables that are included in the input to the Mechanics of Materials Model computer program.

NGP	-	Number of grid points
GP(I,1)	-	X-coordinate of grid point I
GP(I,2)	-	Y-coordinate of grid point I
GP(I,3)	-	Z-coordinate of grid point I
NB	-	Number of beams
IC(I,1)	-	Grid point at end A of beam I
IC(I,2)	-	Grid point at end B of beam I
IC(I,3)	-	Orientation grid point of beam I
IC(I,4)	-	Geometry set number of beam I
IC(I,5)	-	Material set number of beam I
NG	-	Number of geometry sets
BC(I,1)	-	Width of beam along local y-coordinate in geometry set I
BC(I,2)	-	Width of beam along local z-coordinate in geometry set I
NM	-	Number of material sets
XMAT(I,1)	-	Young's modulus in material set I
XMAT(I,2)	-	Poisson's ratio in material set I
XMAT(I,3)	-	Coefficient of expansion in material set I
XMAT(I,4)	-	Zero stress temperature in material set I
XMAT(I,5)	-	Yield stress in material set I
XMAT(I,6)	-	Mass density in material set I

TEMP(1)	-	Temperature at initial conditions
SLOPE	-	Hardening slope for simple material model
N	-	Number of grid points containing degrees of freedom
NI	-	Number of load increments
NIP	-	Number of integration points in each direction in each beam
EE	-	Static analysis: convergence parameter for energy change between two consecutive iterations o Transient Analysis: convergence parameter for change in internal energy for the adaptive time step calculation
JJ	-	Boundary conditions for each degree of freedom JJ = 1: nonconstrained JJ = 0: constrained
ICM	-	Constitutive model indicator ICM = 0: simplified material model ICM = -1: Walker's elastic-plastic-creep material model ICM = 1: state-of-the-art material model
ITRAN	-	Transient problem indicator ITRAN = 0: no transient analysis ITRAN = 1: transient analysis, forces input ITRAN = 2: transient analysis, enforced displacements input
ISIC	-	Indicates modulus slope used for frequency calculation ISIC = 0: initial slope ISIC = 1: current slope (not available in transient problem)
ILA	-	Indicates choice of solving for lowest or all frequencies ILA = 0: lowest frequency ILA = 1: all frequencies

IBUCK	-	Buckling problem indicator IBUCK = 0: no buckling analysis IBUCK = 1: buckling analysis (not available in transient problem)
ISICB	-	Indicates modulus slope used for buckling calculation ISICB = 0: initial slope ISICB = 1: current slope
DF	-	Applied load or enforced displacement for each degree of freedom for an increment
DTEMP(1)	-	Temperature increment
DTEMP(2)	-	Time increment

3.2.4 List of Symbols

List of Symbols
Referenced Within Section 3.2

Symbol	Description	Page
$\{A\}$	Acceleration vector	3.2-4
$\{\Delta F\}$	Incremental force vector	3.2-4
$\{V\}$	Velocity vector	3.2-4
$[M]$	Mass matrix	3.2-4
DT	Time step	3.2-4
λ	Eigenvalue	3.2-4
$[I]$	Identity matrix	3.2-4
$\{x\}$	Eigenvector	3.2-4
f	Frequency	3.2-6
λ_{cr}	Critical buckling factor	3.2-6

3.3 SPECIAL FINITE ELEMENT MODEL

3.3.1 Literature Survey

Numerical technology available for use in nonlinear analyses of turbine engine hot section components was investigated. An extensive literature survey was conducted for MARC by Professor T. J. R. Hughes, Stanford University, as a subcontractor, containing 352 references (Reference 1).

The first topic considered involved recent developments in global solution techniques for nonlinear finite element equations, including time discretization methods and strategies for nonlinear quasi-static analyses. Literature on linear equation solvers was also covered.

As the second item, the finite element basis and approaches for constructing element stiffness matrices were studied with particular emphasis on continuum and shell elements. Special elements were also discussed, including elements for fracture mechanics applications.

The numerical treatment of constitutive models, in particular problems associated with computational plasticity, was surveyed, including the effects of large strains and rotations.

Topics such as the self-adaptive mesh refinement associated with error estimates and error indications, and developments in hardware configurations in association with coding strategies were included in the survey.

A few papers concerning the finite element modeling of hot section components were uncovered and reviewed. These papers were mainly concerned with linear systems with simplified geometry.

In the final section of the survey, new developments in the numerical treatment of contact and friction conditions were studied by virtue of modern mathematical concepts of variational inequalities.

Overall, the current literature indicates that extensive research and development needs to be carried out on new finite element code concepts in order to obtain the significant gains in computational efficiency needed for three-dimensional inelastic analysis of hot section components.

Solution strategies in nonlinear finite element processes have been given much attention in recent years. In particular, a class of computationally efficient iterative solution schemes such as the quasi-Newton type techniques has been developed for solving nonlinear finite element equations. To avoid reassembly and refactorization of the tangent matrix and yet to achieve the quadratic convergence properties of the full Newton-Raphson method, line-search, subspace search and secant search techniques have been introduced in the literature and have proven useful for certain classes of problems. Such techniques are also combined with an automatic load increment size control strategy, usually referred to as arc-length type methods. A sophisticated iterative solution scheme with an adaptive nonlinear incrementation procedure is one of the key ingredients for the solution of the present problem.

Possible exploitation of dynamic relaxation and iterative solvers for linear equations is suggested in the literature survey. The results reported to date show that these methods are perhaps useful for well-conditioned problems, but no convincing numerical results are yet reported for ill-conditioned problems of engineering importance such as plates and shells, meshes with distorted elements, and incompressible problems. Iterative procedures for linear equation systems resulting from nondisplacement methods need to be investigated from a slightly different point of view in order to obtain some computational advantage. It is anticipated that a straightforward implementation of algorithms available in the literature is not robust enough to meet the present purposes.

In the context of nonlinear dynamic analysis of hot section components, a number of time integrators were considered. It was strongly suggested that partition and operator splitting methods needed to be investigated in conjunction with appropriate automatic schemes to determine the time step size. From such a point of view, exploitation of a class of single step algorithms is possible and perhaps most appropriate. All the important algorithms that appeared in recent publications were covered in the literature survey. Progress subsequent to the survey has also been reviewed at MARC.

It should be noted that no systematic investigation to date has been reported on the methodology of adaptive time stepping algorithms. This is in contrast to the numerous reports and scientific papers that have been found for automatic load incrementation in the context of quasi-static finite element analysis. It seems to be a major task to develop a dynamic transient solution algorithm capable of handling nonlinear problems in a stable manner and controlling the time increment size adaptively. Only a few references dealing with a rather primitive version of such a numerical solution were found in the literature survey.

A number of mathematical contributions noted in the survey were associated with a posteriori error estimates and algorithms for adaptive mesh refinement based on these estimates. These techniques were investigated only in the framework of two-dimensional linear elasticity.

As summarized above, no existing method was directly applicable to three-dimensional inelastic analyses of turbine engine hot section components. Existing numerical technologies, together with the development of new methodologies, would be essential ingredients for an efficient finite element procedure. Due to the three-dimensional nature of the problems in the present project, it was anticipated that some sort of iterative approach could substantially improve the efficiency of the computational procedures.

From a computational point of view, algorithmic aspects and coding strategies form the most important ingredients for successful numerical simulation of the present problem. Indeed, a number of papers addressing this aspect of finite element technology were included in the summary. However, the wide variety of hardware configurations currently available does not allow us to establish a single coding strategy to exploit all of the computing power available. It was

observed that a basically sound and transparent code could be modified to improve its performance in a specific hardware environment, but if a code is designed to maximize its performance in a specific hardware and software configuration, then it would become extremely difficult to effectively transplant such a code to different systems.

3.3.2 Formulation Development

3.3.2.1 Introduction

A finite element solution strategy was designed with particular emphasis on three-dimensional inelastic analyses of turbine engine hot section components. Key ingredients employed in this strategy are mixed variational formulations and their iterative implementations; linear isoparametric finite element interpolations with sophisticated integration techniques; advanced techniques in computational plasticity, in particular the integration of rate independent constitutive equations; and a class of single step, second order time integrators.

For the spatial discretization, a version of the Hellinger-Reissner variational formulation for solid mechanics is utilized as the basic variational statement of the problem, where the displacements and strain components are taken as the field variables. A linear Lagrangian finite element basis is used for the interpolation of these variables as well as for the stress-strain law. The radial return concept plays a central role in the computational plasticity. The incremental iterative solution algorithm is, however, cast in the framework of mixed finite elements, which results in a different algebraic system of equations and hence, different convergence properties, which are generally better than those of traditional displacement finite element methods.

The transient algorithms are looked at in a weighted residual manner, i.e., the time-space field is split in a logical fashion with the implicit and unconditionally stable nature of embedded time finite element discretization being maintained, but the evolutional nature of the original problem preserved. One of the major exercises in the formulation development is to construct a reasonable engineering criteria to determine the optimal step size at each time increment.

Thus, for the class of problems stated in the definition of the task, the spatial discretization method and the iterative procedure for linear and nonlinear problems have been firmly established. The current procedures still leave open certain possibilities for further improvement of convergence properties, if higher order solution schemes such as the conjugate gradient method are utilized. The transient algorithm, as well as its theoretical background in conjunction with present spatial discretization techniques, needs further investigation in order to fully utilize the advantages of the present mixed iterative techniques in the context of nonlinear dynamics.

3.3.2.2 Mixed Forms and Iterative Solutions

It is convenient to discuss the framework of the finite element methodology used here in the rather general context of a three-dimensional continuous body. The deformation is assumed to be small. For clarity, the development is presented in terms of classical elastic conditions. The generalization to incremental inelastic analysis is straightforward and involves the use of an appropriate constitutive relationship together with incremental forms of the variational equations.

Consider a deformable body Ω in three-dimensional physical space, of which the boundary $\partial\Omega$ is sufficiently smooth. Motion and deformation of the body is assumed small. The deformation and stress history of the body is characterized by three field variables: the displacement u, the strain ε, and the stress σ. Using lower case subscripts to denote rectangular Cartesian components of vectors and tensors with respect to a fixed spatial reference frame, the governing differential equations are

$$\sigma_{ij,i} = \rho\, a_j - f_j \tag{3.3-1}$$

$$\sigma_{ij} = D_{ijk\ell}\, \varepsilon_{k\ell} \tag{3.3-2}$$

and

$$\varepsilon_{ij} = 1/2\, (u_{i,j} + u_{j,i}) \tag{3.3-3}$$

where ρ is the density of material, a is the acceleration of the body given as a time derivative of the displacements, and D is a fourth order tensor which describes the material response at a given stress and strain state. The vector f is the loading function due to the body force.

For a given initial state, a set of boundary conditions;

$$u_j = \hat{u}_j \quad \text{on} \quad \partial\Omega_1^{(j)} \tag{3.3-4}$$

$$\sigma_{ij} n_j = \hat{t}_i \quad \text{on} \quad \partial\Omega_2^{(i)} \tag{3.3-5}$$

completes the classical statement of the problem. Following the derivation given by Zienkiewicz and Nakazawa (Reference 2), the first variations of the Hu-Washizu variational principle are obtained via the Galerkin method of weighted residuals:

$$\int_\Omega \rho u_j^*\, a_j\, dV + \int_\Omega u_{i,j}^*\, \sigma_{ij}\, dV = \int_\Omega u_j^*\, f_j\, dV + \int_{\partial\Omega_2^{(i)}} u_i^*\, \hat{t}_i\, dS, \tag{3.3-6}$$

$$\int_{\Omega} \varepsilon^{*}_{ij} \, \sigma_{ij} \, dV = \int_{\Omega} \varepsilon^{*}_{ij} \, D_{ijk\ell} \, \varepsilon_{k\ell} \, dV, \tag{3.3-7}$$

and

$$\int_{\Omega} \sigma^{*}_{ij} \, \varepsilon_{ij} \, dv = 1/2 \int_{\Omega} \sigma^{*}_{ij} \, (u_{i,j} + u_{j,i}) \, dv, \tag{3.3-8}$$

where * denotes a virtual quantity. In the above equation the virtual displacement is assumed to satisfy the homogeneous displacement boundary condition.

The above statement can be used as a basis for construction of a finite element procedure. One of the major advantages of this form over the conventional displacement approach is the explicit presence of stress and strain in the variational form and thus in the finite element equations.

This is the main theme of the present formulation development and will be discussed in the following sections.

Use will also be made of the classical virtual work statement

$$\int_{\Omega} u^{*}_{i,j} \, D_{ijk\ell} \, u_{k,\ell} \, dV = \int_{\Omega} u^{*}_{j} \, (f_j - \rho a_j) \, dV + \int_{\partial\Omega_2(i)} u^{*}_{i} \, \hat{t}_i \, dS. \tag{3.3-9}$$

Note here that equations (3.3-2) and (3.3-3) are embedded implicitly in the variational statement.

Direct discretization of the Hu-Washizu principle leads to a finite element equation of the form:

$$\begin{vmatrix} 0 & 0 & B \\ 0 & D & -Q \\ B^T & -Q^T & 0 \end{vmatrix} \begin{Bmatrix} u \\ \varepsilon \\ \sigma \end{Bmatrix} = \begin{Bmatrix} F \\ 0 \\ 0 \end{Bmatrix} \tag{3.3-10}$$

with u, ε and σ being the vector of nodal variables associated with the displacement, the strain and the stress respectively.

Eliminating the stress terms algebraically, a finite element form similar to the Hellinger-Reissner principle is obtained as:

$$\begin{vmatrix} 0 & +BQ^{-1}D \\ +D^T(Q^{-1})^T B^T & -D \end{vmatrix} \begin{Bmatrix} u \\ \varepsilon \end{Bmatrix} = \begin{Bmatrix} F \\ 0 \end{Bmatrix} \tag{3.3-11}$$

from which an iterative procedure is constructed.

Using the discretized form of virtual work statement, equation (3.3-9), the above form is modified.

$$\begin{vmatrix} K & +BQ^{-1}D \\ +D^T(Q^{-1})^TB^T & -D \end{vmatrix} \begin{Bmatrix} u \\ \varepsilon \end{Bmatrix} = \begin{Bmatrix} F + Ku \\ 0 \end{Bmatrix} \tag{3.3-12}$$

with K being the usual finite element stiffness matrix. The recursive form used here is:

$$Ku^{n+1} = F + Ku^n - BQ^{-1}D\varepsilon^n \tag{3.3-13}$$

$$\varepsilon^{n+1} = (Q^{-1})^TB^T u^{n+1} \tag{3.3-14}$$

which is in principle identical to an iterative method proposed by Loubignac (References 3 and 4) and investigated further by Cook (Reference 5). It should be noted that this procedure is used extensively in optimization theory (Reference 6) for a class of minimization problems with more explicit equality and inequality constraints. In finite element computations, solution of incompressible problems has been attempted using this class of iterative techniques, which results in an algorithm of Uzawa (Reference 7). A recent publication by Fortin and Glowinski (Reference 8) covers the theory of the iterative solution for a wide range of constrained problems in mechanics. Nakazawa, et al (Reference 9) show that the high order methods discussed in Reference 8 improve the convergence properties of this solution strategy significantly. The first attempt to unify the concept of an iterative solution for mixed finite element methods is reported in Reference 10 where another alternative economical way for solving mixed finite element equations is discussed.

In the computational procedure, the algebraic form is treated in an incremental way, i.e.,

$$u^{n+1} = u^n + K^{-1}(F - BQ^{-1}D\varepsilon^n) \tag{3.3-15}$$

and

$$\varepsilon^{n+1} = (Q^{-1})^TB^Tu^{n+1} \tag{3.3-16}$$

The stress is recovered directly from the strain, and therefore varies in a similar way as the strain, i.e.,

$$\sigma^{n+1} = D\varepsilon^{n+1} \tag{3.3-17}$$

This completes the discussion of discretization and solution procedures for a general class of problems in solid mechanics.

In the present algorithm, the solution is initialized by the conventional displacement stiffness equations and this stiffness array is used as the pivot in the subsequent iterative solution. Because all the necessary conditions for existence, uniqueness and stability are satisfied, the quality of the converged solution is dictated by the strain interpolation. The displacement plays a rather insignificant role other than as a preconditioner to the iterative approach. This has been noticed in the early papers by Cantin, Loubignac and Touzot (Reference 4).

Using appropriate diagonalization techniques for the matrix Q, the recovery of nodal strain components does not involve a matrix inversion operation, and no significant additional effort is required to compute and iterate on this quantity.

Once the matrix Q is diagonalized, the procedure to recover the nodal stress becomes extremely simple requiring the evaluation of the constitutive law at nodes where the strain is calculated.

The iterative solution procedure is readily applicable to a class of nonlinear material problems such as rate-independent plasticity and involves evaluating the constitutive law at each iteration cycle. This approach results in a scheme similar to the Newton-Raphson method as used in finite element displacement analyses. The only difference occurs in the procedures to evaluate the residuals. Compared with the conventional displacement method, the number of operations required for formation of the residual vector at each iteration is reduced somewhat because the number of nodal points is usually far less than the number of integration points in a given finite element mesh. This saves time in the constitutive calculation.

The iterative procedure developed here provides in principle a powerful vehicle to study large scale inelastic analysis problems in three dimensions. The largest array appearing in this calculation is the same as that in the conventional displacement method; however, the strain and the stress here are evaluated at the nodes, and hence a better approximation for these field variables is obtained. This property, in turn, reduces the necessity of excessively refining the finite element mesh to obtain accurate stress and strain fields.

Numerical instability is often encountered in stress and strain fields calculated from a finite element displacement solution; this is often seen as oscillatory behavior in the numerical approximations and may lead to inaccurate inelastic response of the discretized model. The present approach, being stable in terms of both displacement and strain, eliminates the possible occurrence of such numerical problems.

3.3.2.3 Element Technology

A family of linear Lagrangian finite elements has been used in accomplishing the present task (Reference 11), but the element library is independent of the global solution strategy and higher order elements can be added.

In two-dimensional and axisymmetric cases, four-noded quadrilateral elements with nodal points located at corners are used, with the displacement and strain components taken as the primary variables. The constitutive equation (3.3-2) is evaluated at the same nodes, and parameters associated with it are stored together with the stress components. Eight-noded isoparametric brick elements are utilized in three dimensions, and the same mechanism of representing all the quantities at the nodes is used. For the analysis of plates and shells, a four-noded Lagrangian element is used incorporating the transverse shear terms into a modified variational formulation of Reissner-Mindlin type.

In order to implement the analysis procedures established in the previous section, a number of terms must be integrated to form coefficient matrices. As discussed in the context of penalty finite elements for incompressible problems, due care must be exercised in order to obtain a stable finite element approximation. The integration options for linear quadrilateral elements are four-point and single-point Gaussian quadratures, as well as the four-point trapezoidal rule, as shown in Figure 3.3-1. For the three-dimensional solid elements, eight-point integration rules that correspond to the two-dimensional four-point schemes are employed.

Evaluation of the stiffness matrix K associated with the displacement formulation for the two- and three-dimensional elements may be done using either a standard or a selective reduced integration procedure. In the selective integration procedure, direct (or normal) strain components are evaluated at four/eight Gaussian quadrature points, whereas the shear components are dealt with at the centroid of the element. This simple "trick" greatly improves the behavior of the elements, particularly in bending. In order to account for the isoparametric distortion of elements, the terms in the stiffness equations are represented with respect to a local element Cartesian coordinate system, the definition of which is given by Nagtegaal and Slater (Reference 12) and shown in Figure 3.3-2.

The load vector (including the surface traction term) is integrated using full Gaussian quadrature. The residual vector which appears in Equation (3.3-15) is also fully integrated.

In the strain recovery phase, the use of reduced (single-point Gaussian) quadrature has been found stable and accurate, but the quality of the displacement solution often deteriorates after a few iterations for a given increment. The use of the trapezoidal rule which naturally results in the lumped (diagonal) form of the Q matrix is found to be optimal. For certain cases, the quality of the displacement solution is preserved when this integration procedure is used, without any loss of accuracy in stress and strain approximations.

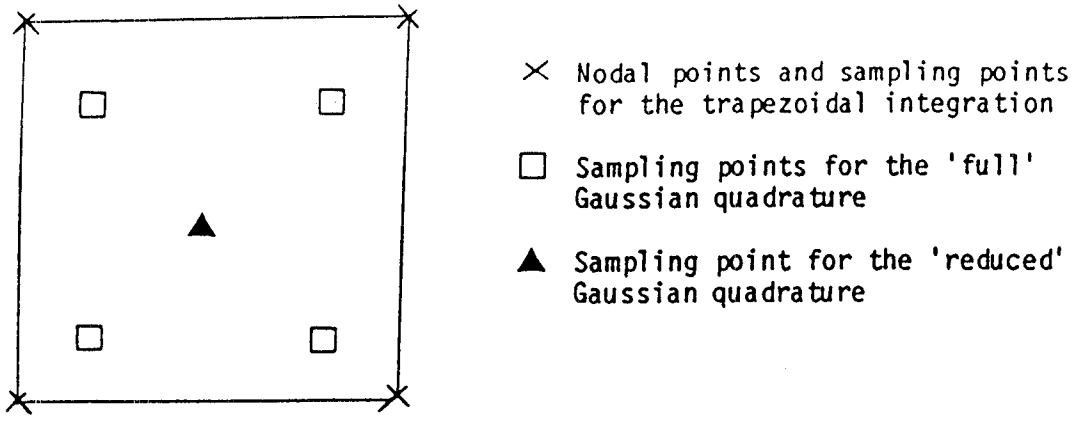

Figure 3.3-1 The Four Noded Linear Lagrangian Element in Two Dimensions

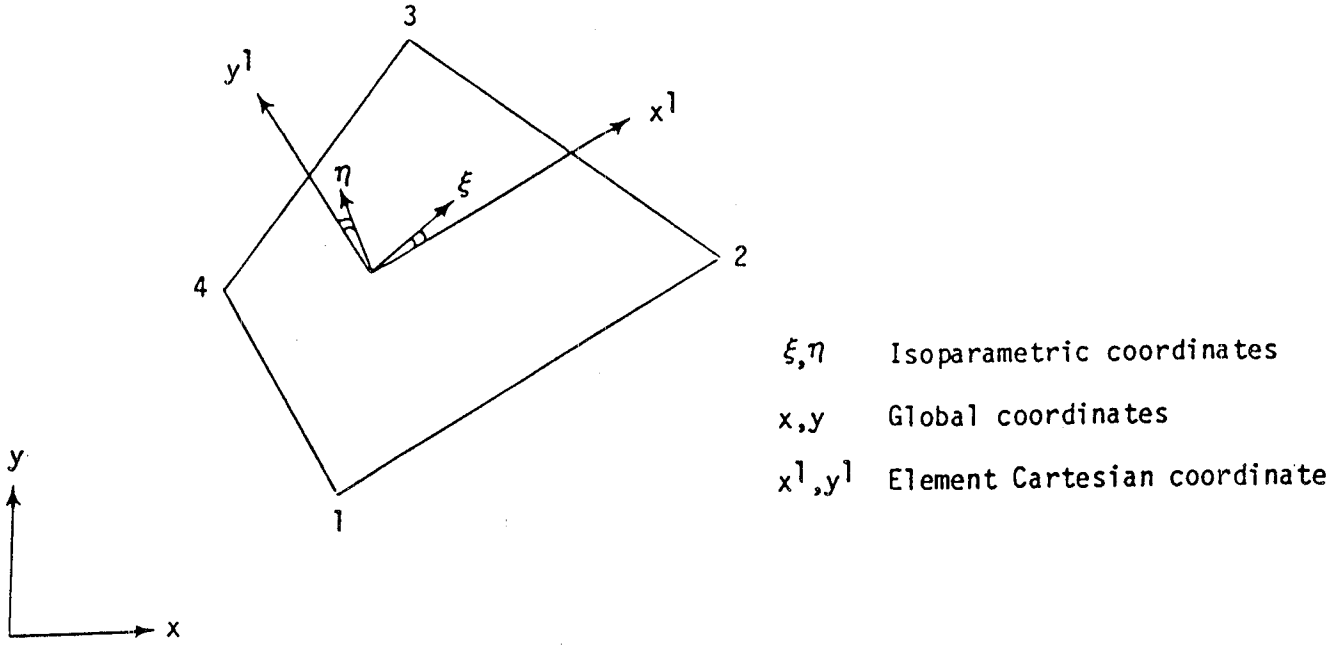

Figure 3.3-2 Coordinate Transformation for Two-Dimensional Elements With Isoparametric Distortion

For the shell element, an adjustable form of the selectively reduced integration technique has been applied to the integration of displacement stiffness terms, to avoid singularity and numerical locking. The same options are made available for the strain recovery at nodal points. To recover the strain at nodes, a local Cartesian coordinate system common to all the elements joined to the node is required. Vector and tensor components, initially defined with respect to the shell element coordinates, are transformed to the local Cartesian system using appropriate operations.

3.3.2.4 Inelastic Constitutive Models

Three inelastic constitutive models have been implemented into the MHOST program. In order of increasing sophistication, these models are as follows:

Approximate Constitutive Model

This model approximates the global stress-strain behavior with a nonlinear pseudo-elastic model. The model is described in detail in a report by Cassenti (Reference 13). A secant modulus procedure is used for the generation of stress increments and constitutive equations. This simple model does not allow for numerous important effects actually occurring in the cyclic loading of hot section components. Nevertheless, it definitely has some usefulness in obtaining some indication of the degree of nonlinearity in simple load simulations.

State-of-the-Art Constitutive Model

This model includes the approaches most commonly used for inelastic analysis of hot section components. It combines state-of-the-art time-independent plasticity with isotropic (and in the near future, also kinematic and combined) strain-hardening, a classical creep model in series with the plasticity model and a thermal expansion capability. In addition, elastic and inelastic properties can be made temperature-dependent. The material may contain initial anisotropic behavior for the elastic properties, yield surface definition and coefficient of thermal expansion.

In the plasticity model, the radial return method is used for stress recovery and the tangent modulus approach is used to generate the stress-strain law. In the creep model, a simple explicit procedure is applied for time integration of the creep strains. Both methods can also be regarded as state-of-the-art methods for implementation of such models.

The state-of-the-art model includes most of the important effects occurring in cyclic loading of hot section components. However, some weaknesses exist in load reversal situations, in particular with respect to interaction between plasticity and creep effects; if these effects are very important, the advanced model should be employed.

Advanced Constitutive Model

The integrated creep-plasticity model orginally developed by Walker (Reference 14) and later modified by Cassenti (Reference 13) was implemented into the HOST program. The model is described in detail in the report by Cassenti (Reference 13). Although both time-independent plasticity and creep effects can be distinguished in the model, definite interactions have been included on the single-point level. In addition, reversed loading effects are included more accurately in this model than in the state-of-the-art model.

An explicit subincrement procedure with optimal time step selection is used in the stress recovery procedure for this model. The elastic (but temperature dependent) stress-strain law is used for the formulation of the stiffness matrix; hence, the iterative algorithm for this model is, in fact, the modified Newton method.

The advanced constitutive model allows accurate material modeling for hot section components. It should be noted, however, that the complexity/generality of the model is also its major drawback. Almost a dozen temperature dependent material constants need to be determined experimentally before the model can be applied.

3.3.2.5 Time Integration

For a class of nonlinear problems to be dealt with in the present task, dynamic effects were taken into account. A recursive form is derived and implemented here, which is conceptually based upon the embedded time (temporal) finite element concept.

The solution of an evolution problem lies in a four-dimensional time-space. Therefore, in the formulation it is necessary to take temporal as well as spatial variations into account using a four-dimensional basis for the discretization. However, as demonstrated in Section 3.3.3.2, the differential operators governing the evolution of nonlinear structural mechanics can be split apart and the dependency of the solution upon each independent variable can now be treated separately. Such a separation of variables is of some importance in dynamic situations, because the differential equation consists of different characteristics with respect to each independent variable, that is hyperbolic in time and elliptic in all spatial dimensions.

To preserve the evolutional nature of the original problem and to take into account the hyperbolic nature of temporal operator, the discretized system of the embedded time finite elements is used recursively from one time level to the next. Hence, the equivalent form is derived by integrating the spatially discretized form of finite element equations in time. It is noted that a non-symmetric weighting function is used in this procedure due to the well-known conditional stability of finite element procedures for hyperbolic systems.

Using the two-noded time element and an appropriate nonsymmetric weighting function, the algebraic system becomes identical to the generalized Newmark-β finite difference expressions.

In each time element, the displacement increment obtained by the integration scheme is fed into the same discrete strain-displacement equation (3.3-14) to obtain the first correction vector, and then the residual vector is updated to produce the new displacement increment. The residual at the end of each time increment is carried to the next time level so that the overall equilibrium is satisfied globally in the sense of embedded time finite element methods.

The size of the time element is controlled adaptively with respect to an energy weighted average of the relative phase errors, based upon the contributions of strain and kinematic energy in the deformation represented by a time element.

3.3.2.6 Eigenvalue Extraction

Eigenvalue extraction is utilized in the MHOST program to obtain both the dynamic model frequencies and collapse load estimates. In addition to the eigenvalues, the eigenvectors are also obtained.

The subspace iteration technique has been implemented in the MHOST program. Using this method, the global stiffness and mass matrices are transformed into a subspace. A threshold Jacobi method has been used to obtain all of the eigenvalues in the subspace. This method has been found to converge very quickly. The program iterates forming new subspaces until convergence is obtained.

This method has been developed for the extraction of a large number of modes in a large system. This is typically what is required for modal dynamic use. The method has not been applied as frequently to the calculation of buckling modes, where only a few modes are required. It is anticipated that this is an area where future work may be fruitful.

An important issue in the successful convergence of this method is in the choice of the initial trial vectors. Currently, a simple scheme is being used, where the degrees of freedom with smallest K/M ratio are given the greatest weight.

Currently the lumped mass matrix is being utilized.

3.3.3 Program Development

3.3.3.1 Introduction

A finite element code (to be referred to as the MHOST program) has been developed by MARC incorporating the formulation and solution strategies previously described. The framework of the code is built on the well established foundation of finite element displacement coding for nonlinear structural analysis.

The mixed interpolations and the iterative procedures are built into the MHOST program as additional operations to the standard procedure, and no major changes are required inside of the finite element computations. One of the major differences, however, from the user's point of view is that all information is available at the nodal points rather than at the element integration points.

The current version of the MHOST program is essentially a vehicle to explore the capability of the present strategy and no attempt has been made to optimize the computational efficiency at the coding level. The program is written in a clear manner in order to achieve high productivity in the formulation and program development.

In this section, a technical note is provided on the overview and control structure of the MHOST program, the element library and the nonlinear solution capability of the system.

3.3.3.2 Overview and Control Structure

The MHOST program is written in FORTRAN IV with commonly accepted options, and has been tested on the PRIME Primos 18.2 FTN compiler and on the IBM/CMS FORTRAN H extended compiler with the optimization level 2. The advantages of a virtual storage system are exploited by storing most of the information in the core memory. and no special file input/output operations are utilized. Hence, the code is portable to other virtual memory systems, with little conversion effort necessary. The code can be run either interactively or in a remote batch mode.

The main functions of the MHOST code are illustrated in Figure 3.3-3, which depicts a number of processors devoted to specific operations. In the following paragraphs, the functions of these processors will be briefly discussed.

A user-friendly, free-format input processor is attached which reads in the data from the main input channel. The input data consist of PARAMETER DATA, MODEL DATA and INCREMENTAL DATA. The PARAMETER DATA specify the size of the model and select the options for the integration and the types of loading. The MODEL DATA provide the definition of the finite element model including the boundary conditions and load data for the first increments. The INCREMENTAL DATA section provides additional loading data and boundary conditions for each load step of the incremental solution.

Data of different types within the three major data blocks are identified using keywords. The keywords available for use in the PARAMETER, MODEL, and INCREMENTAL data blocks are listed and defined in Section 3.3.5.

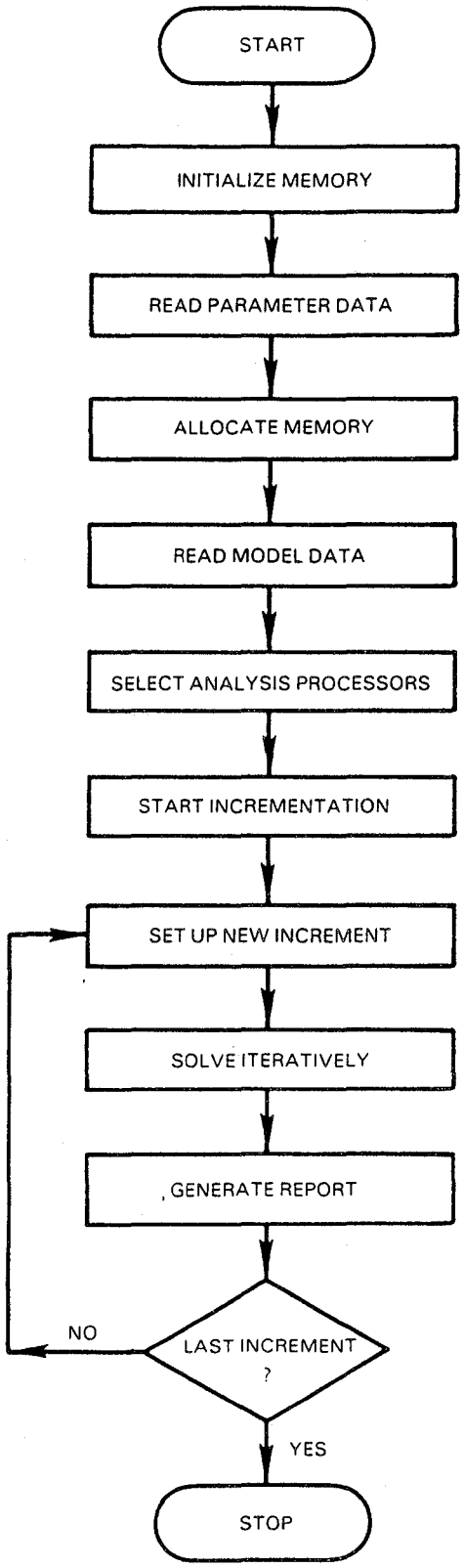

Figure 3.3-3 The MHOST Program Main Control Flow

The input processor passes information to the main finite element processor in which the iterative solution for mixed finite element equations is carried out. The flow chart of this section of the MHOST code is given in Figure 3.3-4, which also includes additional operations to the conventional displacement solution indicated by bold lines.

During an increment, the initial solution of the iteration for the mixed problem is carried out in exactly the same manner as the displacement method, with the converged stress and strain field of the previous increment taken as the initial state to calculate the tangent array. The mixed interpolation then takes over the process, and the tangent array becomes part of the strategy. The nodal strain is recovered from the displacement solution, and then the constitutive equation is integrated at the nodal point level to obtain the nodal stress array. The new residual vector is formed using this new state of stress. The iteration is repeated until the norm of the residual vector becomes less than the prescribed tolerance.

The size of the new incremental load is adaptively calculated when the automatic incrementation routine is invoked. Otherwise, the input data for the next increment are loaded and the above procedure is repeated until the stop flag is set.

The output processor generates a report printout on the line printer channel at the end of every increment. When the restart file and the plot file are requested, this processor generates these files and catalogues them in the system.

As dictated by the mixed formulation of the problem, all the information produced by the MHOST code is associated with nodal points. In the options to generate the line printer file, however, the element integration point information is made available using the values interpolated by the shape function from the nodal values.

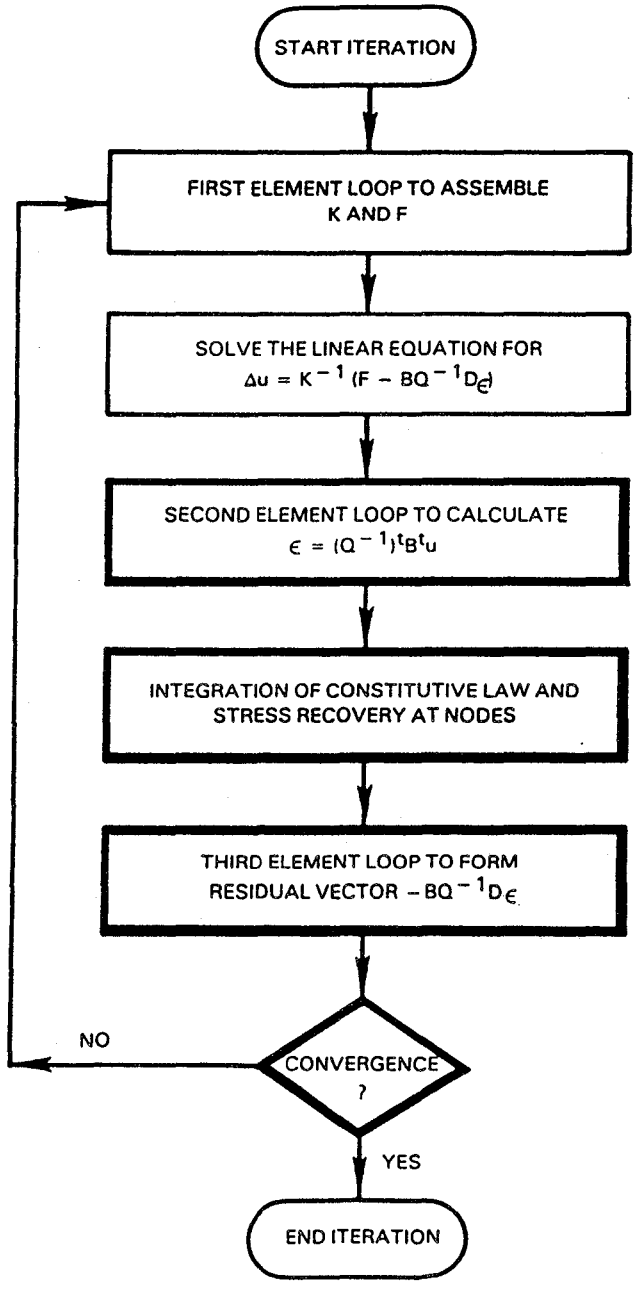

Figure 3.3-4 Detailed Flow Chart for Iterative Solution for Mixed Problem

3.3.3.3 Element Library

The control structure of the code is independent of the element type used in the analysis described in the formulation development Section 3.3.2.2. The operations associated with the element technology are coded in the element library subroutines. This class of subroutines consists of the shape functions, the derivatives of shape functions with respect to the global coordinate system and the element Cartesian coordinate transformations. These individual components are merged into the macro subroutines which assemble matrices used in the solution procedure. These macro subroutines are constructed for every type of geometric feature of the model, i.e., plane stress, plane strain, axisymmetric and, three-dimensional continuum. When the MHOST program is executed, the upper level control routines select the appropriate macro element library subroutines; and then each macro subroutine, in turn, selects the lowest level element library subroutines.

In the current version of the MHOST program, the bottom level element library consists of only two element types, i.e., a four-noded two-dimensional element and an eight-noded three-dimensional element. The structure of this code allows the user to enhance the element library without major difficulties.

The macro level subroutines consist of the lumped mass matrix routine to form Q, and the displacement strain matrix routine to form B. No element level operation is necessary for the stress recovery operations. For shells, the geometrical features of the problem require some coordinate transformations which are defined only at the element level.

3.3.3.4 Nonlinear Analysis Capabilities

The following geometric types are included in the MHOST program:

1. truss in three dimensions,
2. plane stress,
3. plane strain,
4. axisymmetric solid,
5. three-dimensional solid, and
6. shell in three-dimensions.

The nonlinear constitutive equations built in this code are evaluated once at each iteration loop when the nodal stress is recovered after the strain-displacement solution.

The material laws discussed in the formulation development Section 3.3.2.2 are readily built into the present version of the MHOST code leaving the possibility of major modification by means of user subroutines.

3.3.4 Program Validation/Verification

The validation/verification of analysis capabilities is an important step in the computer program development process. Validation/verification of the MHOST finite element program is a joint MARC/Pratt & Whitney effort, and involves comparing MHOST results with those obtained from closed form solutions, the MARC General Purpose Structural Analysis program, and hardware tests.

The simplest validation cases involved subjecting several element types to uniaxial loading. The finite element mesh and applied loads for a plane stress block are depicted on Figure 3.3-5. After three increments of loading into the plastic range, MHOST and MARC results agreed to three significant figures. The mesh shown on Figure 3.3-5 was also analyzed using the four node plane strain quadrilateral element and agreement between results from the two finite element codes was also very good (three significant figures). In addition, a similar mesh of axisymmetric elements was exercised for the case of uniaxial tension. After three increments of loading, results from both codes agreed to two significant figures, except for the plastic strains. Here, MHOST predictions were about 2% smaller than MARC values.

The three-dimensional block shown on Figure 3.3-6 was placed in uniaxial tension by prescribing displacements in the x-direction. The MHOST results exhibited homogeneous uniaxial behavior in the plastic range after three increments of prescribed displacement, and numerical values were in excellent agreement with a closed form solution.

A simple linear temperature analysis case was created by constraining the ends of the mesh shown on Figure 3.3-5 and subjecting it to a uniform increase in temperature. MHOST results were identical to the closed form solution.

The more complex case of the elastic response of a cantilever beam subjected to a moment load was also analyzed using the MHOST program. The rectangular finite element mesh and loading data are shown on Figure 3.3-7. Five Loubignac iterations were performed and the results obtained using various numerical integration procedures are presented in Table 3-I. Run A which employs selective stiffness integration and strain-displacement integration by the trapezoidal rule shows the best (essentially exact) results.

Highly irregular element shapes are often used in models of gas turbine components in order to minimize problem size and, hence, control analysis costs. Since the performance of most quadrilateral and hexahedron elements deteriorates with increasing departure from parallelepiped shapes, the shape sensitivity of these elements must be quantified in order to evaluate the acceptability of meshes proposed for practical applications. The effects of Loubignac iteration on the shape sensitivity of the quadrilateral plane stress element were examined using a cantilever beam modeled with skewed meshes and subjected to a pure moment load as shown on Figure 3.3-8. Results were obtained for three values of the mesh skewing parameter $\Theta(0°, 22.5°, 45°)$ defined on the figure.

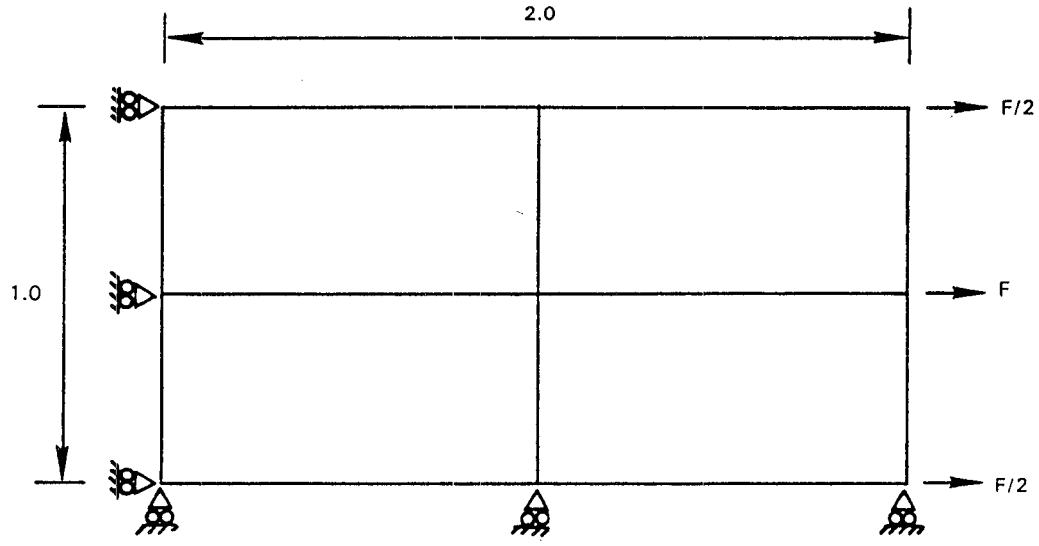

Figure 3.3-5 Finite Element Mesh and Loading Conditions Used for the Validation of Two-Dimensional and Axisymmetric Elements

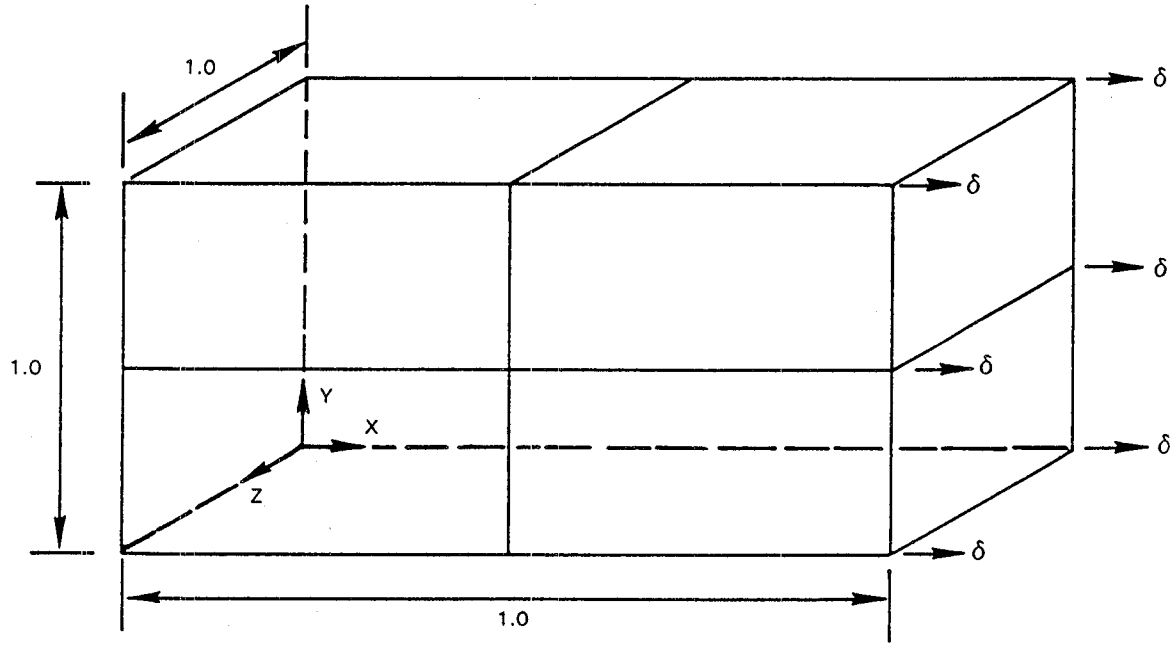

Figure 3.3-6 Finite Element Mesh and Prescribed Displacements Used for the Validation of Three-Dimensional Elements

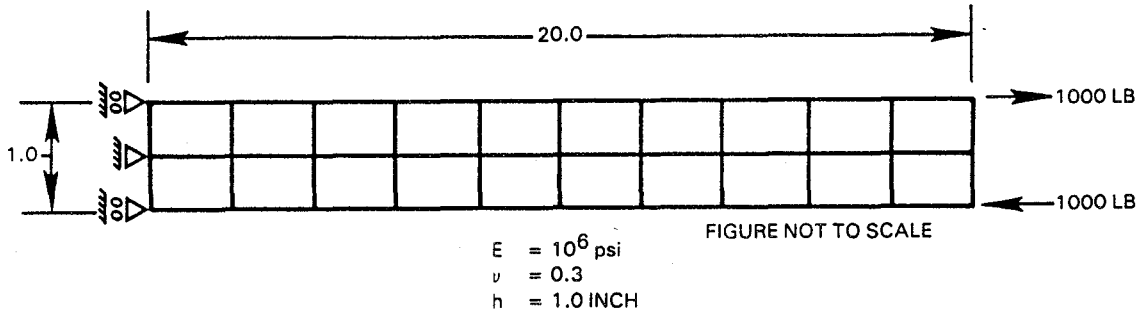

Figure 3.3-7 Cantilever Beam Problem (Plane Stress)

Table 3-I

Cantilever Beam: Loubignac Iteration Comparison

	Exact	Run A	Run B	Run C
Tip Displacement (in)	2.4	2.3988	3.4951	2.2699
Stress (psi)	6000	6005.1	4368.1	5710.7

	Stiffness Integration	Strain-Displacement Integration	Residual Force Integration
Run A	Selective	Trapezoidal	Full Gaussian
Run B	Full Gaussian	Full Gaussian	Full Gaussian
Run C*	Full Gaussian	Trapezoidal	Full Gaussian

*The results are identical to the full Gauss stiffness matrix integration in conjunction with the reduced integration strain recovery integration.

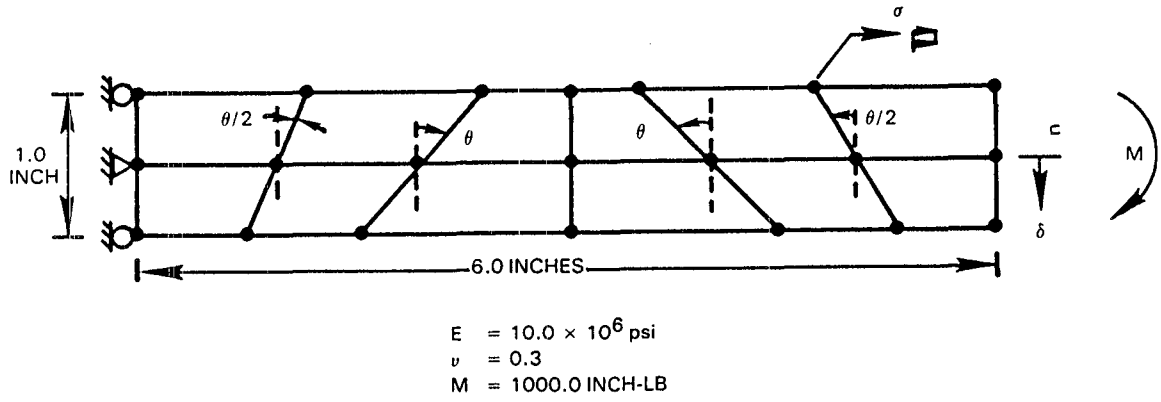

Figure 3.3-8 Cantilever Beam: Shape Sensitivity Study

The behavior of the tip displacement and a typical extreme fiber bending stress are plotted on Figure 3.3-9 as functions of the number of iterations. Values for the cases of full and selective stiffness integration are shown on the figure (strain-displacement integration was performed using the trapezoidal rule in both cases). Displacements and stresses approach exact values as the number of iterations is increased and the improvement in these results is dramatic in the first few iterations. Hence, Loubignac iteration is an effective technique for minimizing the deterioration in accuracy associated with the use of irregular meshes. The positive effects of using selectively reduced element stiffness integration are apparent; two to four fewer iterations are required to obtain results equivalent to full element stiffness integration values.

The MHOST four node shell element was used to analyze a simply supported square plate under the action of a uniform pressure. The finite element model including geometry, loads and boundary conditions is shown on Figure 3.3-10. An elastic analysis with five iterations was performed. The thickness/length ratio for the plate is very small (0.005) so comparisons of MHOST results with the classical thin plate solution in Reference 15 are appropriate. The exact and computed values for lateral displacement and M_y at the center of the plate as well as the values for M_y at the x = 1.0, y = 0.0 location are shown in Table 3-II. The MHOST results at the center of the plate are excellent (errors less than 2 percent) and an adequate representation of the zero moment at mid-edge is also obtained.

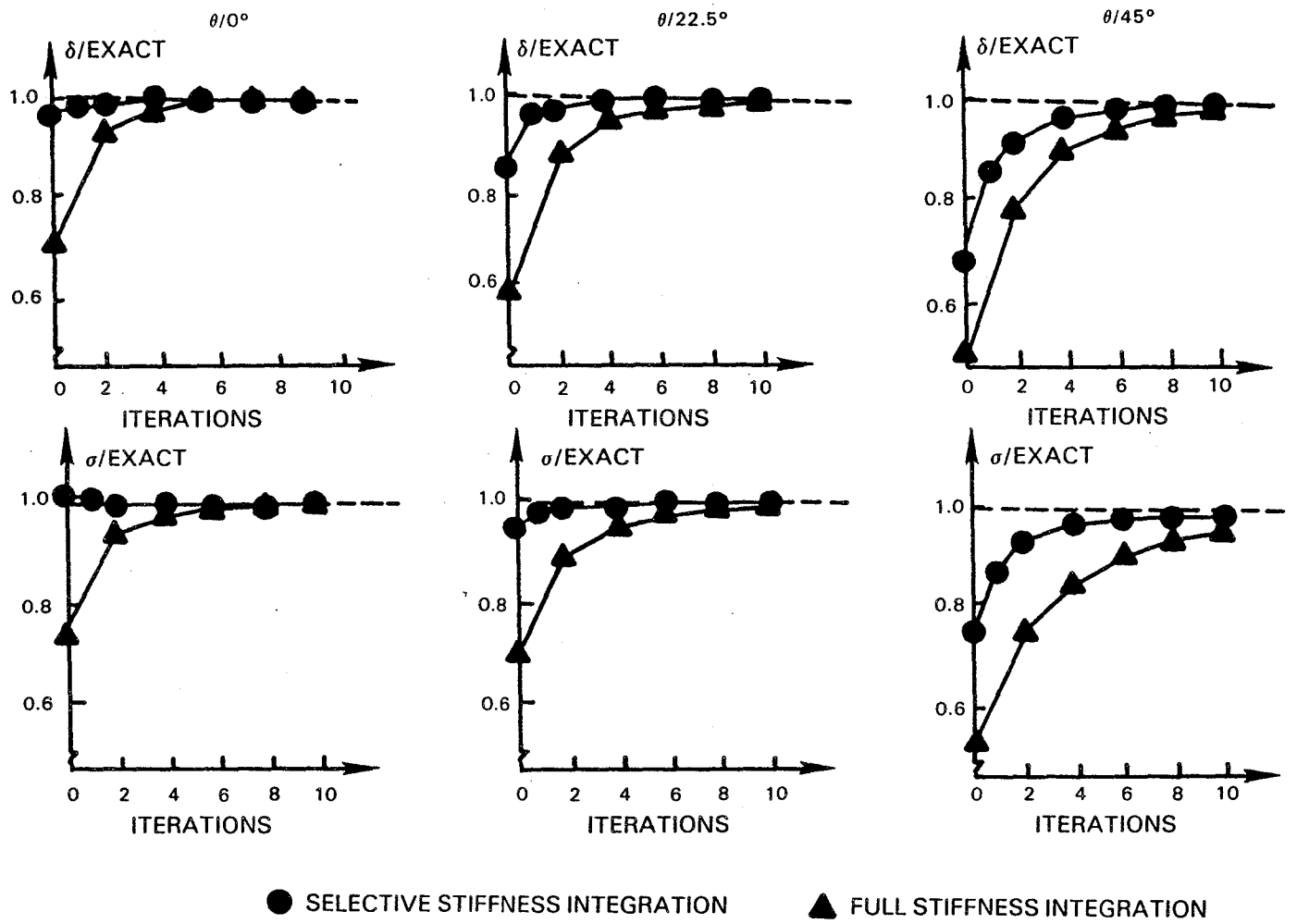

Figure 3.3-9 Convergence of Iterative Procedure for Elastic Cantilever Beam Modeled With Skewed Meshes

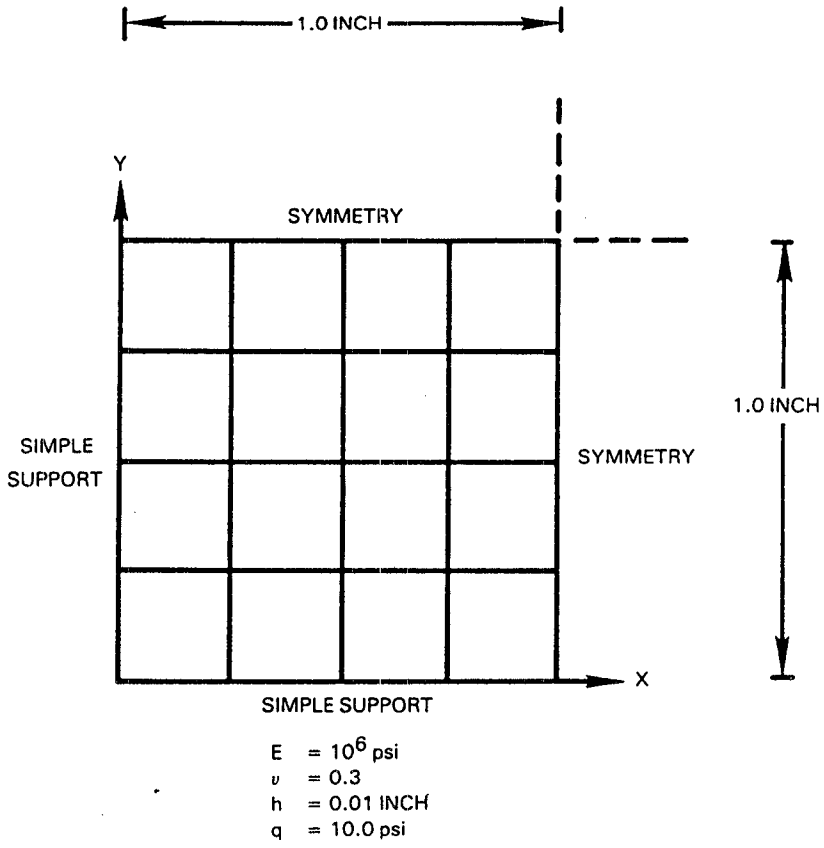

Figure 3.3-10 MHOST Model of Simply Supported Plate

Table 3-II

Simply Supported Plate: Uniform Pressure Load

Item	Exact	MHOST
Center Displacement (in)	-7.093	-7.231
M_y at x = 1.0, y = 0.0 (in-lb/in)	0.00	-0.139
M_y at Center (in-lb/in)	-1.916	-1.932

The MHOST program has been used to determine the elastic-plastic response of a thick cylinder under the action of a uniform internal pressure p_i, Figure 3.3-11. The cylinder has internal radius r=a=1.0 and external radius r=b=2.0, with an axial (i.e., z-direction) thickness of 1.0. The cylinder is modeled by twenty plane strain axisymmetric elements, each with radial thickness 0.05, Figure 3.3-11. Plastic behavior starts at the internal radius and propagates radially outward as p_i increases. The material is elastic-perfectly plastic with yield stress σ_Y=45000. Other material properties are Young's modulus E=30. x 10^6 and Poisson's ratio ν = 0.3.

Results for this case are shown in Figure 3.3-12, where the axial stress σ_Z (normalized) in the elastic region is plotted as a function of the internal pressure loading p_i (also normalized). Here, $k = \sigma_Y/\sqrt{3}$. For completely elastic behavior, the axial stress is constant in the radial direction and varies linearly with p_i along the straight line in Figure 3.3-12. For elastic-plastic behavior, the axial stress σ_Z is constant only for the elastic portion of the cylinder, but varies considerably in the surrounded elastic-plastic region. The value of σ_Z plotted here is that associated with the constant elastic region result. The MHOST program values clearly show very good agreement with the theoretical results obtained by Prager and Hodge (Reference 16).

In addition, a plate with a central hole was analyzed via MHOST and results were compared with MARC values for identical geometry and loading. The finite element mesh for this case is pictured in Figure 3.3-13, where both node and element numbering are indicated. The hole of radius 1.0-inch lies in a 6-inch by 6-inch square region, with symmetry conditions existing along both the horizontal and vertical axes, so that only one-quarter of the region need be considered. Appropriate displacement symmetry boundary conditions are imposed along the left side (i.e., at nodes 28, 30, 25, 20, 22, 24, 35) and along the bottom side (i.e., nodes 15, 18, 10, 3, 6, 9, 31) boundaries. Uniform pressure loading is applied along the top boundary, i.e., along side 33-34 for element 23 and along side 34-35 for element 24. The elastic material properties used are as follows: E = 30. x 10^6, ν = 0.3. The yield stress is 30. x 10^3, with a piecewise linear stress-plastic strain curve applying after yielding.

Comparisons of the results are presented in the next two figures. Figure 3.3-14 shows the normalized σ_Y stress at the most critical internal radius location (i.e., node point 15) as a function of normalized σ_{LOAD} external load. In addition, corresponding values are also presented for the integration point in element 8 lying closest to node point 15. The σ_{NOM} stress is 10 x 10^3 and represents the theoretical external pressure load at which plasticity is theoretically incipient at node point 15. The node point values associated with MARC were obtained from a simple isoparametric bilinear fit of the integration point values of element 8. The straight line unconnected to any data points represents the theoretical purely elastic response at the inner radius. As can be seen from this figure, the σ_Y values agree reasonably well between MHOST and MARC; in fact, overall agreement between the two sets of results improves as the external pressure loading increases. In a similar manner, Figure 3.3-15 shows the plastic strain component, $-\varepsilon_y^{PL}$, varying with normalized external load at the same node and integration point locations. Again, agreement between MHOST and MARC is quite good, even as the external pressure load increases.

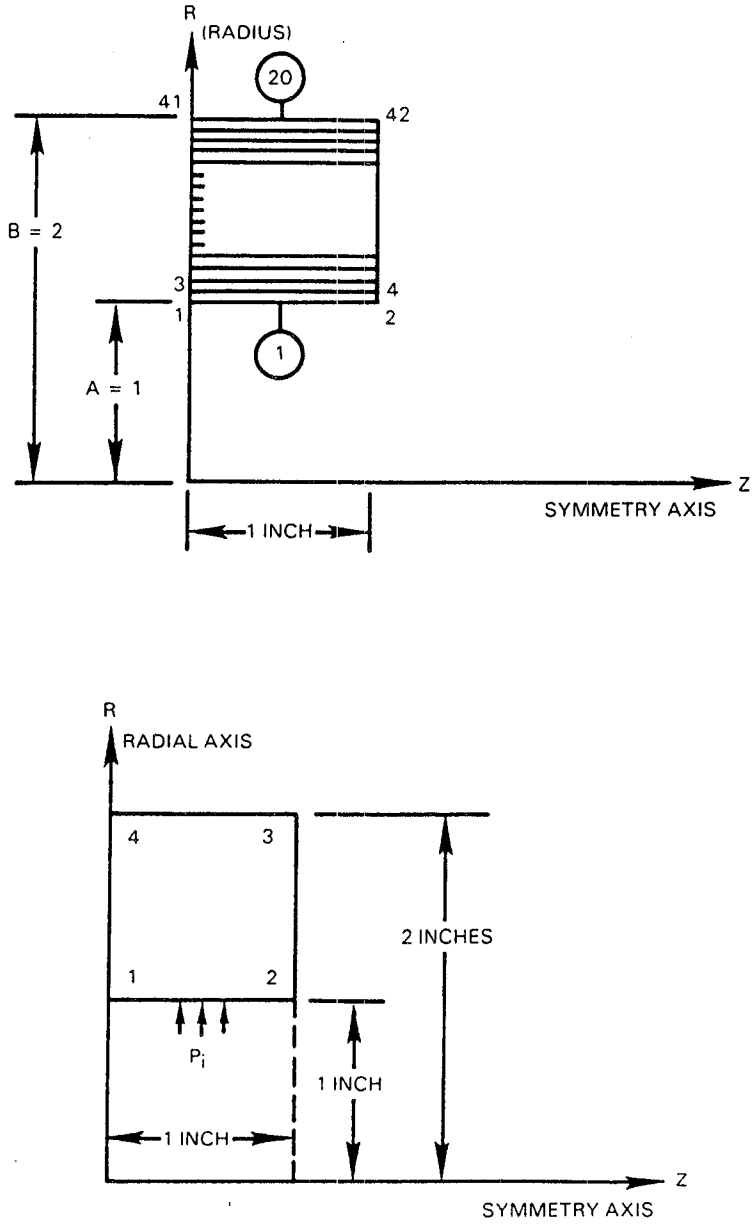

Figure 3.3-11 Thick Cylinder Geometry Mesh

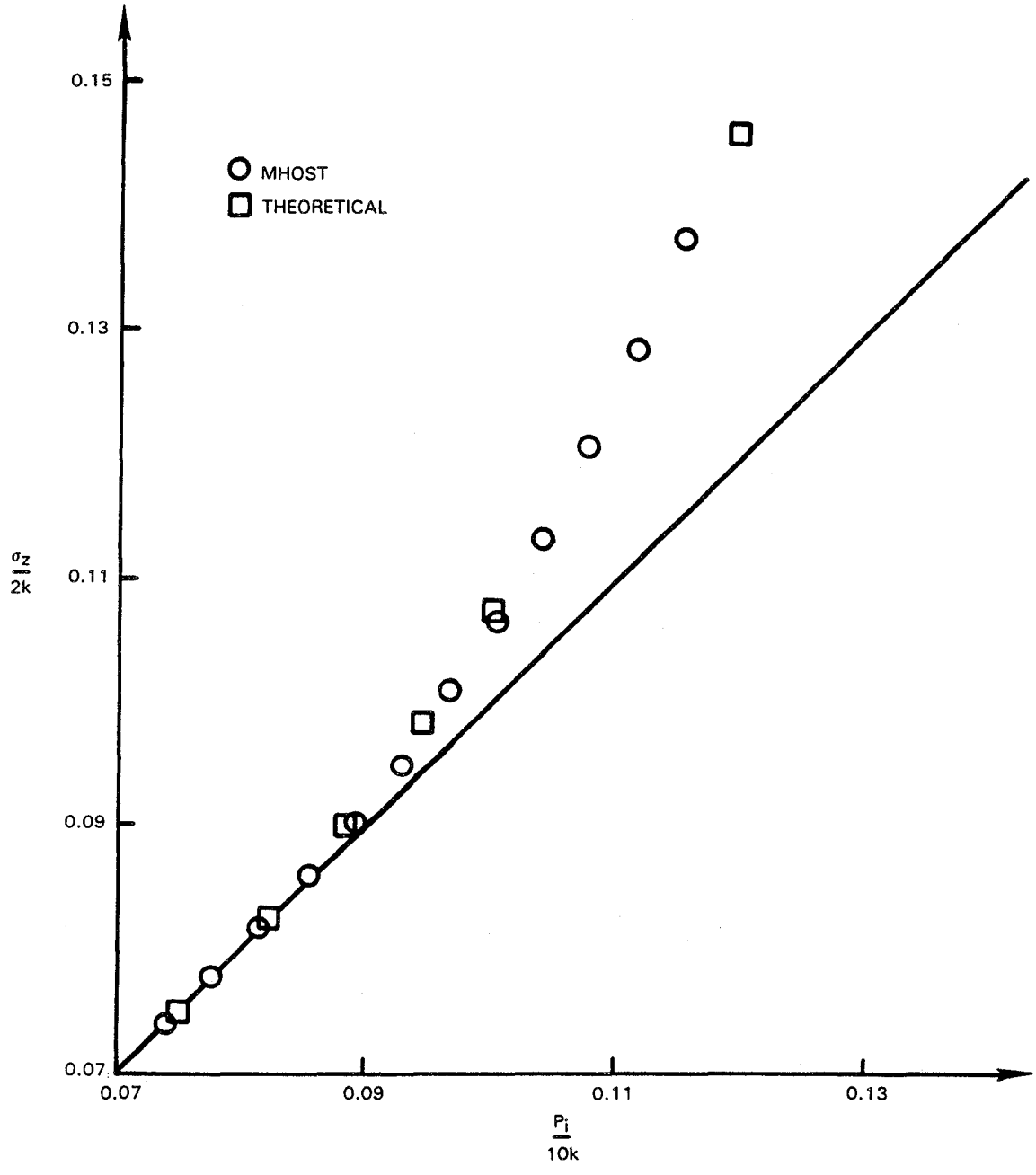

Figure 3.3-12 Axial Stress vs. Internal Pressure Load

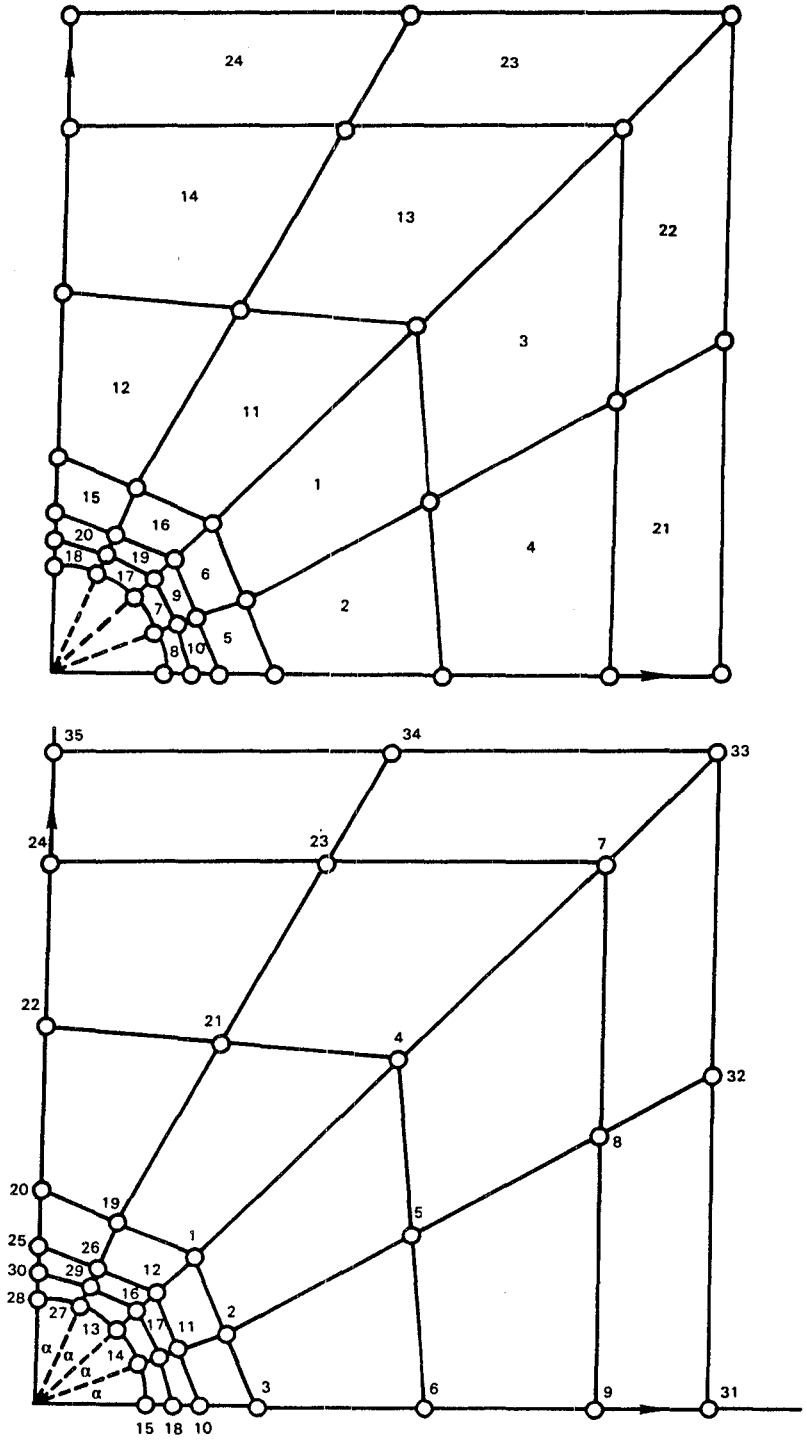

Figure 3.3-13 Finite Element Mesh Node and Element Numbering for Plate With a Hole

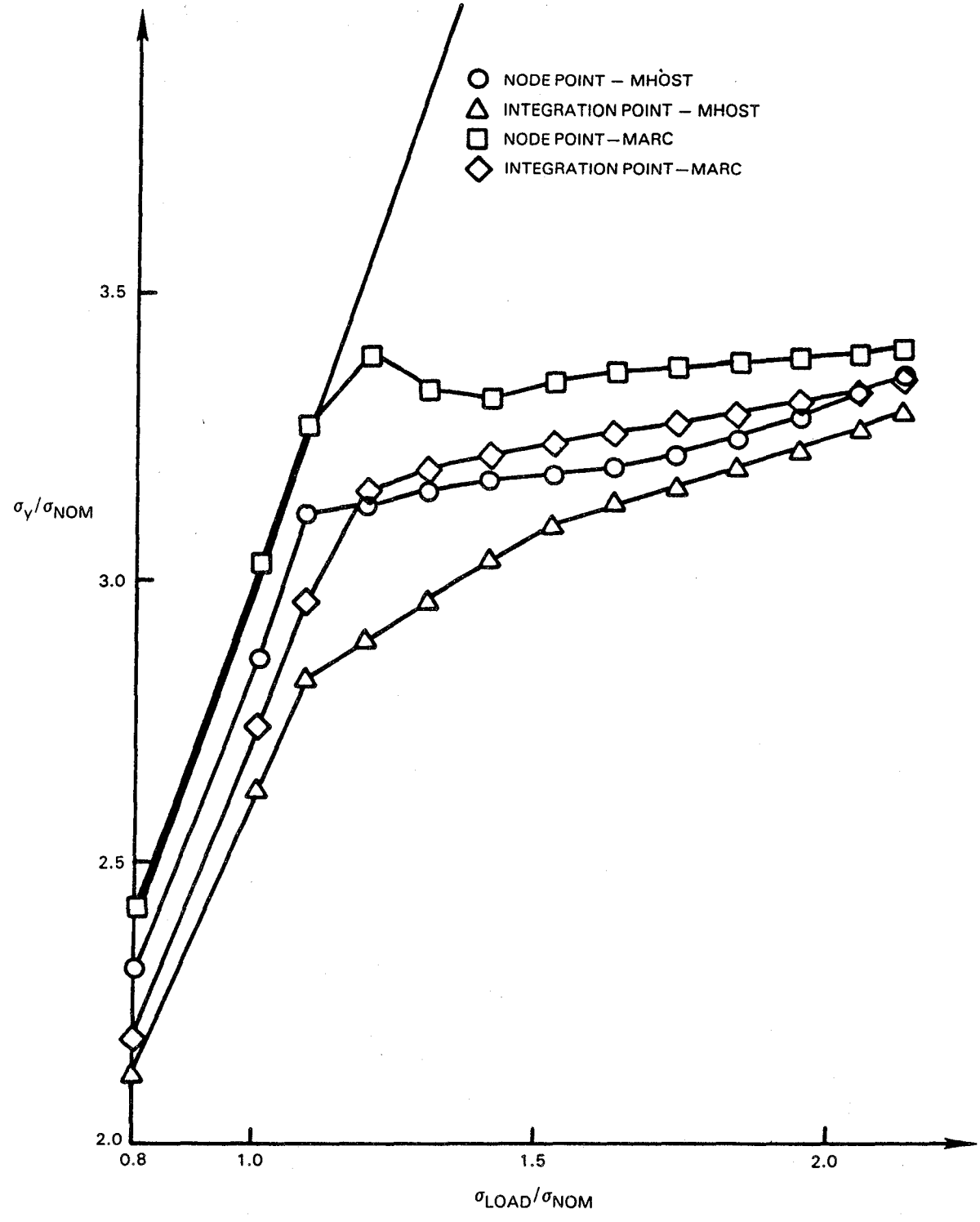

Figure 3.3-14 Normalized σ_y Stress vs. Normalized External Pressure Loading

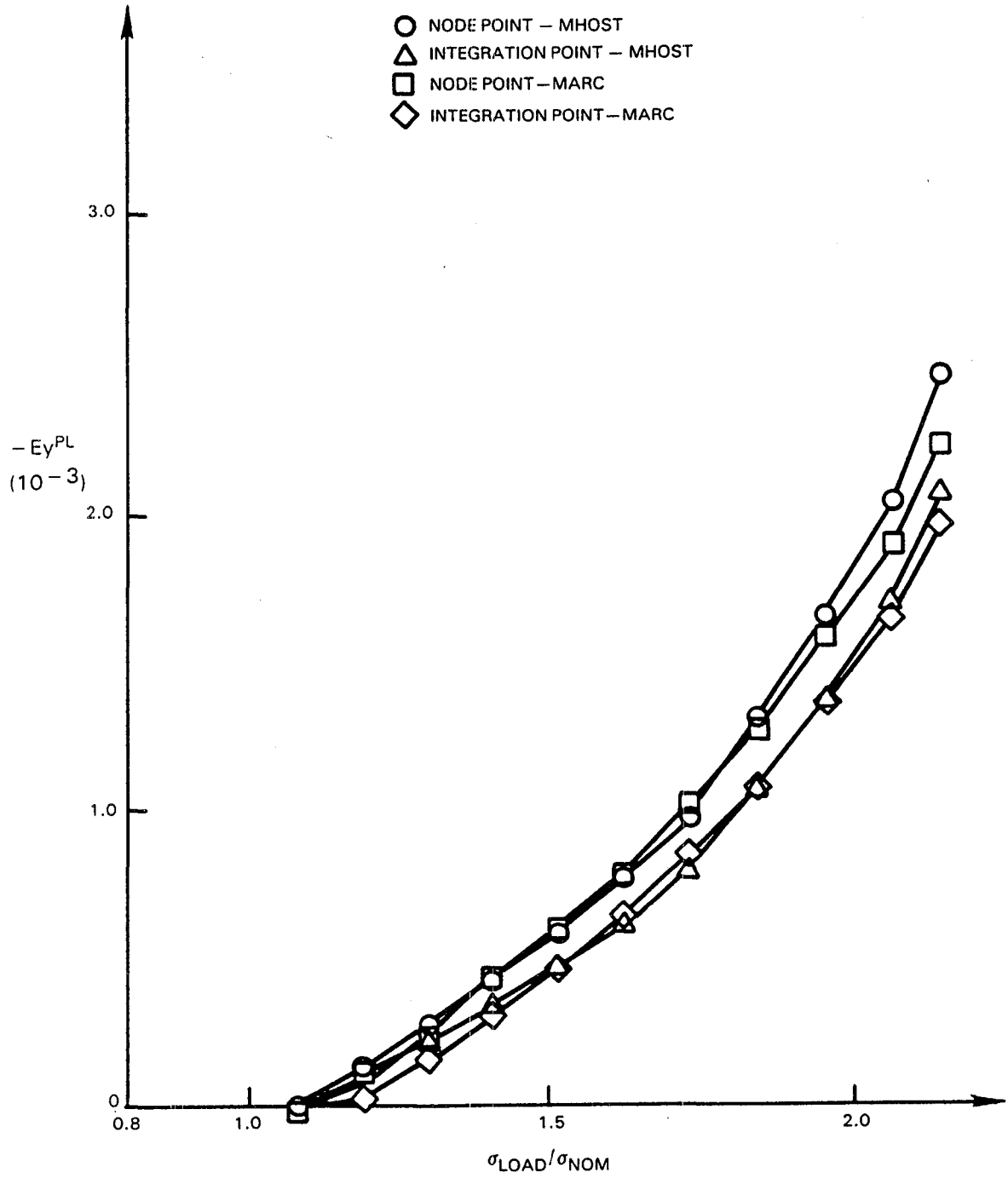

Figure 3.3-15 Plastic Strain ($-\varepsilon_y^{PL}$) vs. Normalized External Pressure Loading

Several structural problems for which test data is available have been selected for analysis using the MHOST program. The first of these configurations is the NASA benchmark notch fatigue test specimen (Reference 17).

Elastic analyses of the flat, double-notched uniaxially loaded specimen were performed using the fine and coarse meshes shown on Figure 3.3-16. In this case, the coarse mesh was defined with one-eighth the number of elements employed in the fine mesh. The elastic strain results from analyses using the two meshes are plotted together with test results in Figure 3.3-17. The microstrain at the surface of the notch for the fine mesh increased from 1705 to 1818 when three Loubignac iterations were employed. The latter value compares favorably with results reported in Reference 17 (1800-1900). Agreement between fine mesh values and test results at other locations is also very good. The microstrain at the surface of the notch produced by the coarse mesh with three iterations (1813) is nearly the same as the iterated fine mesh value and is superior to the standard (no iteration) fine mesh value. This result demonstrates the effectiveness of the iteration procedure in conjunction with coarse meshes and is especially significant because the coarse mesh with iterations used only one-tenth the computer time required to analyze the fine mesh without iterations.

Elastic-plastic analyses of the benchmark notch specimen are now in progress. The advanced constitutive model is being employed in these analyses.

Another MHOST verification problem is related to a combustor application. Conventional full hoop combustors are subjected to large thermal gradients in the radial direction, as well as local streaking in the hoop direction. It is the interaction of these effects that causes failure in the form of low cycle fatigue (LCF) cracking and local oxidation. With these failure mechanisms in mind, advanced combustors have eliminated the radial thermal fight by segmenting the hot wall. This leaves only the local streak temperature variation as a driving force for possible LCF failures. The development and optimization of segmented configurations requires an understanding of the local material behavior in streak locations.

Several years ago, the Material Development Group at Pratt & Whitney instituted an LCF test to rank current and proposed combustor materials. This test thermally cycled a flat disk specimen by periodically imposing a small local hot spot at the specimen's center. The nature of the test, with a small through thickness thermal gradient, causes a bulging or blistering of the hot spot toward the flame which is analogous to combustor streak behavior. Analytic evaluation (MARC) of both this test and combustor components under streak loading confirmed this analogy. In each case, the material in the hot spot showed identical deformations. Furthermore, each showed identical amounts of damage in the form of creep and plastic strains. It has been concluded that the hot spot blister test is a valid simulation of combustor streak behavior. Figure 3.3-18 shows a MHOST finite element solid model of a 1/4 segment of the flat circular specimen. The model consists of 320 solid elements and 615 nodes. Validation/verification analyses are currently in process.

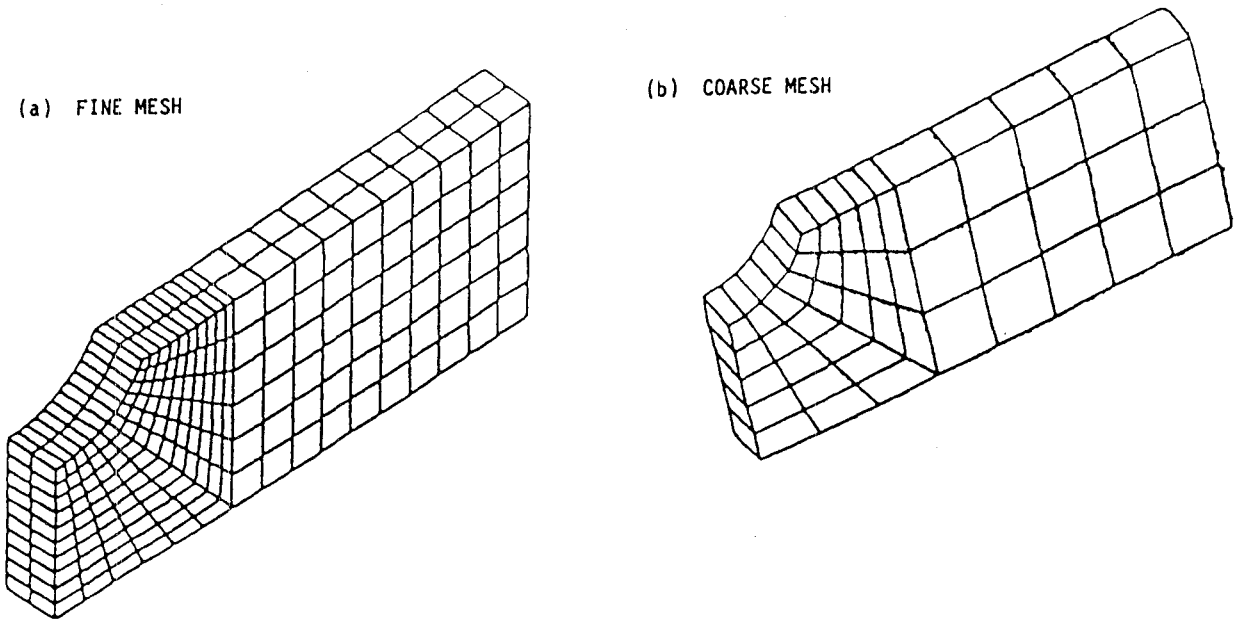

Figure 3.3-16 Three-Dimensional NASA Benchmark Notch Specimen

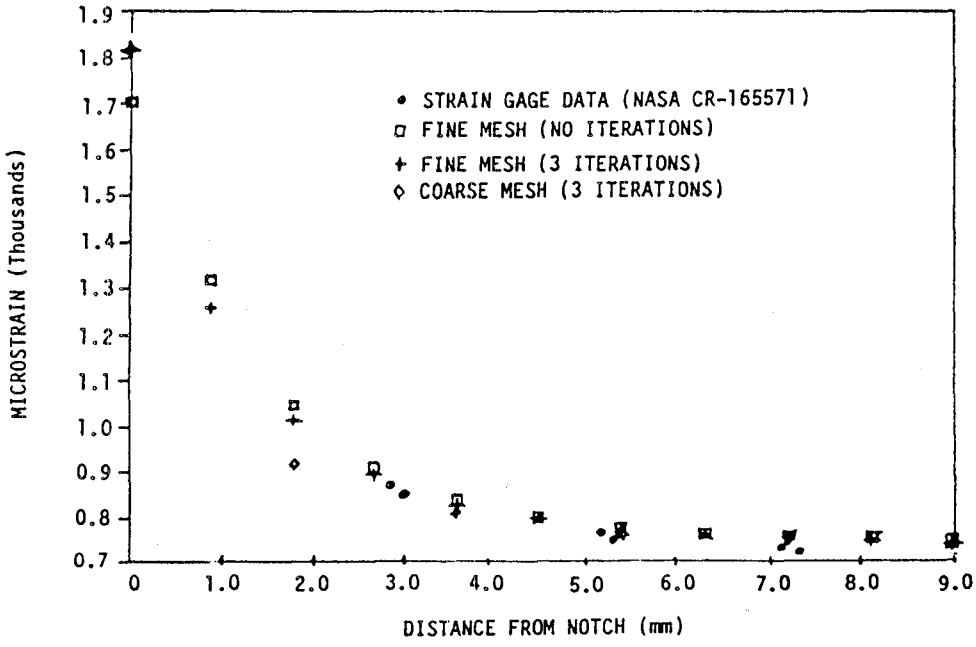

Figure 3.3-17 Comparison of Calculated and Measured Elastic Strains for the NASA Benchmark Notch Specimen

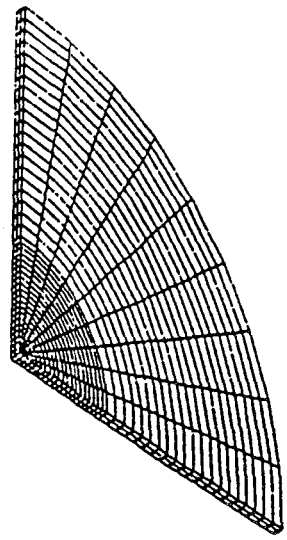

Figure 3.3-18 Simulated Combustor Liner Specimen (One-Quarter Section)

A sophisticated MHOST finite element model of a low pressure turbine vane has been developed to demonstrate the program's applicability to this type of problem. The initial model shown on Figure 3.3-19 contains 424 four-noded shell elements which is consistent with models that would normally be employed in NASTRAN or MARC analyses. However, the enhanced capability of the MHOST code (Loubignac type iteration) should allow the ultimate use of a much coarser model. The loading environment consists of both thermal and aerodynamic pressure loads. Since actual vanes of this type are clustered in groups of three, cyclicly symmetric boundary conditions are used at the inner vane platform to simulate the presence of the additional vanes. Elastic stress/strain distributions predicted by the MHOST analysis will be compared directly to strain gage measurements taken on actual vanes. In addition, a creep analysis will be performed to simulate the 69 hours of hot time accumulated at takeoff power during an in-house endurance test of this vane. The analytical creep predictions will be compared to deflection data from the actual test.

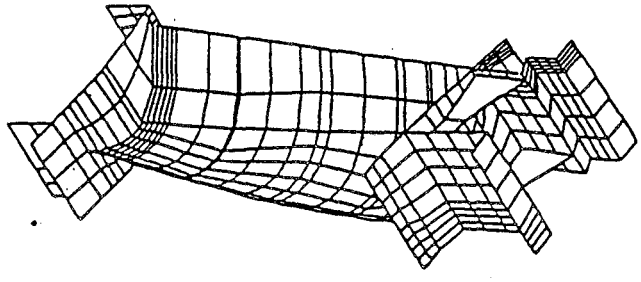

Figure 3.3-19 Turbine Vane Finite Element Model

3.3.5 Input Data Structure for the MHOST Program

The input data for the MHOST program is divided into three major blocks: PARAMETER DATA, MODEL DATA, and INCREMENTAL DATA. Data of different types within the data blocks are identified using keywords as discussed in Section 3.3.3.2. The keywords are listed and defined in this section to provide the potential user of MHOST with an overview of the structure and content of program input.

The PARAMETER DATA serve to specify dynamic array allocations and to control the MHOST module execution sequence. The keywords associated with this data block are listed below:

KEYWORD	SIGNAL TO MHOST PROGRAM
*ANISOTROPY	Anisotropic material data will be input
*BOUNDARY	Displacement boundary conditions will be input
*BUCKLE	Perform a buckling analysis
*CONSTITUTIVE	Use constitutive model (simplified, conventional, or advanced) indicated by parameter value
*CREEP	Perform a creep analysis
*DISTRIBUTEDLOAD	Distributed loads will be input
*DUPLICATENODE	Duplicate nodes will be input
*DYNAMIC	Perform a transient analysis
*ELEMENTS	Use element type indicated by parameter value
*FORCES	Nodal forces will be input
*LOUBIGNAC	Use Loubignac iteration options indicated by parameter values
*MODAL	Perform free vibrations analysis
*NODES	Upper bound to number of nodes indicated by parameter value
*OPTIMIZE	Optimize band-width of stiffness matrix
*PERIODICLOADING	Periodic loads will be input
*PRINTSETS	Upper bound to number of print sets given by parameter value

KEYWORD	SIGNAL TO MHOST PROGRAM
*REPORT	Print interval given by parameter value
*RESTART	A previous analysis is to be continued
*SCHEME	Time integration operator identified by parameter values
*STRESS	Upper bound to number of stress boundary conditions given by parameter value
*TANGENT	Perform modified Newton-Raphson iteration after cycle given by parameter value
*TEMPERATURE	Nodal temperatures will be used in calculations
*THERMAL	Temperature dependent material properties will be used
*TRANSFORMATIONS	Upper bound to number of coordinate transformations given by parameter value
*TYING	Number and form of tying equations given by parameter values
*UCOEFF	User subroutine UCOEFF will be provided
*UDERIV	User subroutine UDERIV will be provided
*UFORCE	User subroutine UFORCE will be provided
*UHOOK	User subroutine UHOOK will be provided
*UPRESS	User subroutine UPRESS will be provided
*UTEMP	User subroutine UTEMP will be provided
*UTHERM	User subroutine UTHERM will be provided

The finite element model is defined with the MODEL DATA. For example, the finite element topology and nodal coordinates, as well as boundary conditions and loads, are specified in this data block. The MODEL DATA keywords are identified below:

KEYWORD	DEFINITION
*BODYFORCE	Body force data
*BOUNDARY	Prescribed displacement data
*COORDINATES	Nodal coordinate data
*DISTRIBUTEDLOAD	Distributed load data
*DUPLICATENODE	Duplicate node data
*ELEMENTS	Element connectivity data
*END	End of MODEL DATA
*FORCES	Nodal force data
*INCREMENTS	Maximum number of increments
*ITERATIONS	Iteration control data
*POSTFILE	Postprocessing file control data
*PRINTOPTION	Output control data
*PROPERTIES	Element properties data
*SAVE	Restart control data
*STOP	End of analysis
*STRESS	Stress boundary condition data
*TEMPERATURES	Nodal temperature data
*TRANSFORMATIONS	Coordinate transformation data
*TYING	Tying equation data
*WORKHARD	Equivalent stress - equivalent plastic strain data

The INCREMENTAL DATA are used to specify the loading history, modifications to boundary conditions, and initial conditions for transient response calculations. Any number of INCREMENTAL DATA blocks may be included in an analysis. The following MODEL DATA keywords may be used in an INCREMENTAL DATA block:

*BODYFORCE
*BOUNDARY
*DISTRIBUTEDLOAD
*END
*FORCES
*ITERATIONS
*POSTFILE
*PRINTOPTION
*SAVE
*STOP
*STRESS
*TEMPERATURES
*TYING

The additional keywords available for use in the INCREMENTAL DATA blocks are defined below:

KEYWORD	DEFINITION
*ACCELERATION	Initial node accelerations data block (transient analysis)
*AUTOINCREMENT	Automatic load increment data
*DISPLACEMENT	Initial nodal displacements (transient analysis)
*ENDINITIALCONDITION	End of initial condition data (transient analysis)
*INITIALCONDITION	Start of initial condition data (transient analysis)
*PERIODICLOADING	Periodic loading data
*PROPORTIONAL	Proportional loading data
*TIME	Time increment data for creep and transient analysis
*VELOCITY	Initial nodal velocities (transient analysis)

3.3.6 List of Symbols

List of Symbols
Referenced Within Section 3.3

Symbol	Description	Page
a_j	Acceleration components	3.3-4
B	Matrix which relates nodal stresses to nodal forces	3.3-5
D	Stress-strain matrix	3.3-5
$D_{ijk\ell}$	Stress-strain tensor	3.3-4
E	Elastic modulus	3.3-20
f_j	Body force components	3.3-4
F	Nodal force vector	3.3-5
h	Thickness of model	3.3-20
K	Conventional displacement method stiffness matrix	3.3-6
M	Moment	3.3-21
n_j	Direction cosines of normal to surface	3.3-4
p_i	Internal pressure	3.3-24
Q	Shape function inner product matrix	3.3-5
R	Radius	3.3-24
t_i	Surface tractions	3.3-4
u	Displacement vector	3.3-4
x,y,z	Coordinates	3.3-9
δ	Displacement component at a point	3.3-19
ε	Nodal strain vector	3.3-5
ε_{ij}	Strain tensor	3.3-4
η,ξ	Isoparametric coordinates	3.3-9

List of Symbols
Referenced Within Section 3.3 (continued)

Symbol	Description	Page
θ	Mesh skew angle	3.3-18
ν	Poisson's ratio	3.3-20
ρ	Density of material	3.3-4
σ	Nodal stress vector	3.3-4
σ_y	Yield stress	3.3-4
σ_{ij}	Stress tensor	3.3-4
Ω	Denotes a deformable body	3.3-4
$\partial\Omega_1$	Denotes surface with prescribed displacements	3.3-4
$\partial\Omega_2$	Denotes surface with prescribed tractions	3.3-4

Superscript	Description	Page
n	Iteration number	3.3-6
PL	Denotes plastic quantity	3.3-29
T	Denotes transpose of a matrix	3.3-5
1	Denotes element coordinates	3.3-9
^	Denotes a prescribed quantity	3.3-4
*	Denotes a virtual quantity	3.3-4

3.3.7 References

1. Fyhrie, D. and T. J. R. Hughes, "A Literature Survey on Finite Element Methodology for Turbine Hot Section Components," MARC Analysis, 1983.

2. Zienkiewicz, O. C. and S. Nakazawa, "On Variational Formulation and its Modifications for Numerical Solution," to be published in Computer Structur., Report No. C/R/429/82, Institute for Numerical Method in Engineering, University College of Swansea, 1982.

3. Loubignac, G., G. Cantin and G. Touzot, "Continuous Stress Fields in Finite Element Analysis," AIAA J., 15, 1983, pp. 1645-1647.

4. Cantin, G., G. Loubignac and G. Touzot, "An Iterative Algorithm to Build Continuous Stress and Displacement Solutions," Int. J. Num. Meth. Eng., 12, 1978, pp. 1493-1506.

5. Cook, R. D., "Loubignac's Iterative Method in Finite Element Elastostatics," Int. J. Num. Meth. Eng., 18, 1982, pp. 67-75.

6. Hestens, M. R., "Optimization Theory: Finite Dimensional Case," Wiley-Interscience, 1976.

7. Temam, R., "The Navier-Stokes Equations," North-Holland, 1976.

8. Fortin, M. and R. Glowinski, "Methodes de Lagrangien Augmente," Dunod, 1982.

9. Nakazawa, S., J. P. Vilotte and O. C. Zienkiewicz, "Variational Formulations and Their Approximations for Incompressible Problems," 5th Int'l Conf. Finite Elements in Flow Problems, Austin, Texas, 1984.

10. Nakazawa, S., "Reducible and Irreducible Finite Element Forms for Linearly Constrained Problems in Mechanics," PVPT Conf., ASME, 1984.

11. Zienkiewicz, O. C., The Finite Element Method, 3ℓ, McGraw Hill, New York, 1977, Chapters 6, 7 and 8.

12. Nagtegaal, J. C. and J. G. Slater, "A Simple Nonconforming Thin-Shell Element Based on Discrete Kirchhoff Theory," AMD-48, ASME, 1981.

13. Cassenti, B. N., "Research and Development Program for the Development of Advanced Time-Temperature Dependent Constitutive Relationships," Final Report, NASA Contract NAS3-23273.

14. Walker, K. P., "Research and Development Program for Nonlinear Structural Modeling with Advanced Time-Temperature Dependent Constitutive Relationships," Final Report, NASA CR-165533, 1981.

15. Timoshenko, S., and S. Woinowsky-Krieger, Theory of Plates and Shells, Chapter 5, McGraw-Hill, 1959.

16. Prager, W. and P. G. Hodge, Jr., Theory of Perfectly Plastic Solids, Chapter 4, John Wiley and Sons, 1963.

17. Domas, P. A., et al, "Benchmark Notch Test for Life Prediction," NASA CR-165571, June, 1982.

3.4 BOUNDARY ELEMENT METHOD

3.4.1 Overview

It is the goal of the Advanced Formulation Development portion of this program to develop a computational technique for the solution of linear, nonlinear and transient problems in gas turbine engine hot section components. This technique is to be distinct from, and complementary to, the finite element method. The existence of such a computational tool will enhance the ability to calibrate the other codes developed under this contract. In addition, it is to be expected that different techniques will prove optimal, in terms of efficiency or accuracy, for particular types of component analyses. Since almost all general purpose structural analysis computer programs presently available employ the displacement finite element method, the new program developed as part of the Advanced Formulation Development effort can be expected to extend the ability to perform realistic analyses of hot section components.

Pratt & Whitney and its subcontractor, the State University of New York at Buffalo, have chosen, with the agreement of the NASA-Lewis program manager, to develop the boundary element method to fulfill the requirements of Task IC, and expect to continue its development throughout the remainder of the Inelastic Analysis Methods program. Very significant progress has been achieved during the first year of the contract effort. The analytical basis for a general purpose structural analysis program employing the boundary element method has been developed. Elastic, inelastic and both periodic and aperiodic dynamic effects have been considered. Numerical methods for the implementation of these analyses have been selected or, in many cases, newly developed. A computer program incorporating these techniques with sufficient generality to allow the analysis of hot section components has been designed, developed and tested.

The first year development effort is discussed in more detail below. Section 3.4.2 reviews the results of a boundary element method literature survey conducted early in the program. Section 3.4.3 summarizes the analytical and numerical basis of the boundary element method for elastic, inelastic and dynamic problems in three dimensions. The overall structure and development of the boundary element method computer program is described in Section 3.4.4. Validation/verification of the resulting code is reviewed in Section 3.4.5.

3.4.2 Literature Survey

3.4.2.1 Introduction

This section contains a brief review of available literature on the boundary element method, applied to problems of linear, nonlinear and dynamic stress analysis. Attention is primarily focused here on the boundary element literature relevant to the present contract.

The earliest work based on the direct boundary element formulation was presented by Jaswon and Ponter (Reference 1) for the Saint-Venant torsion problem of elastic bars, and by Rizzo (Reference 2) for elastostatic problems. In recent years, Cruse, Rizzo, Lachat, Watson, Banerjee, Butterfield, Brebbia, Wilson and others have all contributed to development of the direct boundary element method. At present, higher-order elements, as in the finite element method, have been employed and some standardization of solution procedures has been achieved for linear problems in solid mechanics. A number of textbooks (References 3 through 7) and advanced level monographs (References 8 through 10) provided not only a full description of these developments but also of developments in other fields. Reports by Cruse and Wilson (References 11, 13 and 14) on fracture mechanics, and Mendelson on plasticity (Reference 12) provide very readable accounts of developments in these areas.

In the discussion below, the development of the boundary element method is outlined for several different fields of continuum mechanics.

3.4.2.2 Linear Stress Analysis

The initial application of boundary element methods in elastostatics was to torsion problems of elastic bars. The pioneering work in this area was done by Jaswon and Ponter (Reference 1). Subsequent to their work, computational efficiency and accuracy have both been much improved.

Extension of both direct and indirect integral equation methods to the static stress analysis of three-dimensional bulky solids followed shortly after the successful application of these methods to two-dimensional problems. References 4 and 11 through 23 describe the work of a number of researchers. In particular, Lachat and Watson (Reference 16) and Watson (Reference 17) describe algorithms developed using the direct formulation applied to the stress analysis of thick cylindrical pressure vessels with holes. Banerjee (References 18 and 19) and Banerjee and Butterfield (Reference 20) describe numerical solutions to problems involving pile foundations as well as buried foundations of arbitrary shape.

Cruse, Wilson and others (References 23 through 30) show excellent applications of the boundary element method to two- and three-dimensional problems of linear elastic solids. Alarcon, Brebbia and Dominquez (Reference 31) showed an equivalence between the direct boundary element method and the method of residuals, and solved some simple problems. A more general discretization was presented by Lachat and Watson (References 16 and 17) by introducing higher-order boundary elements, whereby the efficiency and accuracy of numerical calculation were much improved. Anisotropic elastic problems were investigated by Wilson and Cruse (Reference 32). Elastic stress analysis of axisymmetric bodies was carried out by Cruse, Snow and Wilson (Reference 27), and also by Mayer, Drexler and Kuhn (Reference 33), under centrifugal body forces as well as steady state temperature gradients.

If the temperature distribution is known, the uncoupled thermoelastic problem can be treated as an elastostatic problem loaded by a body force corresponding to the temperature distribution. Rizzo and Shippy (Reference 34) used this approach to solve three-dimensional thermoelastic problems for nuclear pressure vessel components and for turbine airfoils. Chaudouet and Loubignac (Reference 35) performed a three-dimensional analysis of the thermoelastic behavior of rollers.

Hansen (Reference 36) and Stern (Reference 37) proposed direct boundary element methods for plate problems formulated in terms of variables having clear physical meanings. Independently, Bezine (References 38 through 40) also proposed similar methods of solution. Wu and Altiero (Reference 41) have recently proposed a new solution procedure for the elastic bending of anisotropic plates and solved some example problems.

Stress intensity factors in elastic fracture mechanics have been calculated with considerable success using boundary element methods (References 23 through 30, and 42 through 47). Results have been obtained for various cracking modes in both two and three dimensions. Recently, crack tip boundary elements have been introduced which take into account the singular behavior of displacements and tractions at crack tips (References 14 through 47). A stress intensity factor was also computed by Snyder and Cruse (Reference 28) for anisotropic elastic plates.

It is clear that solutions to problems in elastostatics based on boundary integral equations have reached such a state of development that it is now possible to undertake elastic and thermoelastic stress analyses of two- and three-dimensional bodies in a routine manner. For instance, Reference 4 discusses the analysis, using an isoparametric boundary element representation, of a disc rim-slot which retains blades in a gas turbine rotor assembly.

3.4.2.3 Dynamic Stress Analysis

As far as the solution of the general transient two-dimensional linear elastodynamic (or viscoelastodynamic) problem is concerned, there are currently three basic approaches available:

1. Determination of the steady-state solution by boundary element method approaches followed by reconstitution of the transient response using Fourier synthesis, as done by Banaugh and Goldsmith (Reference 48), Kobayashi and Niwa, et al (References 49 and 50).

2. Solution of the problem in the Laplace transform domain by boundary element method approaches followed by a numerical inverse transformation to obtain the response in the time domain, as done by Doyle (Reference 51), Cruse and Rizzo (Reference 52), Cruse (Reference 53), and Manolis and Beskos (Reference 54).

3. Time domain formulation and solution of the problem by boundary element method approaches in conjunction with step-by-step time integration schemes. This has been done by Cole, et al (Reference 56), for the anti-plane strain case and by Niwa, et al (Reference 55) for the two-dimensional case.

A comparison of the above three approaches on the basis of their accuracy and efficiency was done by Manolis (Reference 57). It should be noted that in the above papers some simple two-dimensional elastodynamic problems were solved such as: 1) the case of an unlined or lined circular cylindrical cavity under the passage of longitudinal or transverse waves (References 49 and 50), 2) the cases of square or horseshoe shaped cylindrical cavities under longitudinal waves, and 3) the case of wave propagation in half-planes, etc.

In conclusion, it may be mentioned that although the static version of the boundary element method is rather fully developed, this is not the case in elastodynamics. Although in the earlier attempts the dynamic verson of the boundary element method showed considerable promise, the development has not been carried out to the stage where the method could be considered as an established problem solving tool.

3.4.2.4 Nonlinear Stress Analysis

Since material nonlinearities may be introduced into an elastic analysis method as a set of initial strains, stresses or body forces in the same way that thermal loading or centrifugal effects can be introduced, it is hardly surprising that such a successful analysis tool for elastostatics can also be developed for plasticity and creep analysis. However, for the boundary element method, unlike the finite element method, it is possible to provide a brief and yet quite comprehensive review of work published to date on nonlinear problems.

The earliest boundary element formulation for elastoplasticity was due to Swedlow and Cruse (Reference 58). Rzasnicki, et al (Reference 59) proposed an initial strain approach for the three-dimensional analysis of work hardening materials, but only planar problems were solved.

Mendelson, Rzasnicki and Albers (Reference 59) also describe formulations for elastoplastic analysis of torsion and planar problems. Both a biharmonic formulation based on the Airy stress function and the displacement (direct) formulation of Swedlow and Cruse were utilized in numerical solutions (generally for V-notched beams). The elastoplastic solution was of an initial strain type using the method of successive elastic solutions. Boundary and interior discretizations were of the simplest type - straight boundary segments with the midpoint representing the boundary value on the element and an interior grid of essentially rectangles with strains evaluated at midpoints using the (analytically evaluated) integral equations for strain. Recently, Telles (References 60 and 61) has adopted a similar but slightly more sophisticated approach for a variety of problems involving strain hardening and perfect plasticity. In his solutions, a linear variation of boundary displacement and

tractions is adopted, with interior triangular cells in which strains are computed at the vertices. Thus, a linear variation of strain across an interior cell is computed, with an associated improvement in the accuracy of modeling the plastic strain distribution.

Mukherjee and coworkers (References 7, and 64 through 67) have utilized a rate formulation of the inelastic equations and a scheme for integrating forward in time. Material behavior was described either by the equations of power law creep or by a state variable consitutive model which draws no distinction between classical time-independent plasticity and time-dependent creep. The anelastic strain rates at $t=0$ are obtained from the consitutive equations, and a knowledge of these enables boundary displacement and traction rates and interior displacement and stress rates to be obtained. The values of these quantities at a new time $t+\Delta t$ are then obtained by integrating forward in time using an Euler-type strategy with automatic time step control. In Reference 67, a comparison between boundary element and finite element solution times is made, with the boundary element program giving a faster and more accurate solution.

Classical time-independent plasticity solutions have been successfully obtained by Banerjee, et al (References 68 through 72) using an incremental initial stress procedure similar to that used for finite element analysis. Plane, axisymmetric and three-dimensional problems have been solved. The initial stress algorithm is described in some detail in the boundary element method book by Banerjee and Butterfield (Reference 8). This work differs in one particular respect from that of other workers in that strains and stresses are calculated from displacements at the interior cell nodes rather than using the integral equation for strain. This introduces some loss in accuracy but is considerably more efficient computationally. In later work, boundary geometry and unknowns are represented by quadratic elements (References 71 and 75). Cathie and Banerjee (Reference 72) described a generalized formulation to take account of time-dependent inelastic deformation, conventional plasticity, viscoplasticity and creep with a single inelastic algorithm. Other conventional elastoplasticity solutions have also been reported (References 73 and 74).

The boundary element method has recently been extended to the analysis of large deformation problems (References 76 and 77). Although these publications essentially deal with very small test problems involving simple rectangular two-dimensional regions and do not develop the necessary surface or interior identities, feasibility has already been demonstrated.

3.4.3 Formulation Development

3.4.3.1 Summary

Various boundary element formulations for linear, nonlinear and dynamic problems are outlined in this section. The major governing equations are defined and the relevant integral formulations are presented.

An advanced formulation of the boundary element method has been developed for three-dimensional problems of elastoplasticity and viscoplasticity and for dynamics. In this formulation both the surface geometry and unknowns have been represented by isoparametric boundary elements. An efficient mapping scheme has been devised such that the kernel-shape function-jacobian products can be efficiently and accurately evaluated using the standard Gaussian integration formulae. For nonlinear analysis, a fast and accurate solution algorithm has been developed where the previous history of the development of initial stresses and plastic strains is utilized. The dynamic analysis has been developed in such a manner that the steady state (periodic) dynamic as well as transient forced vibration analysis can be carried out using the same implementation.

3.4.3.2 Linear and Nonlinear Stress Analysis

Basic Governing Equations

The governing differential equation for a solid in which the inelastic strain rate $\dot{\varepsilon}^{o}_{ij}$ (i.e., plastic + thermal), and body force excitation rate $\dot{f}$ is present, can be expressed as:

$$\mu \frac{\partial^2 \dot{u}_i}{\partial x_j^2} + (\lambda + \mu) \frac{\partial^2 \dot{u}_j}{\partial x_i \partial x_j} - \left(\lambda \delta_{ij} \frac{\partial \dot{\varepsilon}^{o}_{kk}}{\partial x_j} + 2\mu \frac{\partial \dot{\varepsilon}^{o}_{ij}}{\partial x_j} \right) + \dot{f} = 0 \qquad (3.4\text{-}1)$$

where $\dot{u}$ is the displacement rate

$\dot{\varepsilon}^{o}_{ij} = \dot{\varepsilon}^{p}_{ij} + \delta_{ij} E\alpha\dot{T}$

$\dot{\varepsilon}^{p}_{ij}$ = plastic strain

$\dot{T}$ = temperature

$\dot{f}$ = body force per unit volume and

dots on quantities represent their time derivatives.

The corresponding boundary integral formulation for the problem can be easily shown to be (see Banerjee and Butterfield, Reference 4):

$$[\delta_{ij} - C_{ij}]\,\dot{u}_i(\xi_o) = \int_S [\dot{t}_i(x)G_{ij}(x,\xi_o) - F_{ij}(x,\xi_o)\dot{u}_i(x)]\,dS$$

$$+ \int_V T_{ikj}(x,\xi_o)\,\dot{\varepsilon}^o_{ik}(x)\,dV \qquad (3.4\text{-}2)$$

$$+ \int_V G_{ij}(x,\xi_o)\,\dot{f}_i(x)\,dV$$

where ξ_o is a point on the boundary

$$G_{ij}(x,\xi) = \frac{1}{16\pi\mu(1-\nu)}\,\frac{1}{r}\left[(3-4\nu)\delta_{ij} + \frac{y_i y_j}{r^2}\right]$$

$$F_{ij}(x,\xi) = \frac{1}{8\pi(1-\nu)}\,\frac{1}{r^2}\left[(1-2\nu)\left(n_j\,\frac{yi}{r} - n_i\,\frac{yj}{r}\right) + \left\{\frac{3y_i y_j}{r^2} + (1-2\nu)\delta_{ij}\right\}\frac{y_k n_k}{r}\right]$$

$$y_i = (x_i - \xi_i)\ ,\ r^2 = y_i y_i$$

and

$$T_{ijk}(x,\xi) = -\frac{1}{8\pi(1-\nu)}\,\frac{1}{r^2}\left[\left(\delta_{ik}\,\frac{y_j}{r} + \delta_{jk}\,\frac{y_i}{r} - \delta_{ij}\,\frac{y_k}{r}\right)(1-2\nu) + \frac{3y_i y_j y_k}{r^3}\right]$$

For a linear stress analysis problem, the quantities within the volume integral sign, i.e., $\dot{\varepsilon}^o_{ik}$ $(= \delta_{ij}\,E\alpha\dot{T})$ and $\dot{f}$ are both known. If the body forces $\dot{f}_i$ are conservative, then the volume integral can, if desired, be converted into a surface integral. For nonlinear analysis, $\dot{\varepsilon}^p_{ik}$ is also present, and must be determined at every step of the solution process. The plastic strain is usually a function of the state variables such as the stresses σ_{ij}, plastic strains ε^p_{ij} and temperature T.

Although equation (3.4-2) is written for a surface point ξ_o, it can also be used for an interior point ξ if the term C_{ij} arising from the treatment of the improper integral involving the function F_{ij} is assumed to be zero, i.e.,

$$\dot{u}_j(\xi) = \int_S [\dot{t}_i(x) G_{ij}(x,\xi) - F_{ij}(x,\xi)\dot{u}_i(x)]\, dS$$

$$+ \int_V T_{ikj}(x,\xi)\dot{\varepsilon}^o_{ik}(x)dV + \int_V G_{ij}(x,\xi)\dot{f}_i(x)dV \qquad (3.4\text{-}3)$$

By calculating the strains corresponding to equation (3.4-3) and substituting in the stress-strain relations:

$$\dot{\sigma}_{jk} = \frac{2\mu\nu}{1-2\nu}\,\delta_{jk}\,\dot{\varepsilon}_{mm} + 2\mu\dot{\varepsilon}_{jk} - \left(\frac{2\mu\nu}{1-2\nu}\,\delta_{jk}\dot{\varepsilon}^o_{mm} + 2\mu\dot{\varepsilon}^o_{jk}\right) \qquad (3.4\text{-}4)$$

we can obtain the following expressions for the stresses at an interior point:

$$\dot{\sigma}_{jk}(\xi) = \int_S [\dot{t}_i(x) D_{ijk}(x,\xi) - S_{ijk}(x,\xi)\dot{u}_i(x)]\, dS$$

$$+ \int_V T_{ikj}(x,\xi)\dot{f}_i(x)dV + \int_{V-D} M_{ipjk}(x,\xi)\dot{\varepsilon}^o_{ip}(x)dV \qquad (3.4\text{-}5)$$

$$- \frac{2\mu}{15(1-\nu)}\left[(1+5\nu)\,\delta_{jk}\,\dot{\varepsilon}^o_{mm} + (7+5\nu)\,\dot{\varepsilon}^o_{jk}\right]$$

where D is a small sphere around the source point ξ and the free term on the right hand side is the result of an exact integration over the volume D.

$$M_{ipjk} = \frac{\mu}{4\pi(1-\nu)r^3}\Big[3(1-2\nu)\left(\delta_{jk}r_{,i}r_{,p} + \delta_{ip}r_{,j}r_{,k}\right) - 15r_{,i}r_{,p}r_{,k}r_{,j}$$

$$+ 3\nu\left(\delta_{ij}r_{,k}r_{,p} + \delta_{jp}r_{,i}r_{,k} + \delta_{ik}r_{,p}r_{,j} + \delta_{pk}r_{,i}r_{,j}\right)$$

$$+ (1-2\nu)\left(\delta_{ij}\delta_{kp} + \delta_{ik}\delta_{jp}\right) + (4\nu-1)\delta_{jk}\delta_{ip}\Big]$$

If the strains are purely deviatoric, then $\dot{\varepsilon}^o_{mm} = 0$ and equation (3.4-5) can be simplified, resulting in a small saving in computation.

Equation (3.4-5) is not only invalid on the surface but also is difficult to evaluate numerically at points close to it. For points on the surface, the stresses can be calculated by constructing a local Cartesian coordinate system with the axes 1 and 2 directed along the tangential directions and the axis 3 in the direction of the outward normal. The stresses referred to these local axes (indicated by overbars) are then given by:

$$\bar{\sigma}_{11} = \frac{\nu}{1-\nu}\bar{t}_3 + \frac{E\nu}{1-\nu^2}(\bar{\varepsilon}_{11} + \bar{\varepsilon}_{22}) + \frac{E}{1+\nu}\bar{\varepsilon}_{11}$$

$$\bar{\sigma}_{12} = \bar{\sigma}_{21} = \frac{E}{2(1+\nu)}\bar{\varepsilon}_{12}$$

$$\bar{\sigma}_{22} = \frac{\nu}{1-\nu}\bar{t}_3 + \frac{E\nu}{1-\nu^2}(\bar{\varepsilon}_{11} + \bar{\varepsilon}_{22}) + \frac{E}{1+\nu}\bar{\varepsilon}_{22} \qquad (3.4\text{-}6)$$

$$\bar{\sigma}_{33} = \bar{t}_3$$

$$\bar{\sigma}_{32} = \bar{\sigma}_{23} = \bar{t}_2$$

$$\bar{\sigma}_{31} = \bar{\sigma}_{13} = \bar{t}_1$$

where E is the Young's modulus and $\bar{\varepsilon}_{ij}$ defines the components of the elastic strains (i.e., total-inelastic) in the local axes system. This method of evaluating the stresses on the surface was originally devised by Cruse (Reference 25).

The development presented here has assumed that all of the integral equations discussed are written over the entire structure to be analyzed. This restriction is not essential. In fact, in practical analysis it is almost always desirable to subdivide a complex structure into two or more subregions (referred to in this program as Generic Modeling Regions, or GMRs). The integral equations are written separately on each GMR, and the overall structure is then assembled by enforcing appropriate compatibility and equilibrium conditions on the boundaries between GMRs. This tactic can improve the numerical stability of the resulting equation system and also results in very considerable reductions in computer time for both elastic and inelastic problems.

Solution Algorithm

If we discretize the boundary using n isoparametric quadratic surface elements and the likely elastoplastic region using m isoparametric quadratic hexahedral cells, then the complete state of the structure can be defined in terms of the nodal values of displacement and traction. The surface and volume integrals of equation (3.4-2) can then be expressed as a sum of integrals over surface elements and volume cells. Each of these integrals can be evaluated numerically. We can thus derive an algebraic representation of equation (3.4-2) as:

$$\underset{\sim}{A}\,\dot{\underset{\sim}{x}} = \underset{\sim}{B}\,\dot{\underset{\sim}{y}} + \dot{\underset{\sim}{C}} \tag{3.4-7}$$

where $\dot{\underset{\sim}{x}}$ and $\dot{\underset{\sim}{y}}$ are unknown and known boundary tractions and displacements, respectively, and:

$$\dot{\underset{\sim}{C}} = \underset{\sim}{G}\,\dot{\underset{\sim}{f}} + \underset{\sim}{T}\,\dot{\underset{\sim}{\varepsilon}}^{o}$$

couples the effect of the volume cells to the boundary solution.

It should be emphasized that for a linear analysis, $\dot{\underset{\sim}{C}}$ is completely prescribed and equation (3.4-7) can be solved directly.

Similarly, the interior equations for displacements and stresses may be cast in the form:

$$\dot{\underset{\sim}{u}}^{i} = \underset{\sim}{A}^{i}\,\dot{\underset{\sim}{x}} + \underset{\sim}{B}^{i}\,\dot{\underset{\sim}{y}} + \dot{\underset{\sim}{C}}^{i} \tag{3.4-8}$$

$$\dot{\underset{\sim}{\sigma}}^{i} = \underset{\sim}{D}^{i}\,\dot{\underset{\sim}{x}} + \underset{\sim}{S}^{i}\,\dot{\underset{\sim}{y}} + \dot{\underset{\sim}{M}}^{i} \tag{3.4-9}$$

where the superscript i is used to designate interior field point.

The solutions for a nonlinear analysis can be developed as an accelerated elastoplastic algorithm or a viscoplastic algorithm depending on the nature of the constitutive model involved. For conventional elastoplastic constitutive relations, an initial stress (defined as $\dot{\sigma}^{o}_{ij} = D^{e}_{ijkl}\dot{\varepsilon}^{o}_{kl}$ where $\underset{\sim}{D}^{e}$ is the elastic constitutive matrix) algorithm would be as follows:

1. Obtain an elastic solution and scale to first yield. Hence, determine $\dot{\underset{\sim}{x}}$, $\dot{\underset{\sim}{u}}^{i}$, $\dot{\underset{\sim}{\sigma}}^{i}$

2. Evaluate $\dot{\underset{\sim}{x}}$, $\dot{\underset{\sim}{u}}^{i}$, $\dot{\underset{\sim}{\sigma}}^{i}$ for a small load increment with an initially estimated value of $\dot{\underset{\sim}{\sigma}}^{o}$ obtained from the extrapolation of the previously generated history of initial stresses (if no prior plastic history exists, assume $\dot{\underset{\sim}{\sigma}}^{o} = 0$)

3. Accumulate all incremental quantities of stress, displacement

4. Calculate with the new stress history the current constitutive matrix and determine the initial stresses

5. Calculate new $\dot{\underset{\sim}{x}}$, $\dot{\underset{\sim}{u}}^i$, $\dot{\underset{\sim}{\sigma}}^i$ with $\dot{\underset{\sim}{y}} = 0$ (i.e., no boundary loading change)

6. Return to step 3 if $\dot{\underset{\sim}{x}}$ is greater than an acceptable norm

7. Return to step 2, the next load increment.

During the early part of the loading, the algorithm will require a few iterations for each load increment (since no history of generation of initial stresses exists). From the second or third increment onwards the solution converges after one or two iterations.

If a viscoplastic model, including thermally induced plastic creep strain behavior, is used the solution is best obtained using a current rather than an incremental form of equations (3.4-7) through (3.4-9). These equations, if written in non-rate form, are valid expressions of the elastic problem given the boundary conditions and an initial strain field. Providing the developing initial strain field in the plasticity and creep problem is integrated in a sufficiently accurate manner, the solution to the nonlinear problem at any time may be obtained using current values. Advantages are that the algorithm is simplified, errors introduced through the accumulation of incremental quantities are minimized and the equilibrium equations are satisfied at each stage of the calculation.

The essentials of the viscoplastic solution algorithm are as follows:

1. Evaluate $\underset{\sim}{x} = \underset{\sim}{A}^{-1} \underset{\sim}{B}\, \underset{\sim}{y} + \underset{\sim}{C}$

   $$\underset{\sim}{\sigma}^i = \underset{\sim}{D}^i \underset{\sim}{x} + \underset{\sim}{S}^i \underset{\sim}{y} + \underset{\sim}{M}^i$$

   for the prescribed boundary loading with the vector $\underset{\sim}{y}$ and initial viscoplastic strain $\underset{\sim}{\varepsilon}^{vp} = 0$

2. Scale elastic solution to yield point for plasticity problem and apply a small load increment $\lambda \underset{\sim}{y}$ where λ is fraction of the total load to be applied in an incremental analysis

3. Evaluate $\dot{\underset{\sim}{\varepsilon}}^{vp}$ using the constitutive equation at the time t

4. Select Δt and compute $\underset{\sim}{\varepsilon}^{vp}$ from a suitable integration of $\dot{\underset{\sim}{\varepsilon}}^{vp}$ at time $t + \Delta t$

5. Resolve equations in step 1

6. Return to step 3 until $\dot{\underset{\sim}{\varepsilon}}^{vp}$ is negligible or $t > t_{max}$, the time up to which the solution is required.

5. For plasticity applications return to step 2 for the next load increment.

The algorithm outlined above would be successful if the chosen $\Delta t < \Delta t_{critical}$ where $\Delta t_{critical}$ is obtained from the careful study of the governing stiff differential equation:

$$\dot{\varepsilon}^{vp} = \frac{\partial \varepsilon^{vp}}{\partial t} = F(\sigma, \varepsilon^{p}) \qquad (3.4\text{-}10)$$

A good working rule often adopted in practice is that the creep strain rate must not exceed a certain fraction of the total elastic strains at a critical section of the structure, i.e.,

$$\dot{\underset{\sim}{\varepsilon}}^{vp} < \alpha \, \underset{\sim}{C}^{e} \, \underset{\sim}{\sigma}$$

where $\underset{\sim}{C}^{e}$ is the elastic compliance matrix

$\underset{\sim}{\sigma}$ is the stress state

α is a value between 0.1 to 0.5.

3.4.3.3 Dynamic Stress Analysis

Governing Equations

The governing differential equations for the response of a three-dimensional solid in the absence of body forces can be expressed as:

$$(c_1^2 - c_2^2)\, u_{i,ij} + c_2^2\, u_{j,ii} = \ddot{u}_j \qquad (3.4\text{-}12)$$

where $u_i(x_j,t)$ are the components of the displacement vector, indices i and j correspond to Cartesian coordinates x_j, commas indicate differentiation with respect to these coordinates, dots indicate differentiation with respect to time t and summation over repeated indices is understood; c_1 and c_2 are the propagation velocities of dilatational (P-wave) and distorsional (S-wave) waves, respectively, given in terms of the Lamé constants λ and μ and the mass density ρ of the material by

$$c_1^2 = (\lambda + 2\mu) / \rho \quad c_2^2 = \mu/\rho \qquad (3.4\text{-}13)$$

The constitutive equations are of the form

$$\sigma_{ij} = \rho \left[\left(c_1^2 - 2c_2^2 \right) u_{r,r}\delta_{ij} + c_2^2 \left(u_{i,j} + u_{j,i} \right) \right] \qquad (3.4\text{-}14)$$

where $\sigma_{ij}(x_j,t)$ are components of the stress tensor and δ_{ij} is the Kronecker delta.

The Laplace transform with respect to time of a function $f(x_j,t)$ is defined as:

$$L(f) = \bar{f}(x_j,s) = \int_0^\infty f(x_j,t)e^{-st}dt \qquad (3.4\text{-}15)$$

where s is the transform parameter.

Application of the Laplace transform to equations (3.4-12), (3.4-13) and (3.4-14) under zero initial conditions yields

$$\left(c_1^2 - c_2^2 \right) \bar{u}_{i,ij} + c_2^2\, \bar{u}_{j,ii} - s^2\, \bar{u}_j = 0 \qquad (3.4\text{-}16)$$

$$\bar{\sigma}_{ij} = \rho \left[\left(c_1^2 - 2c_2^2 \right) \bar{u}_{r,r}\delta_{ij} + c_2^2 \left(\bar{u}_{i,j} + \bar{u}_{j,i} \right) \right] \qquad (3.4\text{-}17)$$

$$\bar{\sigma}_{ij} n_j = \bar{t}_i \qquad (3.4\text{-}18)$$

If a homogeneous, isotropic and linear elastic body is under the influence of harmonic forcing functions of time prescribed through boundary conditions of the form

$$t_j(x_k,t) = \bar{t}_j(x_k,\omega)\, e^{i\omega t} \tag{3.4-19}$$

where ω is the circular frequency and t_j the amplitude of the forces, then the displacement vector will be of the form

$$u_j(x_k,t) = \bar{u}_j(x_k,\omega)\, e^{i\omega t} \tag{3.4-20}$$

where u_j is its amplitude. Substitution of equation (3.4-20) in (3.4-12) and (3.4-14) and cancellation of the common factor $e^{i\omega t}$ yields

$$\left(c_1^2 - c_2^2\right) \bar{u}_{i,ij} + c_2^2\, \bar{u}_{j,ii} + \omega^2\, \bar{u}_j = 0 \tag{3.4-21}$$

$$\bar{\sigma}_{ij} = \left[\left(c_1^2 - 2c_2^2\right) \bar{u}_{r,r}\delta_{ij} + c_2^2 \left(\bar{u}_{i,j} + \bar{u}_{j,i}\right)\right] \tag{3.4-22}$$

$$\bar{\sigma}_{ij} n_j = \bar{t}_i \tag{3.4-23}$$

where $\bar{\sigma}_{ij}$ denotes the stress amplitude. A comparison of equations (3.4-16) - (3.4-18) with equations (3.4-21) - (3.4-23) indicates that any method for solving the Laplace transformed general transient problem can also be used to solve the steady-state problem as a special case, if the complex Laplace transform parameter s is replaced by $-i\omega$ in the formulation. The solution $\bar{u}_i$ and $\bar{\sigma}_{ij}$ will be, of course, in terms of the frequency ω so that no inversion is required. The approach implies that the formulation corresponding to algorithms of Laplace inversion working with complex data will be used.

The corresponding boundary element formulation in the transformed space (s,x_i) follows from the above differential equation. Thus for a boundary point ξ_0, we have

$$\left[\delta_{ij} - \bar{C}_{ij}(\xi_0)\right]\bar{u}_i(\xi_0,s) = \int_S \left[\bar{G}_{ij}(x,\xi_0,s)\bar{t}_i(x,s) - \bar{F}_{ij}(x,\xi_0,s)\bar{u}_i(x,s)\right] dS \tag{3.4-24}$$

where s is either the transform parameter or $-i\omega$, and ω is the circular frequency

$$\bar{G}_{ij}(x,\xi_0,s) = \frac{1}{4\pi\mu}\left[\psi\delta_{ij} - \phi r_{,i}r_{,j}\right] \quad \bar{F}_{ij}(x,\xi_0,s) = \frac{1}{4\pi}\left[\alpha\left(\delta_{ij}\frac{\partial r}{\partial n} + r_{,i}n_j\right)\right.$$

$$\left. + \beta\left(n_i r_{,j} - 2r_{,i}r_{,j}\frac{\partial r}{\partial n}\right) + \gamma\, r_{,i}r_{,j}\frac{\partial r}{\partial n} + \delta r_{,j}r_{,i}\right]$$

$$\psi = \left(\frac{c_2^2}{s^2r^2} + \frac{c_2}{sr} + 1\right)\frac{e^{-sr/c_2}}{r} - \frac{c_2^2}{c_1^2}\left(\frac{c_1^2}{s^2r^2} + \frac{c_1}{sr}\right)\frac{e^{-sr/c_1}}{r}$$

$$\phi = \left(\frac{3c_2^2}{s^2r^2} + \frac{3c_2}{sr} + 1\right)\frac{e^{-sr/c_2}}{r} - \frac{c_2^2}{c_1^2}\left(\frac{3c_1^2}{s^2r^2} + \frac{3c_1}{sr} + 1\right)e^{-sr/c_1}$$

$$\alpha = \frac{\partial\psi}{\partial r} - \frac{\phi}{r}, \quad \beta = -\frac{2\phi}{r}, \quad \gamma = -2\frac{\partial\phi}{\partial r} \quad \text{and} \quad \delta = \left(\frac{c_1^2}{\partial c_2^2} - 2\right)\left(\frac{\partial\psi}{\partial c_2^2} - \frac{\partial\phi}{\partial r} - \frac{2\phi}{r}\right)$$

Note that although the functions $\bar{G}$ and $\bar{F}$ become identical to their static counterparts G and F as ω tends to zero it is important to evaluate this limit carefully because of the presence of ω in denominator. As ω increases these functions remain well behaved.

Equation (3.4-24) can also be written for an interior point ξ by simply assuming $\bar{C}_{ij} = 0$ and $\xi = \xi_0$. This gives the required identity for calculating the interior displacements. The interior stresses can be obtained from:

$$\bar{\sigma}_{jk}(\xi) = \int_S \left[\bar{T}_{ijk}(x,\xi,s)\bar{t}_i(x,s) - \bar{E}_{ijk}(x,\xi,s)\bar{u}_i(x,s)\right] dS \qquad (3.4\text{-}25)$$

where:

$$\bar{T}_{ijk} = \left[\left(c_1^2 - 2c_2^2\right)_{\backslash} \delta_{jk} \frac{\partial \bar{G}_{im}}{\partial \xi_m} + c_2^2 \left(\frac{\partial \bar{G}_{ik}}{\partial \xi_j} + \frac{\partial \bar{G}_{ij}}{\partial \xi_k}\right)\right]$$

$\bar{E}_{ijk}$ = same as $\bar{T}_{ijk}$ with $\bar{G}$ replaced by $\bar{F}$

$$\frac{\partial \bar{G}_{ij}}{\partial \xi_k} = -\frac{1}{4\pi\mu}\left[\frac{\partial \psi}{\partial r}\delta_{ij}r_{,k} - \frac{\partial \phi}{\partial r}r_{,i}r_{,j}r_{,k} - \phi\left(r_{,i}r_{,jk} + r_{,j}r_{,ik}\right)\right]$$

$$\frac{\partial \bar{F}_{ij}}{\partial \xi_k} = -\frac{1}{4\pi}\left[\frac{\partial \alpha}{\partial r}r_{,k}\left(\delta_{ij}\frac{\partial r}{\partial n} + r_{,j}n_i\right) + \alpha\left(\delta_{ij}\left(\frac{\partial r}{\partial n}\right)_{,k} + r_{,jk}n_i\right)\right.$$

$$+ \frac{\partial \beta}{\partial r}r_{,k}\left(r_{,i}n_j - 2r_{,i}r_{,j}\frac{\partial r}{\partial n}\right) + \beta\left(r_{,ik}n_j - 2r_{,ik}r_{,j}\frac{\partial r}{\partial n} - 2r_{,i}r_{,jk}\frac{\partial r}{\partial n}\right.$$

$$\left. - 2r_{,i}r_{,j}\left(\frac{\partial r}{\partial n}\right)_{,k}\right) + \frac{\partial \gamma}{\partial r}r_{,k}\left(r_{,i}r_{,j}\frac{\partial r}{\partial n}\right) + \gamma\left(r_{,ik}r_{,j}\frac{\partial r}{\partial n} + r_{,i}r_{,jk}\frac{\partial r}{\partial n}\right.$$

$$\left. + r_{,i}r_{,j}\left(\frac{\partial r}{\partial n}\right)_{,k}\right) + \frac{\partial \delta}{\partial r}r_{,k}\left(r_{,i}n_j\right) + \delta\left(r_{,ik}n_j\right)\Bigg]$$

The corresponding equations for the stresses on the surface are identical with those for the static case with dynamic elastic constants given by equation (3.4-13).

Numerical Implementation

Since the basic governing equations for a dynamic analysis in the transformed space (either in s or ω space) are virtually identical to the corresponding equations for the static analysis, the numerical implementation developed for the static case can be used to extract solutions for the dynamic problem for one value of the transform parameter s or frequency parameter ω. It should also be noted that any internal viscous dissipation of energy (damping) can easily be accounted for by replacing the elastic moduli λ and μ by their complex counterparts λ^* and μ^*:

$$\mu^* = \mu(1 + 2i\beta)$$
$$\lambda^* = \lambda(1 + 2i\beta) \qquad (3.4\text{-}26)$$

leaving Poisson's ratio unaltered.

The parameter 2β, by analogy with single degree of freedom systems may be termed the damping ratio and is given by:

$$\beta = \omega\eta/2\mu \qquad (3.4\text{-}27)$$

where η is the coefficient of viscosity in the Kelvin-Voigt model.

For a general transient case the solution must be transformed back to real time by a suitable inversion process. Let $f(t)$ be a real function of t, with $f(t) = 0$ for $t < 0$. The Laplace transform $\bar{f}(s)$ of $f(t)$ is defined by equation (3.4-15) and its inversion formula is given by:

$$f(t) = \frac{1}{2\pi i} \int_{x-i\infty}^{x+i\infty} \bar{f}(s)e^{st}\, ds \qquad i = \sqrt{-1} \qquad (3.4\text{-}28)$$

where $x(>0)$ is arbitrary, but greater than the real part of all the singularities of $\bar{f}(s)$, and s is a complex number with $Re(s)\beta > 0$.

In the present applications $\bar{f}(s)$ is too complicated to be inverted analytically and is available in numerical form. In those cases a numerical inversion of the Laplace transform is imperative.

The method of inversion used is that of Durbin (Reference 78) and is actually an efficient improvement of the method of Dubner and Abate (Reference 79) which is based on the finite Fourier cosine transform. Durbin (Reference 78) combined both finite Fourier cosine and sine transforms to obtain the inversion formula:

$$f(t_j) \simeq 2\left(e^{\beta j \Delta t/T}\right)\left[-\frac{1}{2}\,Re[\bar{f}(\beta)] + Re\left\{\sum_{n=0}^{N-1}(A(n) + iB(n))W^{jn}\right\}\right] \qquad (3.4\text{-}29)$$

where

$$S_n = \beta + in\frac{2\pi}{T} \qquad i = \sqrt{-1} \qquad W = e^{i2\pi/N}$$

$$A(n) = \sum_{\ell=0}^{L} Re\left\{\bar{f}\left(\beta + i(n + \ell N)\frac{2\pi}{T}\right)\right\} \qquad (3.4\text{-}30)$$

$$B(n) = \sum_{\ell=0}^{L} Im\left\{\bar{f}\left(\beta + i(n + \ell N)\frac{2\pi}{T}\right)\right\}$$

$$n = 0, 1, 2, 3, \ldots, N \qquad \ell = 0, 1, 2, 3, \ldots, L$$

and f(t) is computed for N equidistant points $t_j = j\Delta t = jT/N, j = 0, 1, 2, \ldots, N-1$. It is suggested that for LxN ranging from 50 to 5000 one should select $\beta T = 5$ to 10 for good results, where T is the total time interval of interest. The computations involved in equation (3.4-29) are performed by employing the Fast Fourier algorithm of Cooley and Tukey (Reference 80). The algorithm employed here was used with considerable success by Manolis and Beskos (Reference 54). In the case of the Fourier transform ($s = -i\omega$), the above algorithm is equivalent to a Fourier synthesis. In this work we have used L=1, N=50 and βT=6, although as mentioned above these values can be adjusted to improve accuracy.

The only topic remaining for discussion is the direct transform, i.e., to find the Laplace or Fourier transform of a given forcing function in time. If the forcing function is piecewise linear in time, which is an excellent approximation for functions that are densely sampled, then the following exact formula can be used:

$$\bar{f}(s) = \sum_{i=1}^{N-1} \frac{1}{\Delta t\, s^2} \left\{ \Delta F \left(e^{-st_i} - e^{-st_{i+1}} \right) + s\, \Delta t \left(F_i e^{-st_i} - F_{i+1} e^{-st_{i+1}} \right) \right\} \quad (3.4\text{-}31)$$

where F_i is the value of f at time t_i and $\Delta F = F_{i+1} - F_i$.

It should be noted that the Laplace transform solution is essentially a superposition of a series of steady state solutions and is therefore applicable only to linear elasto-dynamic problems. For nonlinear problems the solution must be obtained in the real time domain. The boundary integral formulation for the time embedded elasto-dynamic analysis has already been developed. This formulation can be extended to deal with nonlinear dynamic problems.

The present steady state dynamic algorithm can also be used to determine the various vibration modes of a structural component. Unfortunately, the algorithm is computationally inefficient. A new real variable version of the eigenvalue analysis is currently being developed which is likely to prove useful. The present steady state dynamic analysis is ideally suited for the stress analysis of components at a given value of frequency parameter ω.

For buckling analysis, the necessary boundary integral formulation has not yet been developed. Although it is possible to construct an integral representation, it is doubtful if it can be made sufficiently computationally efficient to be a viable alternative.

3.4.4 Computer Program Development

3.4.4.1 Introduction

The mathematical goal of the computer program development is the accurate and efficient implementation of the analysis described in Section 3.4.3. By itself, this is a significant task. While many of the capabilities required have been demonstrated in special purpose computer programs or discussed in the open literature, no program (even for two-dimensional analysis) includes all of the required capabilities. The construction of a three-dimensional code including elastic, nonlinear and dynamic capabilities was a most challenging task.

Of equal importance is the degree of generality required in the definition of component geometry, loading and material properties. This is necessary if the program is to be applicable to real problems in the aerospace industry. Since no general purpose boundary element program existed as a starting point, or even a model, it was necessary to develop, during a single year, a new general purpose system for structural analysis.

During the past year, the computer program BEST (Boundary Element Stress Technology) has been developed. It is capable of carrying out elastic, inelastic and dynamic analyses for real component geometries. The capabilities of the program have been calibrated by comparison with analytical solutions, other numerical stress analyses and data. In addition, the code was written with sufficient generality to allow the incorporation of new technology, developed during the remainder of this contract, without major recoding of the already completed portions of the program.

The development of the computer program BEST is discussed in the following sections.

3.4.4.2 Global Program Structure

BEST is designed to be a fully general structural analysis system employing the boundary element method. The program is written using standard IBM FORTRAN IV. Development has been carried out at Pratt & Whitney using an IBM 3081 in both batch and interactive modes and at SUNY-B on an HP9000 minicomputer system. In both cases the required code and workspace fit in core without requirement for overlays. The nature of the method is such that, for any realistic problem, not all required data can reside simultaneously in core. For this reason extensive use is made of both sequential and direct access scratch files.

The overall structure of BEST is shown in Figure 3.4-1. The program first executes an input segment which is common to all types of analysis. After the input has been processed, there are three major branches, corresponding to elastic, inelastic and dynamic analysis.

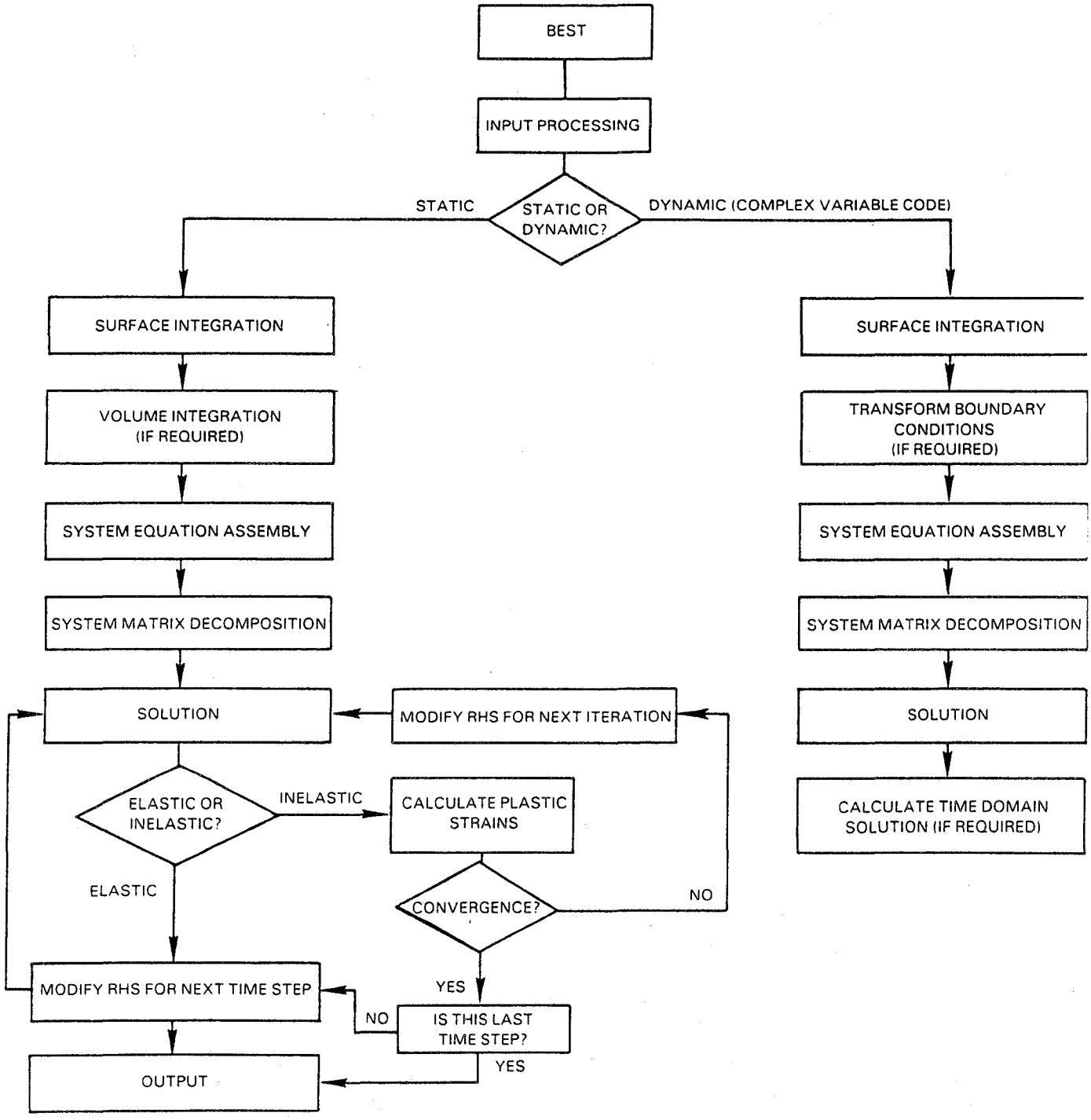

Figure 3.4-1 BEST - Overall Program Structure

If only an elastic analysis is required, the necessary surface integrals are calculated and assembled into the set of system equations using specified boundary conditions. The system matrix is then decomposed and saved on disk, followed by the calculation of the solution vector. The full displacement and traction solution on each boundary element is then reconstructed from the solution vector. In a time dependent problem the process of constructing the load vector for the system equations is repeated at each time step, but the integration, formation and decomposition of the system matrix are done only once.

If a dynamic analysis is to be carried out, a branch is taken immediately after the input processing. The main differences between the elastic and dynamic portions of the code are:

1. in the calculation of Laplace transforms of the boundary conditions (in the aperiodic case),

2. in the use of complex versions of the quasi-static elastic routines connected with surface integration, system matrix assembly and system matrix decomposition, and

3. in the use of the transform of the (complex) dynamic point load solution in place of the Kelvin solution.

In the case of inelastic analysis the elastic branch is followed through the calculation of the surface integrals required for both system matrix creation and the evaluation of elastic stresses at the points used to describe the volume distribution of inelastic strain. The system matrix is decomposed once, for the initial elastic solution, and the decomposed form is saved for repeated use during the plasticity calculations. The main difference between the elastic and inelastic analyses is the iterative process (carried out at each load or time step) in which the inelastic strain distribution is evaluated and employed in volume integrals which modify the system equation load vector. This process is nested inside the time stepping procedure of the elastic code.

It should be noted that, in the present version of BEST, the inelastic volume integration routines are used to deal with both thermal stresses (due to either transient or steady state temperature fields) and inhomogeneous elastic material properties. Effort during the second year of the program will be devoted to developing a more efficient treatment of these effects in purely elastic problems.

Various aspects of the computer program are discussed below.

3.4.4.3 Program Input

The input for BEST is free field. Meaningful keywords are used to identify data types and to name particular data sets. The overall input structure is shown in Figure 3.4-2. The input is divided into four major types:

1. Case Control Cards

The case control cards define global characteristics of the problem. In addition to the problem title, these input items define the ways in which the problem departs from a static, homogeneous elastic analysis. The reading or writing of restart data is also defined at this point. In all cases the absence of a case control card will cause the program to default to the simplest case, a standard elastic analysis.

2. Material Property Definition

The material property input allows the definition of elastic and, if required, inelastic material properties for a variety of materials. For isotropic, homogeneous materials both Young's modulus and the coefficient of thermal expansion can be prescribed in tabular form for a user-defined set of temperatures. Temperature independent values of density and Poisson's ratio are defined.

If inelastic material properties are required, the particular constitutive model to be used must first be chosen. The constants required to initialize the model for a given material are then input, together with a material identifier.

For both elastic and inelastic properties, provision is made to link BEST to existing user material properties libraries. In this case the user is responsible for providing code to access the local libraries.

3. Geometry Input

Geometry input is defined one GMR (generic modeling region, or subregion) at a time. To initiate the input, a tag is provided to identify the GMR, a material name and reference temperature are defined to allow initialization of material properties and various flags are input (if required) to identify behavior other than static elastic within the GMR.

The next block of geometry input consists of the Cartesian coordinates of the user input points for surface and volume geometry definition, together with identifiers (normally positive integers) for these geometric nodes.

Following the definition of an initial set of nodal points, the surface connectivity of the GMR is defined through the input of one or more named surfaces. Each surface is made up of a number of elements, with each element defined in terms of several geometric nodes. All surface element types presently employed represent surface geometry using the quadratic isoparametric shape functions (Figure 3.4-3). Three sided elements, defined using six rather than eight geometric nodes, are used for mesh transition purposes. The terms quadrilateral and triangle are normally used to refer to the eight and six noded elements, although the real geometry represented is, in general, a nonplanar surface patch.

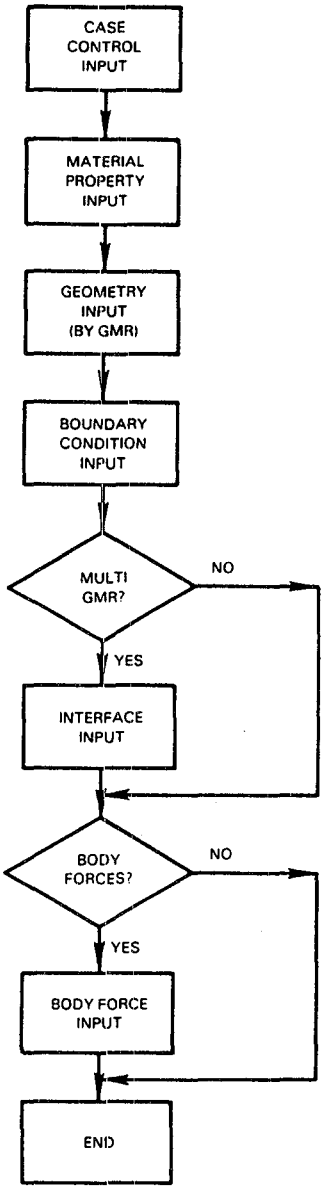

Figure 3.4-2 BEST - Input Structure

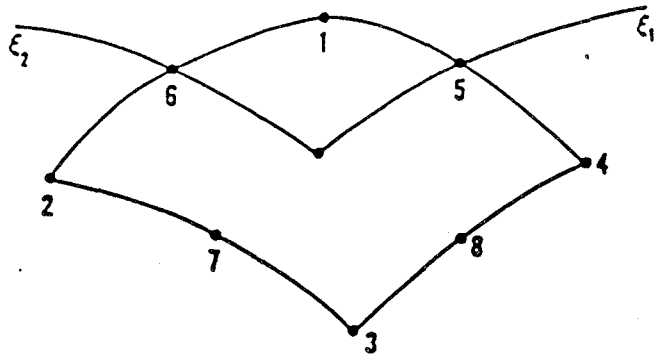

$$X_i(\xi) = M^\alpha(\xi)\, X_i^\alpha \qquad \alpha = 1,2,\cdots,8$$

$$M^1(\xi) = \tfrac{1}{4}(\xi_1+1)(\xi_2+1)(\xi_1+\xi_2-1)$$

$$\vdots$$

$$M^5(\xi) = \tfrac{1}{2}(\xi_1+1)(1-\xi_2^2)$$

$$\vdots$$

Figure 3.4-3 Quadratic Isoparametric Shape Functions

Over each element the variation of displacement and traction can be defined using either the linear or quadratic isoparametric shape functions. Linear and quadratic elements can share a common side, which is then constrained to have linear displacement and traction variation.

In addition to the element types mentioned above, elements which extend to infinity are provided. These elements are designed to allow modeling of structures connected to ground, and automatically incorporate appropriate decay conditions. The characteristics of the various element types are summarized below.

Element Type	Geometry Nodes	Displacement/Traction Nodes
Linear Quadrilateral	8	4
Linear Triangle	6	3
Quadratic Quadrilateral	8	8
Quadratic Triangle	6	6
Linear Infinite	8	2
Quadratic Infinite	8	3

The geometry input includes the option to duplicate surfaces. Once a given surface has been completely defined, a copy of it can be automatically created, with arbitrary translation and rotation. In this case the program will internally define and number any new nodes required, and will construct all element definitions. The surface referenced can be from the current GMR, or from any GMR previously defined.

The final input for each GMR is the definition of volume cells (presently restricted to twenty node isoparametric elements) for that portion of the GMR in which volume effects (inelastic or thermal) are anticipated. The nodes of the (partial) volume discretization lying on the surface of the GMR need not be coincident with nodes of the surface discretization.

4. Boundary Condition Input

The final input section provides for the definition of boundary conditions, as functions of both position and time. Data can be input for an entire surface, or for a subset (elements or nodes) of a surface. Input can be in global coordinates, or can define rollers or pressure in the local coordinate system. Input simplifications are available for the frequently occurring cases of boundary data which is constant with respect to space and/or time variation. Each boundary condition set can be defined at a different set of times.

Special types of boundary conditions which are available include interfaces (fixed or sliding contact) between two GMRs, cyclic surfaces (to allow efficient modeling of structures with periodic geometry and loading) and springs to ground.

In addition to the boundary condition types defined above, two types of body force loading (thermal and centrifugal) can be defined.

3.4.4.4 Surface Integral Calculation

Following the processing of the input data, the surface integrals occurring in equations (3.4-2) and (3.4-3) are evaluated numerically. This is the most time consuming portion of most elastic analyses, and contributes heavily to the cost of inelastic analysis. In BEST the results of these integrations are stored as they are calculated, rather than being assembled into the final equation system immediately. Although this is somewhat more costly in terms of storage and CPU (central processing unit) time, it has led to much greater clarity in the writing of the initial version of BEST. In addition, it provides much greater flexibility in the implementation of various restart and boundary condition options.

The basic outline of the surface integration process is shown in Figure 3.4-4. The calculations proceed first by GMR (generic modeling region), then by source point (the equation being constructed) and finally by surface element. The results for each source point/surface element pair are written to disk. All of the calculations are carried out and stored in the global (Cartesian) coordinate system.

The calculations connected with the creation of the system equations are the more complex. In this case either singular or nonsingular integrals can be encountered. The integrals are singular if the source point for the equations being constructed lies on the element being integrated. Otherwise, the integrals are nonsingular, although numerical evaluation is still difficult if the source point and the element being integrated are close together.

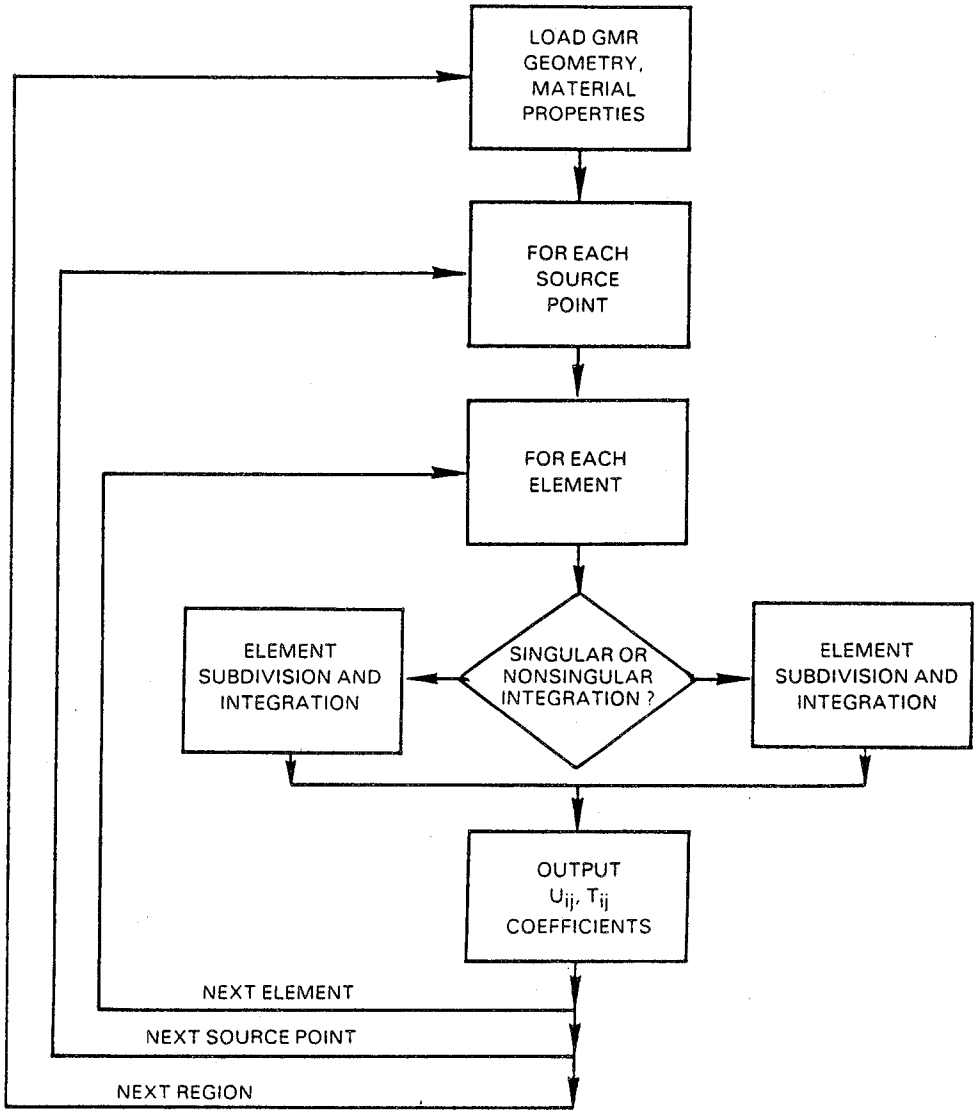

Figure 3.4-4 BEST - Surface Integral Calculations

In both the singular and nonsingular cases Gaussian integration is used. The basic technique is developed in Reference 4, and was first applied in the three-dimensional boundary element method by Lachat and Watson (Reference 16). In the nonsingular case an approximate error estimate for the integral was developed based on the work of Stroud and Secrest (Reference 81). This allows the determination of element subdivisions and orders of Gaussian integration which will retain a consistent level of error throughout the structure. Numerical tests have shown that the use of 3x3, 4x4 and 5x5 Gauss rules provide the best combination of accuracy and efficiency. In the present code the 4x4 rule is used for nonsingular integration, and error is controlled through element subdivision. The origin of the element subdivision is taken to be the closest point to the source point on the element being integrated.

If the source point is very close to the element being integrated, the use of a uniform subdivision of the element can lead to excessive computing time. This frequently happens in the case of aerospace structures, due either to mesh transitions or to the analysis of thin walled structures. In order to improve efficiency, while retaining accuracy, a graded element subdivision was employed. Based on one-dimensional tests, it was found that the subelement divisions could be allowed to grow geometrically away from the origin of the element subdivision. Numerical tests on a complex three-dimensional problem have shown that a mesh expansion factor as high as 4.0 can be employed without significant degradation of accuracy.

In the case of singular integration (source point on the element being integrated) the element is first divided into triangular subelements. The integration over each subelement is carried out in a polar coordinate system with origin at the source point. This coordinate transformation produces nonsingular behavior in all except one of the required integrals. Normal Gauss rules can then be employed. The remaining integral (that of the traction kernel T_{ij} times the isoparametric shape function which is 1.0 at the source point) is still singular, and cannot be numerically evaluated with reasonable efficiency and accuracy. Its calculation is carried out indirectly, using the fact that the stresses due to a rigid body translation are zero (Reference 16). It has been found that subdivision in the circumferential direction can be required to preserve accuracy in the singular integration. A maximum included angle of 15 degrees is used. Subdivision in the radial direction has not been required.

The modifications required in the surface integrals for the solution of dynamic problems are primarily the replacement of a number of routines with complex variable versions of the same code and the substitution of the transform of the dynamic kernel function. Modification of the calculation of the singular T term is also required, since the rigid body argument cannot be used directly. It has been found, however, that the singular behavior of this term is entirely due to the static kernel. The modifications required for the dynamic solution can be calculated entirely in terms of nonsingular numerical integrals.

The surface integrals required for calculation of displacement and stress at interior or surface points are of the same type as those involved in the generation of the system equations, except that only nonsingular integrals are involved. If the source point involved is located on the surface of the body, then numerical integration is not required. Instead, the required quantities are calculated using the displacements and tractions on the element (or elements) containing the source point, as discussed in Section 3.4.3.2.

3.4.4.5 Volume Integral Calculations

The calculation of volume integrals is required in both the construction of the system equations and the evaluation of interior stresses and displacements. In a purely elastic context this requirement is due primarily to the presence of body forces. In the case of inelastic analysis the inelastic strain distribution must also be integrated for each source point/volume cell pair.

The three volume integrals involved in the analysis: G, T and M, all exhibit singular behavior as the load point and the source point coincide. The order of the singularities for G, T and M are $(1/r)$, $(1/r^2)$ and $(1/r^3)$, respectively.

The overall strategy used in the volume integration is very similar to that described for the surface integration in the preceding section; i.e., based on the consistent level of error throughout the volume, Gaussian integration has been used to evaluate both the singular and nonsingular integrals.

Nonsingular integrals involving T and M have been evaluated using 3x3x3, 4x4x4 or 5x5x5 Gauss rules depending on the distance between the source point and field point. If the source point lies in the neighboring cell, the cell is subdivided into several sub-cells. The corresponding integrals involving the weakly singular function G have been evaluated using Gaussian integration rules of one order less than those mentioned above.

Singular integrals involving the functions G and T were evaluated using a spherical polar mapping with the origin at the field point. The cell is subdivided into several tetrahedra through the field point and the resulting sub-cell integrations are carried out by mapping each of these sub-cells into a unit cube. The kernel-shape function products are thus made to behave like a regular integrand. Gauss rules of 3x3x3 (for G) and 4x4x4 (for T) are used for evaluating these sub-cell integrals.

Singular integrals involving the functions M times the shape function N require some very special attention. For node at which the shape function is zero, the behavior of these integrands is similar to the singular integrals involving the function T as described previously; and accordingly they have been treated in a similar manner. Those involving the shape function attaining a value of 1.0 at the singular point (a situation which is equivalent to the case of traction kernel F times the shape function 1.0 at a singular node at the surface) cannot be evaluated accurately without a massive amount of computational effort. Fortunately, the free term obtained by the exact integration over a spherical exclusion (see equation 3.4-5) accounts for 95% to 98% of the contribution from this integral; accordingly, this integral has been assumed to be zero.

3.4.4.6 System Matrix Assembly

The assembly of the system equations is a multistep process, as shown in Figure 3.4-5. The process is the same for elastic, inelastic and dynamic problems. The assembly process is carried out differently in the present program than in previous two- and three-dimensional codes. This is due to the fact that the present program is aimed largely at the solution of nonlinear problems. Since the nonlinear effects are accounted for in the load terms of the equation system, and since these effects depend both on the present load state and on the past history of the system, it is not possible to calculate all of the system load vectors prior to the beginning of the solution process. As a result, the assembly process must be designed to facilitate the updating of the load vector, based on material response as well as time dependent loads.

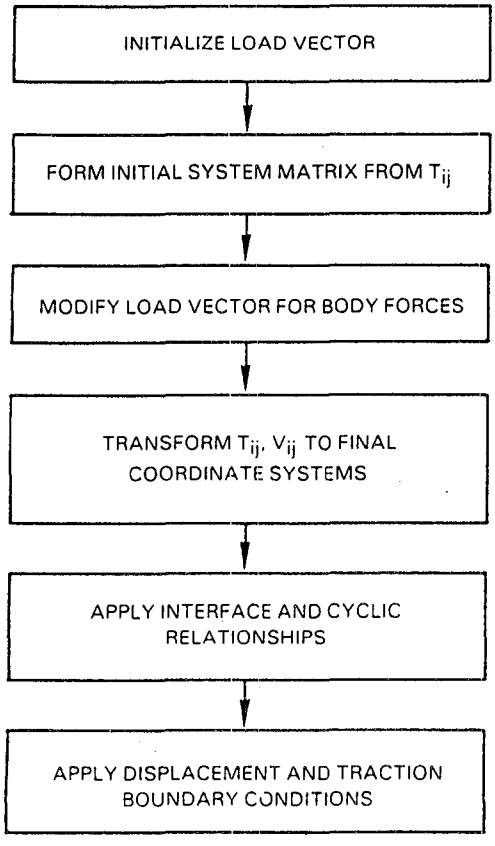

Figure 3.4-5 BEST - System Matrix Assembly

The first step in the assembly process is the reduction of the rectangular matrix of T integrals to a square matrix. This matrix is the prototype of the system matrix. The columns of this matrix are transformed or replaced, as required by the boundary conditions, as the assembly process proceeds.

A key problem in the entire process is the proper definition of appropriate coordinate systems, on a nodal basis. This is a problem common to any direct boundary element method program which treats structures with nonsmooth surfaces. It arises because the tractions at a point are not uniquely determined unless the normal direction to the surface varies continuously at the point in question.

The original surface integral calculations are all done in global coordinates. If a displacement boundary condition is specified at a given node, in global coordinates, then no new coordinate system definition is required. It is only necessary to keep track of the subset of elements, containing the given node, on which the fixed displacement is to be reacted. However, if a displacement is specified in a nonglobal direction at a given node, then a new nodal coordinate system must be defined and, potentially, updated as further boundary conditions are processed. The associated nonzero reactions must then be expressed in the new coordinate system.

After all required local coordinate systems have been defined, any modified boundary conditions required by the presence of body forces are calculated. There are a variety of methods of accounting for body force distributions. The one employed in the multi-GMR version of BEST is a modification of the integral equations resulting from the representation of the solution as the sum of a complementary solution and a particular integral. The boundary conditions must be modified to reflect displacements or tractions due to the particular integral. This results in changes to any explicitly specified boundary conditions and in the introduction of potentially nonzero boundary conditions on any surfaces previously defined implicitly as being traction free.

Following this preparatory work, the final assembly of the system equations is carried out. It is performed in three major steps:

1. Transformation of the columns of the matrices to appropriate local coordinate systems and incorporation of any boundary conditions involving springs.

2. Incorporation of compatibility and equilibrium conditions on interfaces between GMRs and on cyclic surfaces. On interfaces either a completely glued condition (full displacement compatibility) or a sliding condition (only normal displacement compatibility) is available.

3. Application of specified displacements and tractions.

Two particular features of the equation assembly deserve special comment. First, in multi-GMR problems the system matrix is not full. Rather, it can be thought of as consisting of an NxN array of submatrices, each of which is either fully populated or completely zero. Only the nonzero portions of the system equations are preserved during system matrix assembly. In order to improve the numerical conditioning of the system matrix for the solution process, the columns are reordered to number variables lying on the same interface, but belonging to two different GMRs, as close together as possible. The rows of the system matrix are placed in the same order as the columns.

Second, rather than simply assembling an explicit load vector at each time point in the solution process, load vector coefficient matrices are assembled and stored. These allow the updating of the load vector at any required time point simply by interpolating the time dependent boundary conditions and performing a matrix multiplication. This capability is particularly important in inelastic analysis, since frequent updating of the load vector is required. A similar process is used in the calculation of interior and boundary stresses.

3.4.4.7 System Equation Solution

A new solver was written for BEST. It operates at the submatrix level, using software from the LINPACK package (Reference 82) to carry out all operations on submatrices. The system matrix is stored, by submatrices, on a direct access file. The decomposition process is a Gaussian reduction to upper triangular (submatrix) form. The row operations required during the decomposition are stored in the space originally occupied by the lower triangle of the system matrix. Pivoting of rows within diagonal submatrices is permitted.

The calculation of the solution vector is carried out by a separate subroutine, using the decomposed form of the system matrix from the direct access file. The process of repeated solution, required for problems with time dependent and/or nonlinear behavior, is highly efficient.

3.4.4.8 Inelastic Solution Process

The inelastic solution algorithm starts with an elastic analysis of the problem for the first loading increment (complete with the specified boundary and body force loading). At the end of the elastic increment the state variables are calculated and the nonlinear consitutive equations are established. The difference between the correct stresses or strains and the elastic stresses or strains are estimated. These are used to compile a new boundary condition vector (the right-hand side of the system equation). The process is essentially repeated until the constitutive equations yield the stresses that are negligibly different from the calculated stresses using equation (3.4-5). A new loading increment is taken and the process is repeated for each subsequent increment (see Section 3.4.3.2).

During such an incremental solution process, a considerable saving in the computing time has been achieved by introducing:

a. a solver which allows for resolution of the same system equations for different right-hand sides so that the decomposition of the system matrix is done only once.

b. a routine for the extrapolation of the plastic strains based on the previous loading history and the generation history of the plastic strains.

Although the extrapolation of the plastic strains does sometimes affect the accuracy of the nonlinear solution, the savings could be very considerable since usually one iteration may lead to 95% of the desired results.

The nonlinear solution algorithm and the associated routines are included within the program BEST in such a manner that their presence will not affect the efficiency of an elastic analysis.

Various levels of constitutive relations have been programmed within BEST. These include a kinematic elastoplastic hardening model, and a viscoplastic kinematic hardening model of Walker admitting thermally dependent hardening.

3.4.4.9 Output

The output from BEST is relatively straightforward. It consists of nine sections, as follows:

1. Complete echo of the input data set.

2. Summary of case control and material property input.

3. Complete definition for each GMR, including all surface and volume nodes, surface elements and volume cells.

4. Complete summary for each boundary condition set, including the elements and nodes affected.

5. Boundary solution (on an element basis), including displacements and tractions at each node of each element. The resultant load on each element and on the entire GMR is calculated and printed.

6. Displacement, stress and strain on a nodal basis, at all surface nodes, for each GMR.

7. Displacements at all volume cell nodes.

8. Stresses at all volume cell nodes.

9. Strains at all volume cell nodes.

Items 5 through 9 are printed at each user-requested time point. In the case of a plastic analysis, an extra print of the elastic solution at first yield is also provided.

Sample output pages are included in Section 3.4.7, following the input description.

3.4.5 Program Validation/Verification

3.4.5.1 Validation of Elastic Capabilities

The newly developed three-dimensional boundary element program (BEST) has a great variety of input and analysis options. More will be added in the future. It is clearly impossible to design and execute a test case examining every possible combination of these options. BEST has, however, been subjected to an extensive validation effort.

A simplified tabulation of the elastic validation cases which have been used is presented in Figure 3.4-6. Major program capabilities are shown along the diagonal boundary. The box at the intersection of a row and column represents a possible test case combining two capabilities. The presence of an L, Q or M in such a box signifies that a test case has been successfully run using linear, quadratic or mixed variation of displacement and traction. In many cases a single test problem involves several capabilities. This is indicated by multiple entries in Figure 3.4-6. In most cases the test problems have been run repeatedly during the BEST development effort, in order to verify the continued correct operation of existing capabilities after the addition of code enhancements.

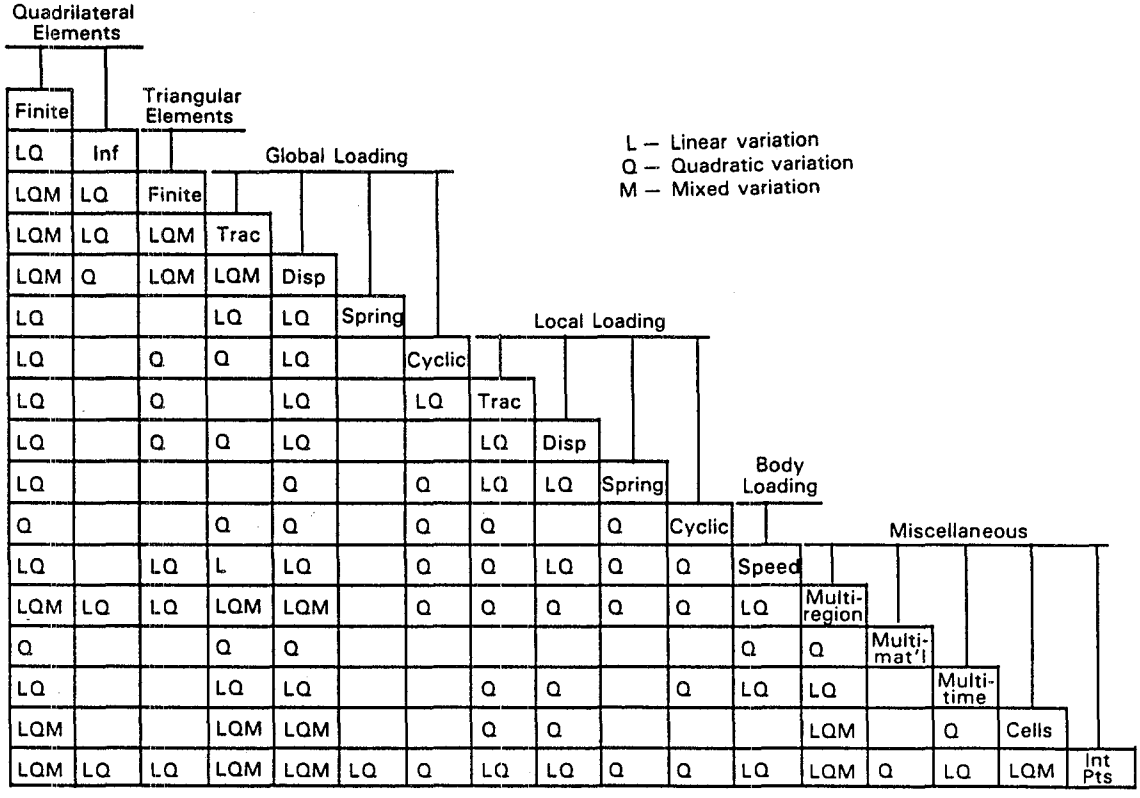

Figure 3.4-6 BEST - Elastic Validation Matrix

A small subset of the validation cases, testing particularly important or basic capabilities, is discussed below. Except as otherwise indicated, all stresses are surface stresses, calculated using the displacements and tractions on the boundary. Unless otherwise noted, displacements are given in inches and stresses in lb/in^2. In many cases both full and hidden line plots of the meshes are shown.

1. Cube in Tension (Figure 3.4-7)

A cube was modeled using five quadrilateral and two triangular elements. The cube was subjected to a uniform displacement. Using a sufficiently accurate numerical integration, it is possible to achieve five place agreement with the exact solution.

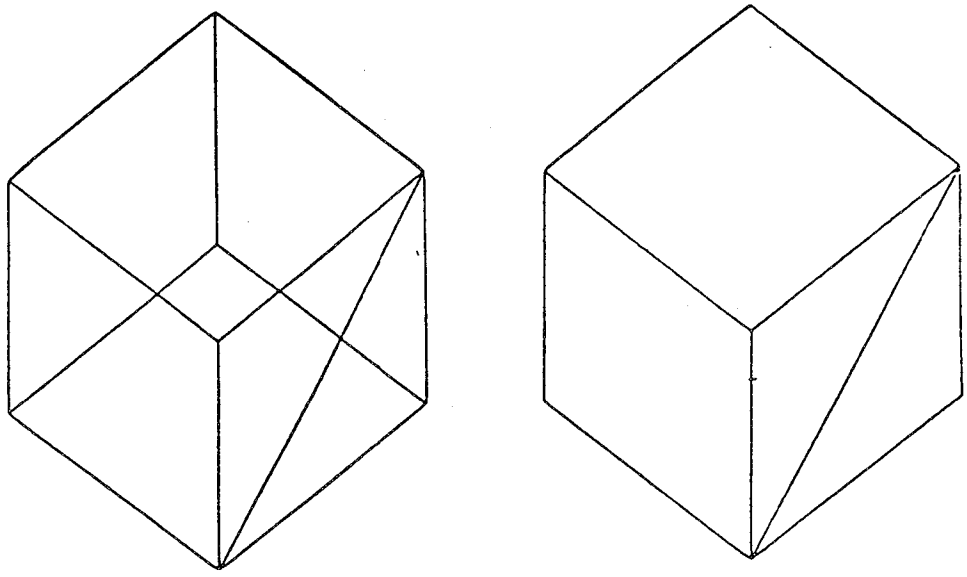

	Analytical	BEST
U_x	0.001	0.001
U_y	0.00035	0.00035
U_z	0.00035	0.00035
T_x	16126	16126
T_y	0	0
T_z	0	0

Figure 3.4-7 Cube in Tension

2. Pressurized Thick Cylinder (Figure 3.4-8)

A 22.5 degree sector of a thick cylinder was modeled using six quadrilateral surface patches. In this problem two of the elements (the cylinder ID and OD) possess curvature. The problem was solved using both linear and quadratic variation of displacement and traction. The displacements from both analyses showed good agreement with analytical results. Quadratic variation was, however, required to obtain good stress results at the surface nodes. The use of more surface patches in the radial direction would further improve the agreement between the calculated and analytical values of the radial stress.

This problem also tests the use of local coordinate systems, since the load is defined as a pressure (traction normal to the surface) on the ID of the cylinder, and rollers (zero normal deflection) are imposed on the 0 and 22.5 degree planes.

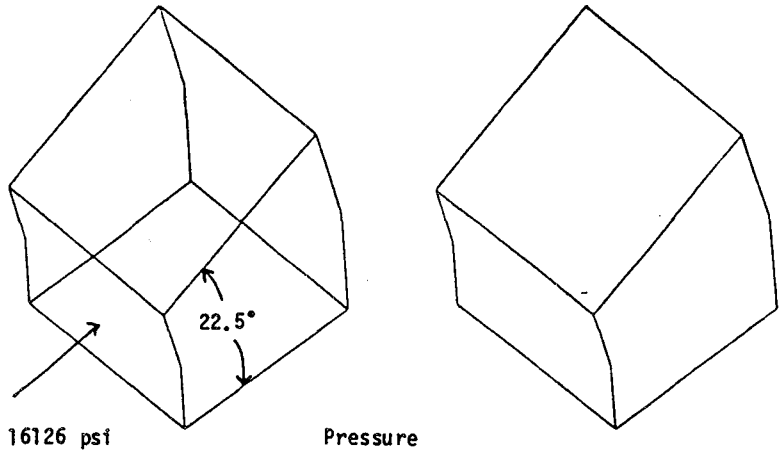

			BEST	
		Analytical	Linear	Quadratic
ID	U_R	5.90×10^{-3}	5.79×10^{-3}	5.91×10^{-3}
	σ_R	-16126	-9334	-14699
	σ_θ	41928	38869	41839
OD	U_R	4.80×10^{-3}	4.70×10^{-3}	4.81×10^{-3}
	σ_R	0	-5023	991
	σ_θ	25802	24818	25812

Figure 3.4-8 Pressurized Thick Cylinder

3. Rotating Thick Cylinder (Figure 3.4-9)

The geometry and mesh for this problem are identical to (2), above. Note that for this problem the use of quadratic variation is required to obtain acceptable results for either displacement or stress.

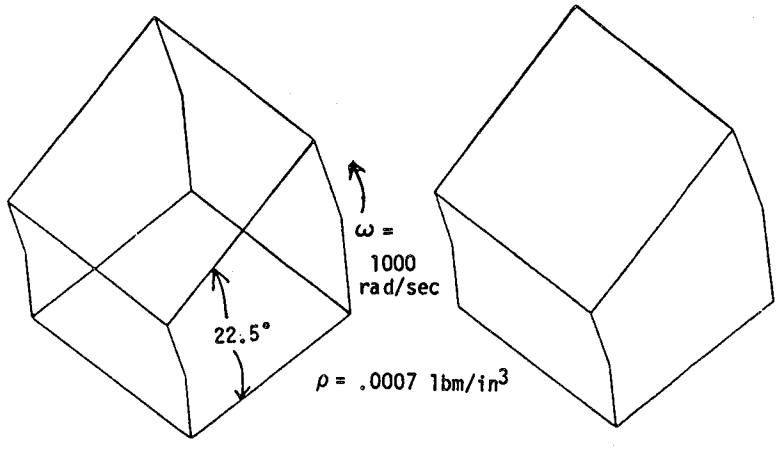

			BEST	
		Analytical	Linear	Quadratic
ID	U_R	7.13×10^{-4}	6.76×10^{-4}	7.13×10^{-4}
	σ_R	21	507	131
	σ_θ	5752	5211	5732
OD	U_R	6.29×10^{-4}	5.94×10^{-4}	6.29×10^{-4}
	σ_R	21	-370	94
	σ_θ	3390	3132	3368

Figure 3.4-9 Rotating Thick Cylinder

4. Multi-GMR Cylinder (Figure 3.4-10)

In this problem a 22.5 degree sector of a thick cylinder was again analyzed. In this case, however, several added features are present. First, the mesh is larger (twelve elements rather than six). Second, the structure is broken into two GMRs along the 11.25 degree plane. Third, the boundary conditions on the 0 and 22.5 degree planes are cyclic symmetry between these two surfaces, rather than the roller boundary conditions used in (2) and (3). In this case only the results for quadratic variation of displacements and tractions are shown. Once again, good agreement between the calculated and analytical results was obtained.

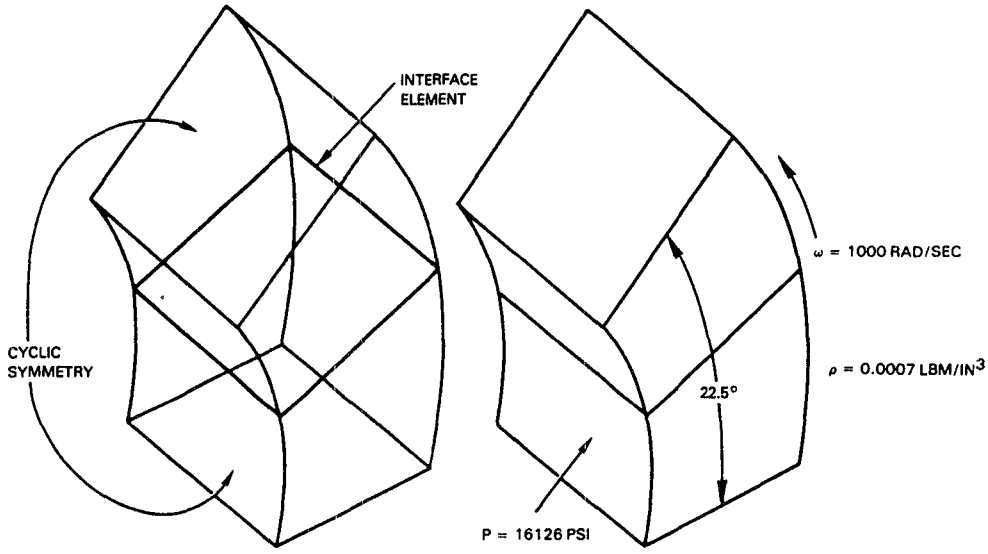

		PRESSURE		SPEED	
		ANALYTICAL	BEST	ANALYTICAL	BEST
ID	U_R	5.90×10^{-3}	5.91×10^{-3}	7.13×10^{-4}	7.13×10^{-4}
	σ_R	-16126	-16126	21	0
	σ_θ	41928	41997	5752	5751
OD	U_R	4.80×10^{-3}	4.81×10^{-3}	6.29×10^{-4}	6.29×10^{-4}
	σ_R	0	0	21	0
	σ_θ	25802	25865	3390	3371

Figure 3.4-10 Thick Cylinder - Multi-GMR

5. Half-Space Loaded with a Circular Punch (Figure 3.4-11)

This problem was designed to test both the infinite elements incorporated in BEST and the ability to calculate stress and displacement at points in the interior of a region.

The problem is the classical one of a half-space loaded with a uniform pressure over a circular region. In the figure the dashed outer lines of the mesh are boundaries at infinity. Use of the mesh shown, consisting of twelve finite quadratic elements and four infinite elements, gave good agreement between calculated and analytical results for the displacement and stress under the center of the punch.

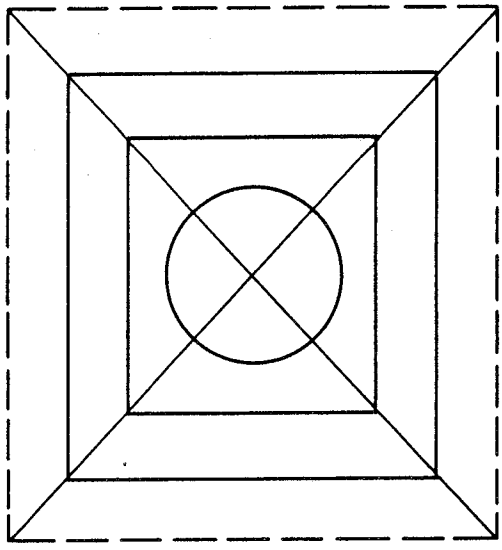

		DISPLACEMENT (BELOW CENTER OF PUNCH)		STRESS (BELOW CENTER OF PUNCH)	
	DEPTH	ANALYTICAL	BEST	ANALYTICAL	BEST
SURFACE POINT	0	1.29×10^{-3}	1.25×10^{-3}	16100	16100
INTERIOR POINTS	0.1	1.23×10^{-3}	1.20×10^{-3}	16060	16550
	0.4	1.02×10^{-3}	9.71×10^{-4}	14180	14054
	1.6	4.49×10^{-4}	4.25×10^{-4}	3780	3547
	6.4	1.21×10^{-4}	1.19×10^{-4}	290	246

Figure 3.4-11 Half-Space Loaded With a Circular Punch

6. Long Beam on an Elastic Half-Space (Figure 3.4-12)

In this problem a long beam is attached to an elastic half-space and loaded in tension. This problem is of interest primarily as a starting point for later dynamic/transient analyses. Note that the correct solution for the tip deflection of the beam is essentially the sum of the extension of the beam in simple tension and the displacement of the half-space under a patch load.

It is of particular interest to note that it was never possible to obtain an acceptable solution to this problem when it was run as a single region, using either linear or quadratic variation. This is due to the fact that, when considered as a single region, much of the beam is effectively located at infinity. To obtain accurate results would require a much more extensive mesh on the surface of the half-space, losing all the advantage gained by the use of infinite elements. Assigning the beam and the half-space to separate GMRs eliminates this problem, leading to reasonable results (-5% error) for linear variation and very good results (less than 1% error) for quadratic variation.

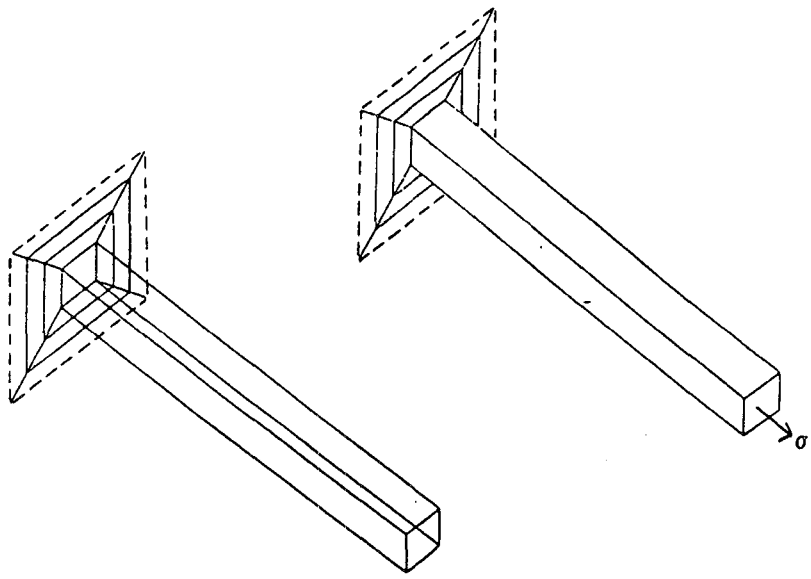

- - - - - BOUNDARY AT INFINITY

	Displacement at Tip of Beam
Analytical	1.13×10^{-2}
One Region, Linear Variation	5.00×10^{-4}
One Region, Quadratic Variation	6.91×10^{-4}
Two Regions, Linear Variation	1.05×10^{-2}
Two Regions, Quadratic Variation	1.12×10^{-2}

Figure 3.4-12 Beam on an Elastic Half-Space

3.4.5.2 Validation of Inelastic Algorithms

The main portions of the code which are unique to inelastic analysis are the constitutive modules and the routines for calculating volume integrals of various kernel function/inelastic strain (or stress) products over twenty node isoparametric cells. All of the other basic functions of the program are identical with the elastic version and do not, therefore, require separate validation. Several simple problems have been run to verify the unique features of the inelastic code.

1. Cube under Uniform Thermal Expansion

An unconstrained unit cube was subjected to a uniform thermal expansion. Since the cube is unconstrained, the final stress should be zero and the final direct strains should be those due to the temperature change. To obtain these results using the inelastic code requires that all of the inelastic volume integrals be properly implemented. The problem was run

twice. In the both cases the surface was modeled using six (quadratic) elements. In the first analysis, a single volume cell was used. In the second, the cube was divided into four cells, requiring calculations at interior, as well as surface, points.

The results were excellent for both analyses.

2. Cube in Simple Tension (Figure 3.4-13)

A cube in simple tension, represented by six surface elements and one 20 noded cell was loaded in simple tension. The cube was modeled as an elastic linearly strain hardening plastic body. The analysis was carried out up to the fourth increment beyond the yield point. Excellent agreement with analytical results were obtained. The same problem was also analyzed with 12 surface elements and 4 volume cells (in order to test the volume integration routines for neighboring cells); the results were found to be essentially similar for both cases.

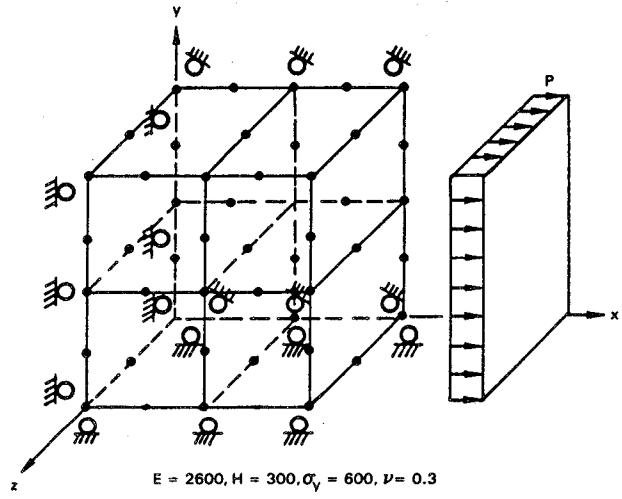

Figure 3.4-13 Elastic-Plastic Cube in Tension

3. Pressurized Thick Cylinder (Figures 3.4-14 through 3.4-17)

An internally pressurized thick cylinder (inner radius a=1, outer radius b=2.0) was modeled using six surface elements and one cell. Axial deflection on the front and back faces was constrained to simulate plane strain. Three-dimensional load-deflection results are compared to plane strain results in Figure 3.4-14. Even with this simple model, good accuracy was achieved over a significant range of nonlinearity when compared with the two-dimensional model.

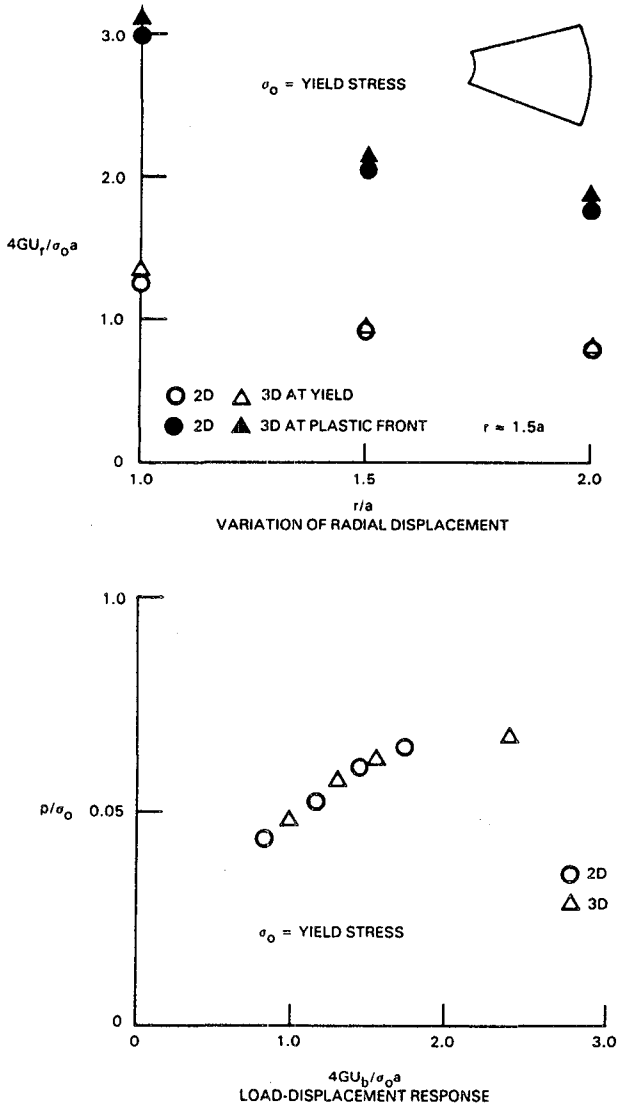

Figure 3.4-14 Load Displacement Response for One Cell

Figure 3.4-15 shows a similar comparison with the two-dimensional results for a discretization using ten surface elements and two volume cells. Since the two-dimensional program is probably the most accurate boundary element method program analysis to date, it serves to establish the correctness of the three-dimensional analysis.

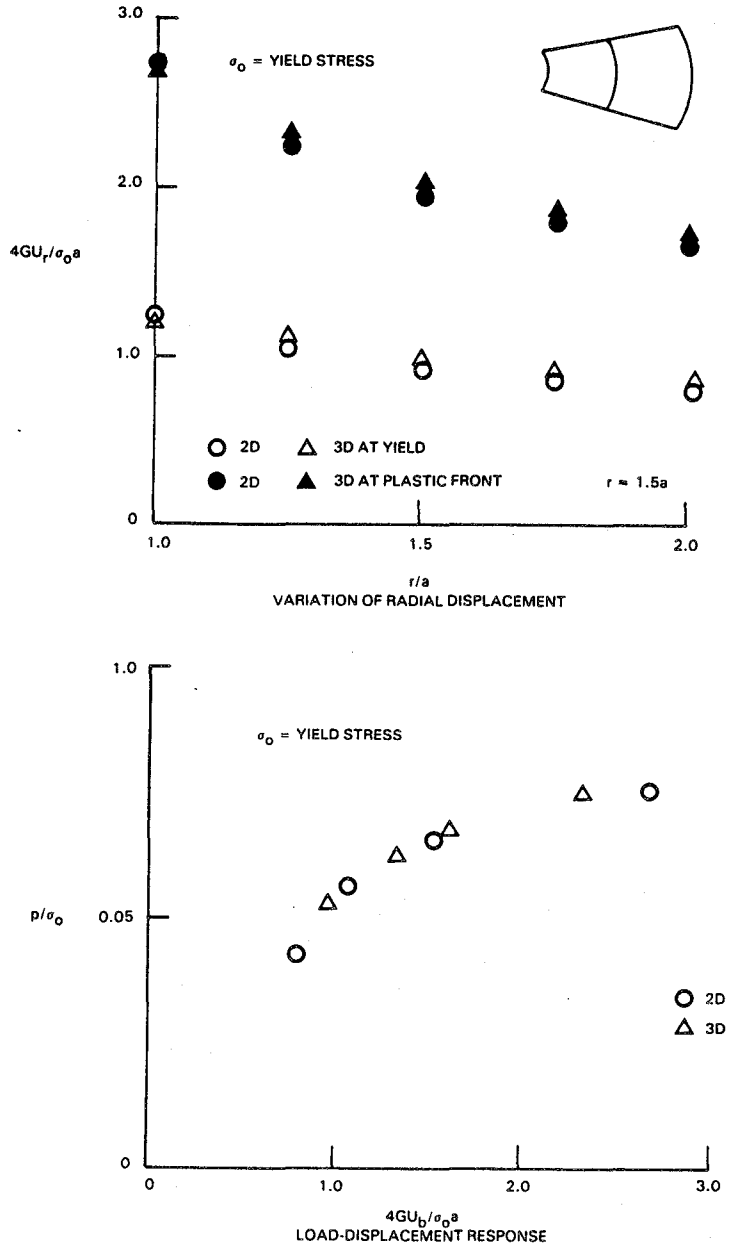

Figure 3.4-15 Load Displacement Response for Two Cells

Figure 3.4-16 shows the convergence of the radial displacement solution when the plastic front has reached the middle of the cylinder (r=1.5a) for the three-dimensional solution, where it can be seen that even a two-cell (10 boundary elements) representation provides a satisfactory solution. Similar convergence studies on the overall load-displacement response are shown in Figure 3.4-17, where the two-cell results are almost indistinguishable from the exact analytical solution.

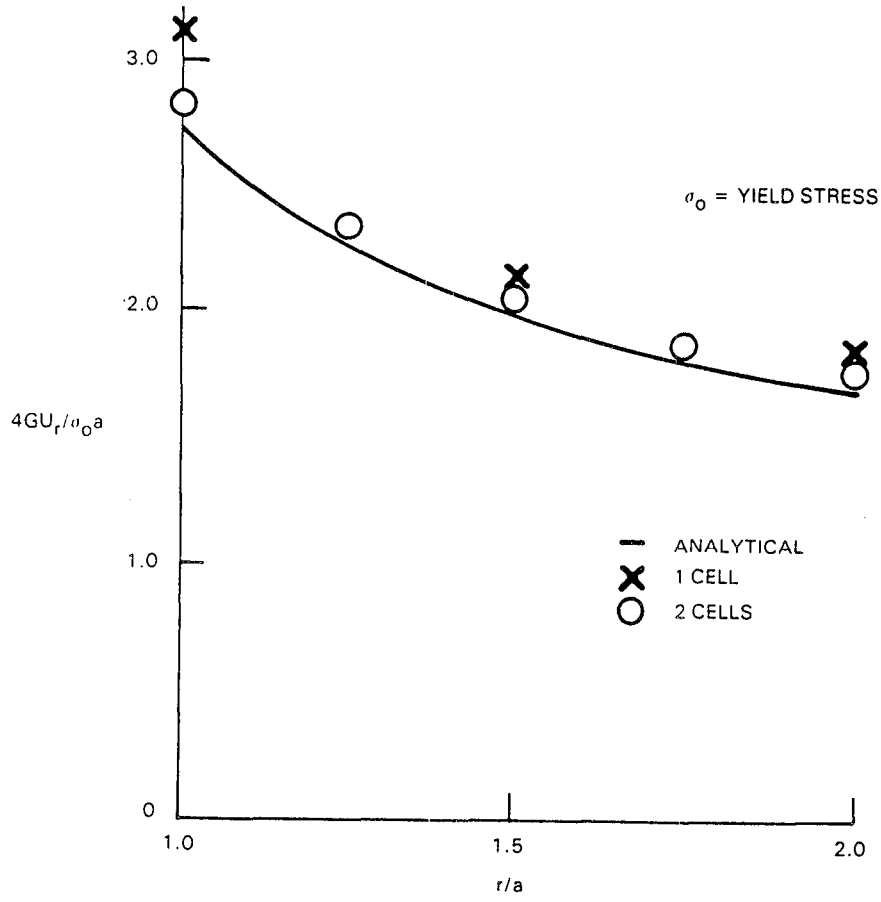

Figure 3.4-16 Variation of Radial Displacement When the Plastic Front Is At $r \approx 1.5a$ for a Three-Dimensional Analysis

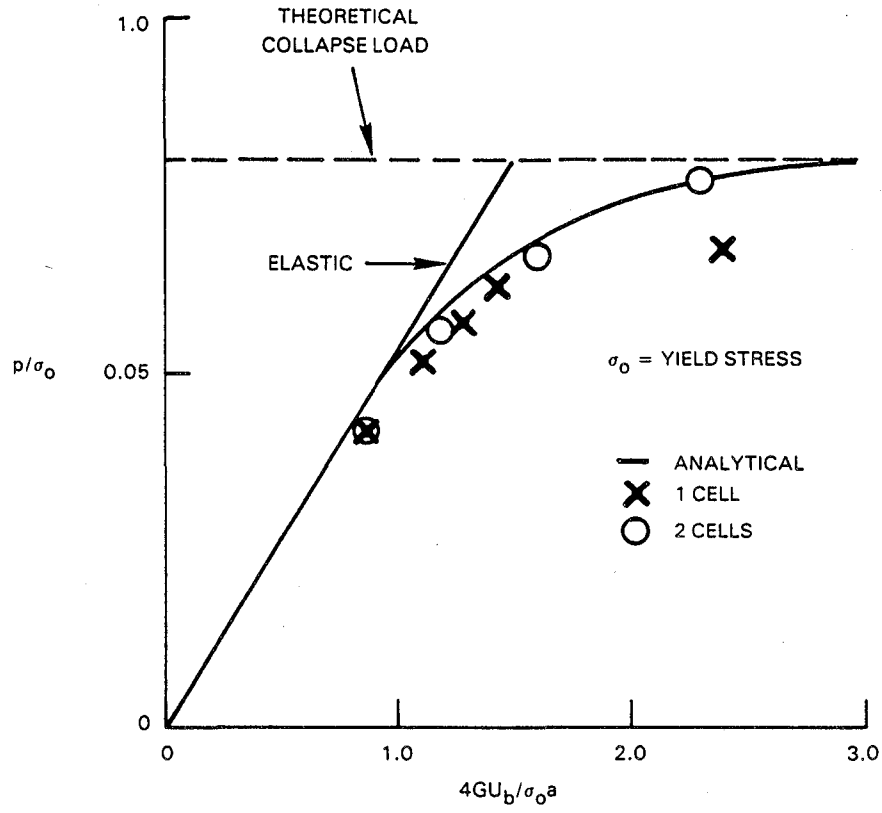

Figure 3.4-17 Convergence of the Load Displacement Response for the Three-Dimensional Analysis of a Thick Cylinder

4. Perforated Plate in Axial Tension (Figures 3.4-18 through 3.4-20)

Figure 3.4-18 shows the discretization for a perforated plate under axial loading (the X-direction). Thirty boundary elements (8 noded) and six cells (20 noded) have been used to define the problem. It is important to note that the cells are defined only in the high stress concentration region where yielding is likely to occur.

Figure 3.4-19 shows the overall load-displacement behavior obtained from the three-dimensional analysis compared with plane stress boundary element method results. Figure 3.4-20 shows the same comparison for the longitudinal stress distribution at the root of the plate. The results of the analyses agree very well with each other, indicating that the numerical implementation of nonlinear analysis within BEST is at least as accurate as the existing two-dimensional boundary element program.

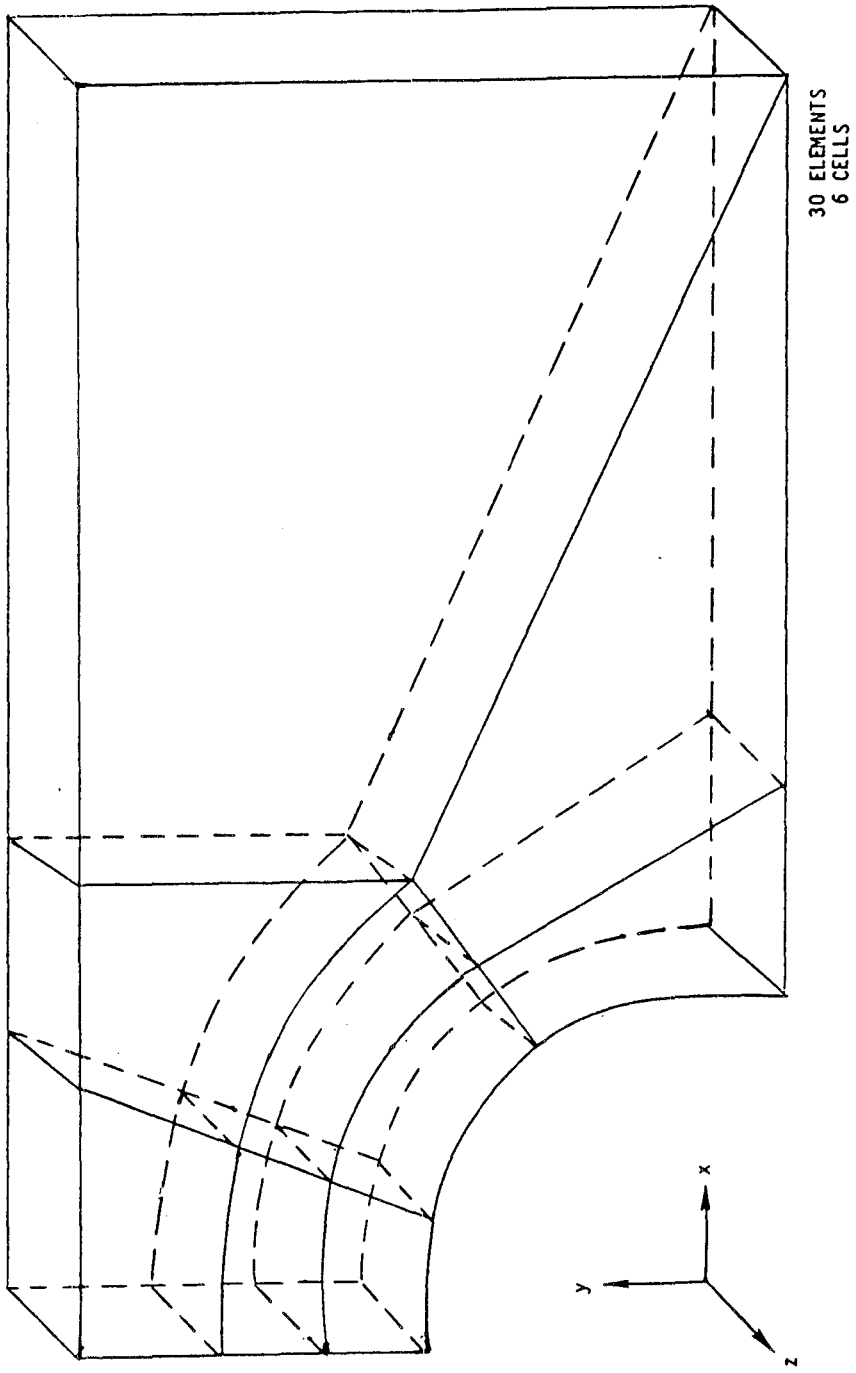

Figure 3.4-18 Perforated Plate in Tension

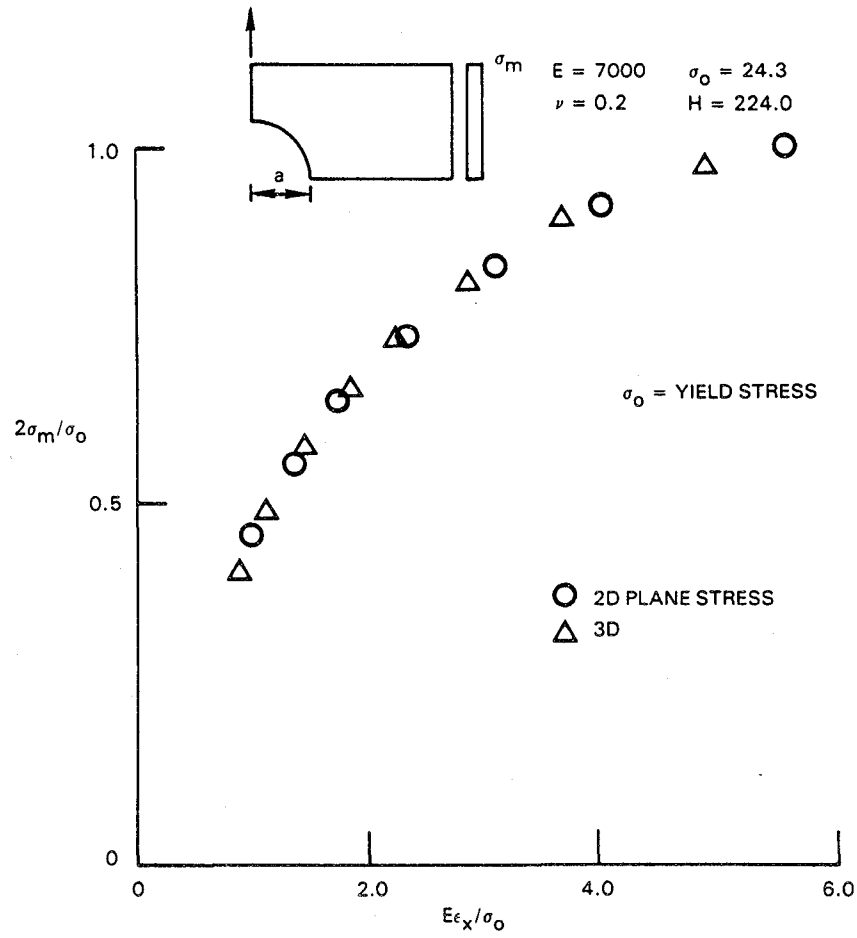

Figure 3.4-19 Stress-Strain at the Root of the Perforated Plate

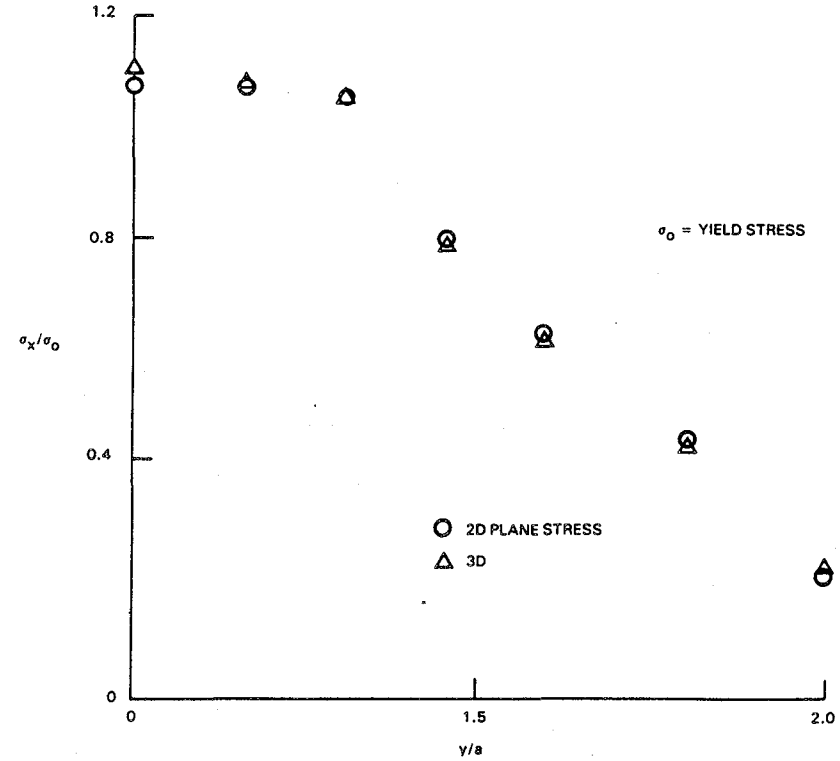

Figure 3.4-20 Perforated Plate - Stress Spread at $\sigma_m = 1.6(\sigma_m)$ at Yield

3.4.5.3 Validation of Dynamic Analysis

The dynamic/transient capabilities of the present program are implemented using transform techniques. The problem is recast in the Laplace or Fourier transform domain. In the case of a time harmonic loading the boundary element algorithm is exactly analagous to that for the static elastic case, except carried out in complex arithmetic. In the case of a more complex loading function (either a discrete sum of harmonic terms or an aperiodic loading), an appropriate transform of the boundary condition is taken, and the system equations are created and solved for a set of values of the transform parameter. The time domain solution must then be numerically reconstructed from the transform solution.

Test cases have been developed to test the time harmonic solution, the numerical transform inversion and the ability to solve problems with nonharmonic loading.

1. Cantilever Subject to Harmonic End Shear (Figure 3.4-21)

A long cantilever was modeled using a total of eighteen quadratic surface patches. A time harmonic shear load at a frequency of 314 radians/second was applied to the free end of the beam. The excellent agreement between the calculated three-dimensional response and analytical results (based on beam theory) for the envelope of the vibrating beam is shown in the referenced figure.

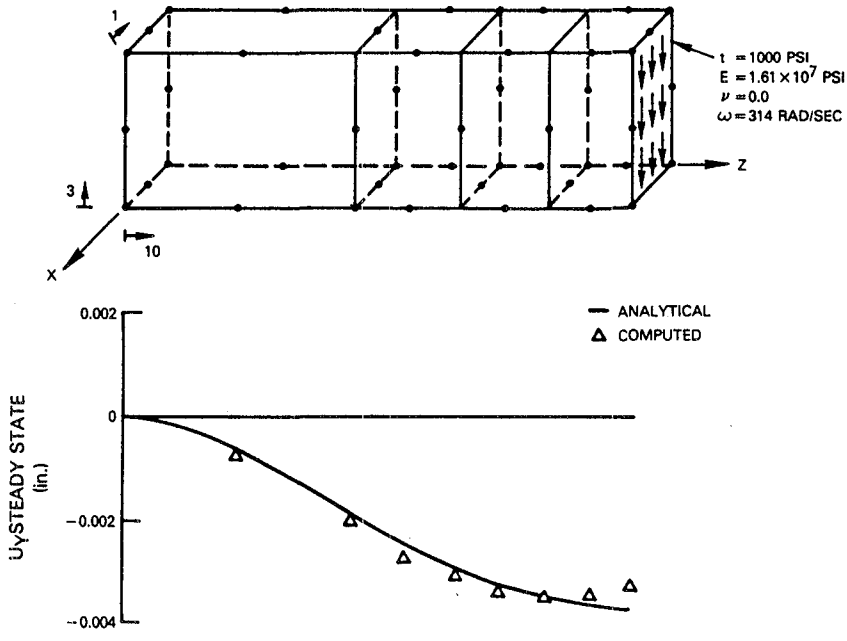

Figure 3.4-21 Cantilever Subject to Harmonic End Shear

2. Cantilever Subject to Harmonic Transverse Load (Figure 3.4-22)

The same model discussed in (1) was subjected to a time harmonic patch load. The agreement between the three-dimensional calculations and beam theory was, once again, excellent.

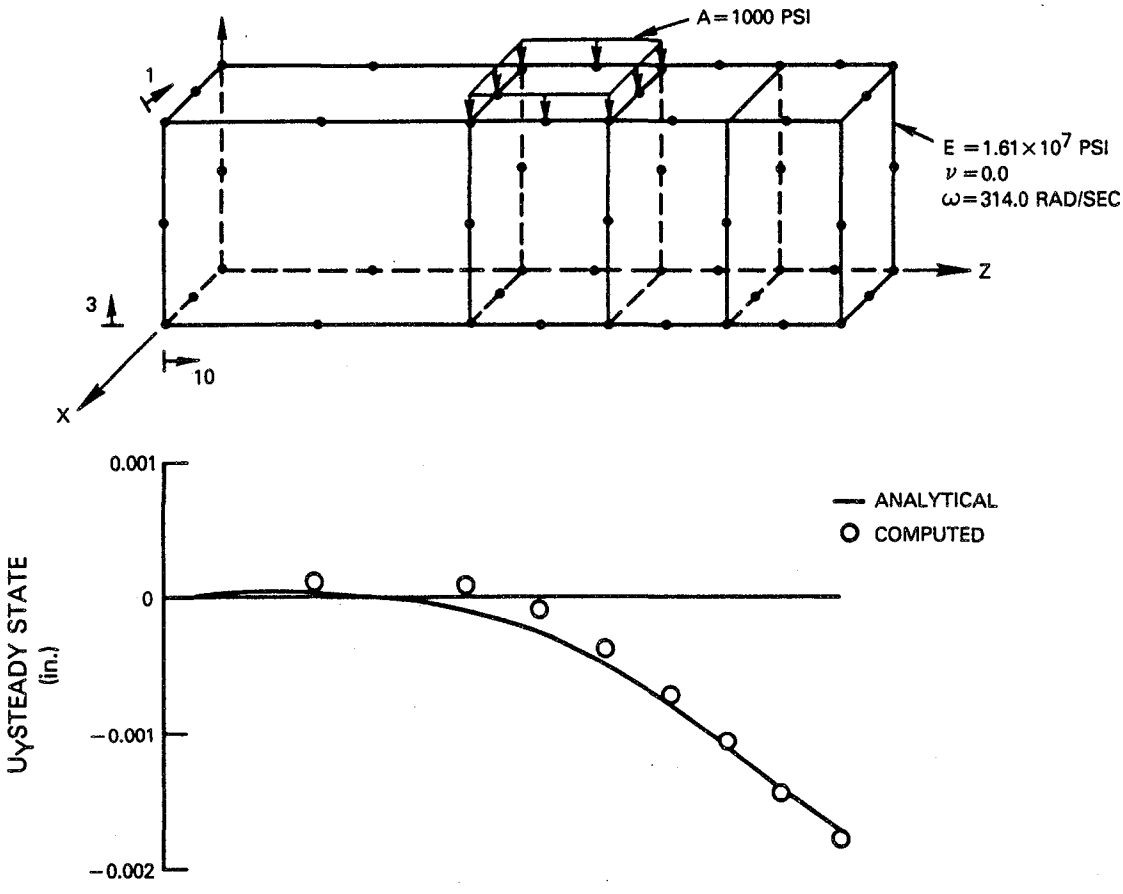

Figure 3.4-22 Cantilever Subject to Harmonic Transverse Load

3. Test Problem for a Time Dependent Analysis (Figures 3.4-23 and 3.4-24)

In order to test the numerical accuracy of the inversion of the transform domain solution, a problem of cantilever subjected to a time dependent loading at the free end was analyzed.

Figure 3.4-23 shows the surface discretization used for the problem as well as the calculated displacement response. The end displacement agrees very well with the exact analytical solution. The difference is mainly due to the way the applied loading was represented by the direct transform algorithm for a piece-wise linear approximation, as shown in Figure 3.4-24.

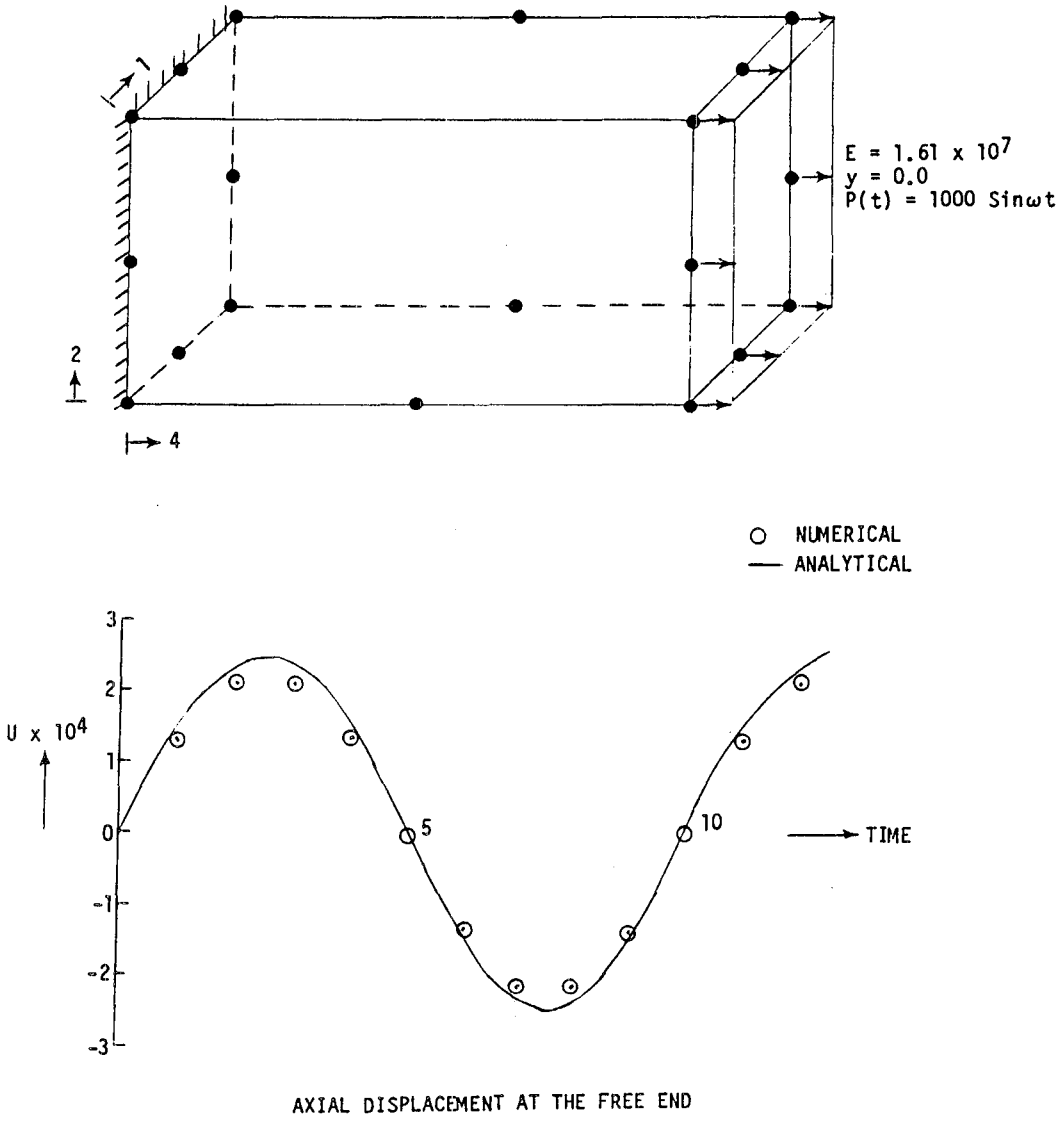

Figure 3.4-23 Transient Analysis of a Cantilever Subjected to a Harmonic Axial Loading

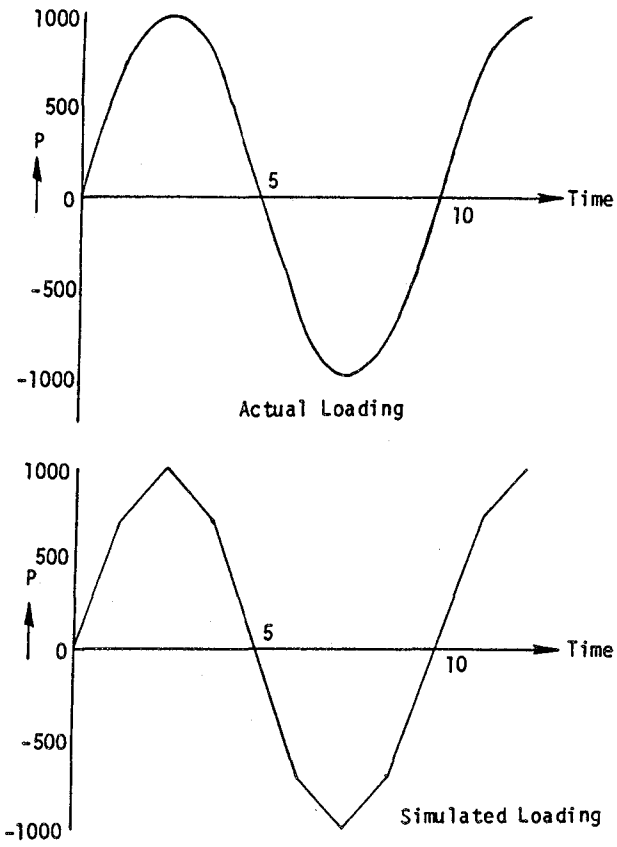

Figure 3.4-24 Cantilever Loading - Actual vs. Simulated

3.4.5.4 Notched Specimen Verification

Verification of this initial version of BEST is being carried out using test data and previous analytical results for notched specimens. The work done to date relates to specimen loading within the elastic range. The inelastic and creep analysis of one of these specimens is now being performed.

1. C-Notch Low Cycle Fatigue Specimen (Figure 3.4-25)

The C-notch low cycle fatigue specimen, as shown in the referenced figure, is designed to place a large volume of material in a plane strain, high stress condition. The specimen has, since its design several years ago, been subjected to a variety of elastic and inelastic analysis as well as to strain gage testing for specimen calibration.

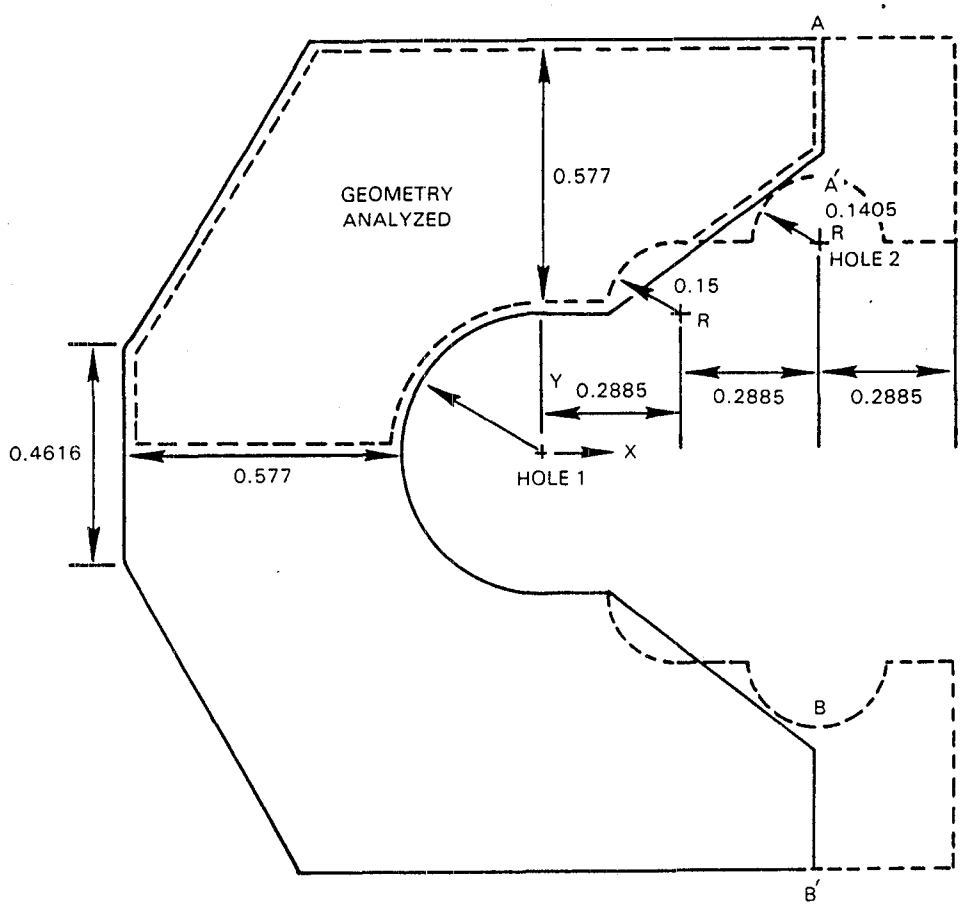

Figure 3.4-25 Cross Section of C-Notch Low Cycle Fatigue Specimen

In the present verification program the specimen was analyzed using BEST. The portion of the specimen which was analyzed is indicated in Figure 3.4-25. The mesh used is shown, in both full and hidden line views, in Figure 3.4-26. The analysis was carried out using both linear and quadratic variation of displacement and traction.

Key stress results are summarized in the table below. The plane strain results were obtained from a variety of two-dimensional codes. The baseline results were obtained from a very detailed three-dimensional analysis. The NASTRAN results cited were obtained using a mesh of twenty node isoparametric elements. The surface mesh refinement in the NASTRAN analysis was approximately equivalent to that in the BEST analysis.

	Plane Strain	Baseline	NASTRAN	BEST Quadratic	BEST Linear
σ_{xx} (midplane)	250	252	224	248	191
σ_{xx} (free surface)	---	150	136	158	138
σ_{zz} (midplane)	76	75	67	70	--

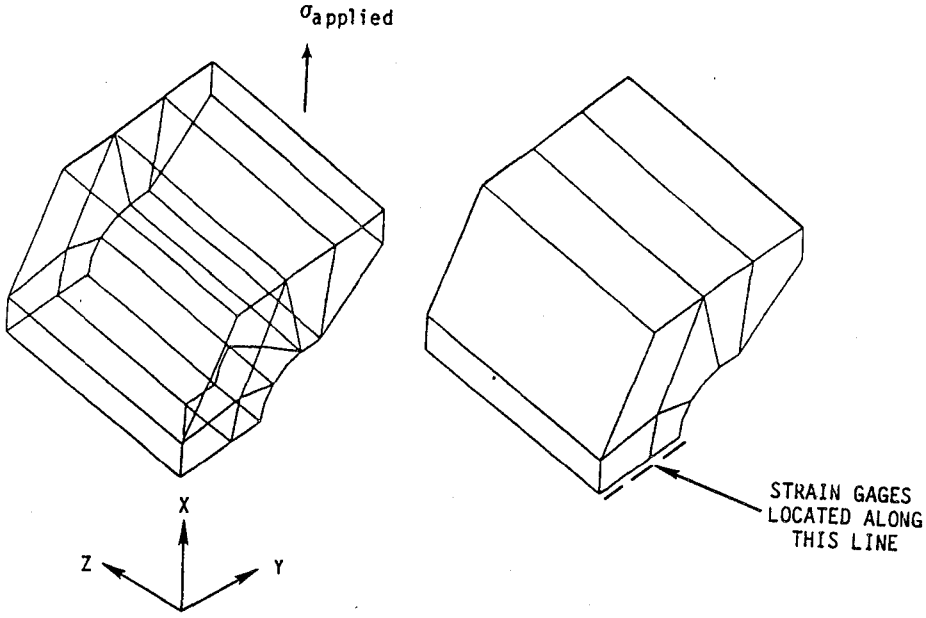

Figure 3.4-26 BEST Model for Analysis of C-Notch Low Cycle Fatigue Specimen

It is clear from the results above that BEST (using quadratic variation) is equivalent in accuracy to the previous baseline solution and to the plane strain results, and is superior to three-dimensional finite element analysis for an equivalent mesh.

It is also clear that the use of linear variation for the full model does not provide sufficiently accurate results. The linear results could be improved by mesh refinement, but the use of quadratic variation over the same mesh is more efficient both in input preparation and analysis cost.

The results of the quadratic BEST analysis are compared to strain gage data in Figure 3.4-27. The gages were located on the free surface of the specimen along the line shown in Figure 3.4-26. Agreement between the three-dimensional calculations and the data is generally good.

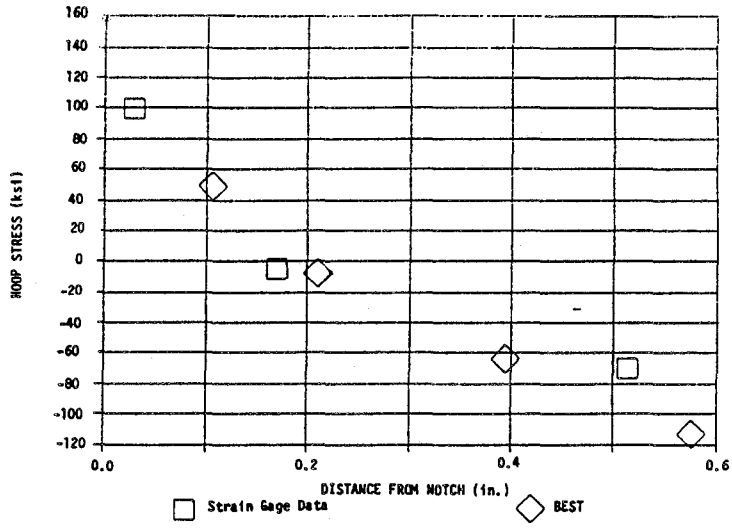

Figure 3.4-27 Comparison of Strain Gage Data With BEST Results for C-Notch Specimen

2. Benchmark Notch Specimen (Figure 3.4-28)

The benchmark notch specimen is a double edge notch specimen developed by General Electric/Louisiana State University (GE/LSU) under NASA-Lewis Contract NAS3-22522 (Reference 83). A significant volume of well documented data was provided as part of the referenced contract. These data have been used to verify the elastic capabilities of BEST. Verification of the inelastic capabilities of BEST, using this same data base, is now underway.

The specimen geometry is defined in Figure 3.4-28. Stress analysis was carried out for the gage section only, a procedure already known to be satisfactory (Reference 83). Three different models were used, all idealizing one-quarter of the specimen gage section. Detailed comparison of results was carried out among the BEST analyses, GE/LSU finite element results and Pratt & Whitney finite element results obtained using both MARC and MARC-HOST. While these comparisons are not discussed here, it should be noted that, with sufficient mesh refinement, equivalent results were obtained with all analysis tools.

The discussion in this report is directed at the comparison of BEST results with the GE/LSU strain gage data. The major characteristics of all of the BEST analyses are summarized in the table below. The maximum peripheral strain in the notch (at the free surface) is given for each analysis. All analysis methods and the test data show that this value should be between 1700 and 1800 (microstrain).

Model	Elements	Variation	Equations	GMRs	CPU Time (seconds)	Max Strain
1	50	linear	156	1	64	1688
2	50	quadratic	456	1	234	1780
3	22	linear	78	2	20	1594
4	22	quadratic	210	2	60	1742
5	22	mixed	117	2	31	1729
6	10	linear	36	1	10	1186
7	10	quadratic	96	1	28	1605

It is clear from the table that models 2, 4 and 5 all yield results of accuracy entirely comparable with the strain gage data. The variation in peak strain among these three is within $\pm 1.5\%$. It is also clear that the most cost effective analysis is that which combines substructuring with mixed linear and quadratic variation. As was the case for the C-notch specimen, fully linear analysis cannot give acceptably accurate results without unacceptable mesh refinement.

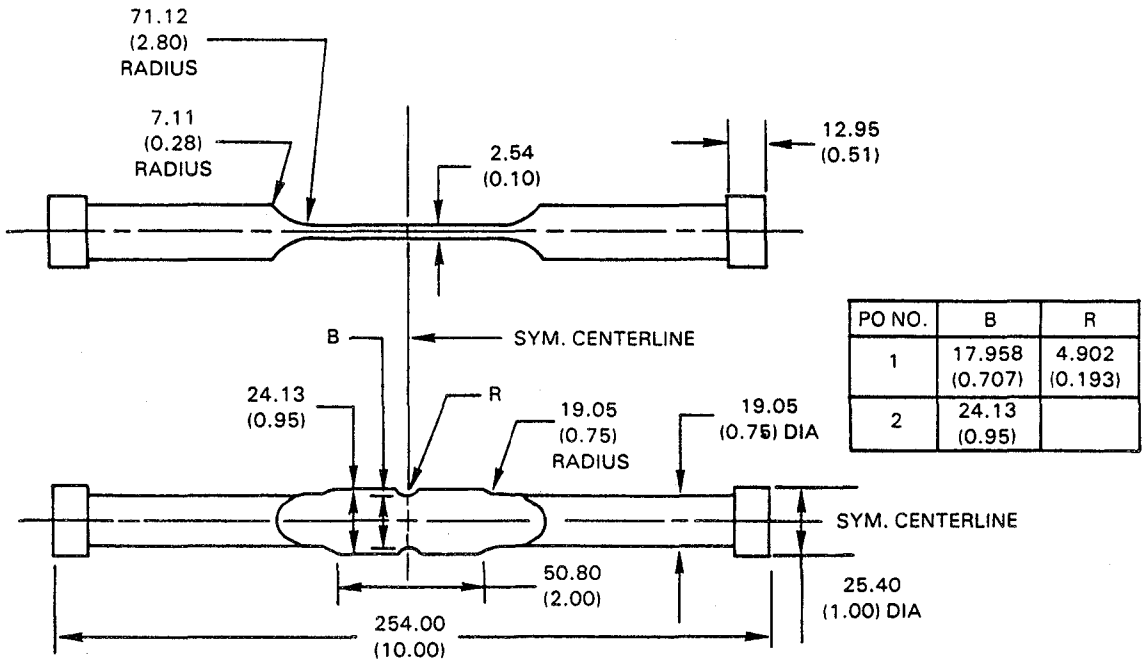

PO NO.	B	R
1	17.958 (0.707)	4.902 (0.193)
2	24.13 (0.95)	

Figure 3.4-28 Double Edge Notch Specimen Used in Contract NAS3-22522

The mixed model is shown in Figure 3.4-29, in both full and hidden line views. In this model eight of the twenty-two elements (those in and near the notch) were quadratic, while the remaining fourteen were linear. The visible elements in the hidden line plot are identified as linear or quadratic. The fully linear and quadratic models (4 and 6) utilized an identical surface discretization to that shown. The results of these three analyses (4, 5 and 6) are plotted with the GE/LSU strain gage results in Figure 3.4-30. Both the fully quadratic and mixed analyses are in excellent agreement with the strain gage data. The difference between the two analyses is far less than the normal scatter in strain gage data. The fully linear analysis, however, does not give either an accurate peak strain or a correct representation of the strain distribution near the notch.

Also shown in Figure 3.4-29 is a pattern of eight volume cells. These cells are used for the representation of inelastic strain in the nonlinear analysis of the specimen under various loadings. The cell pattern was designed to include the portion of the specimen gage section which experiences inelastic response during the tests described in Reference 83.

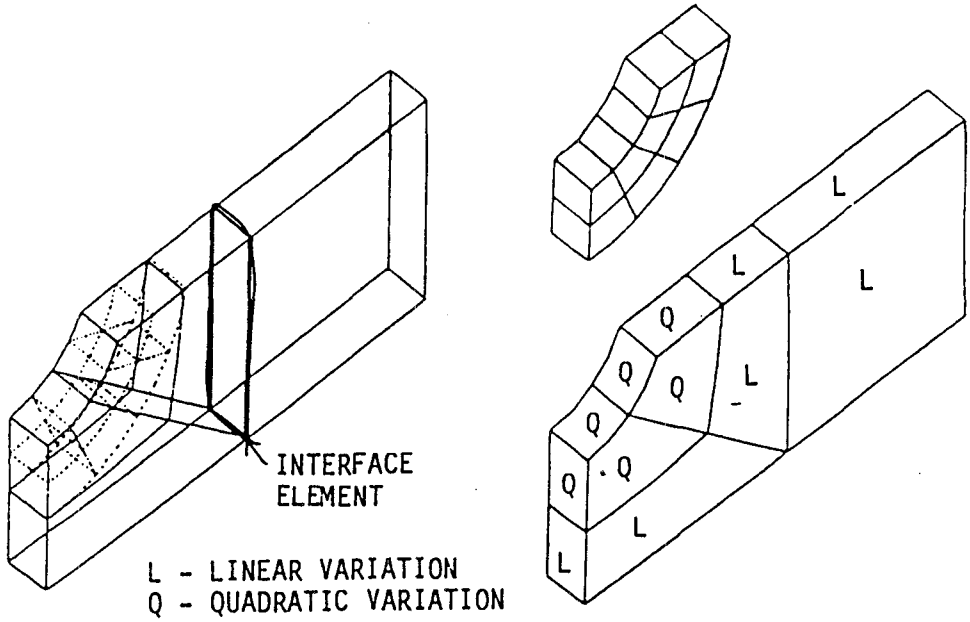

Figure 3.4-29 Optimized Model for Analysis of Benchmark Notch Specimen

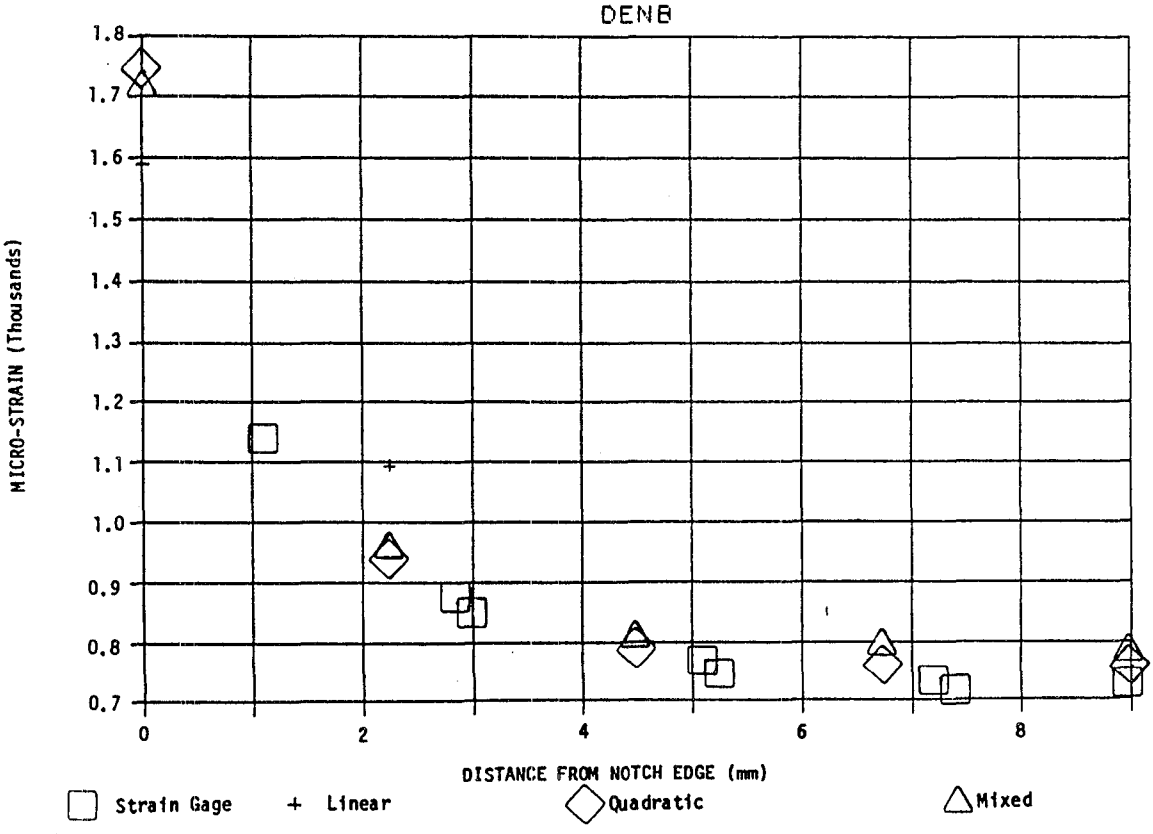

Figure 3.4-30 Comparison of BEST Results With Strain Gage Data

3.4.5.5 Hot Section Component Analysis

In order to evaluate the capabilities of the present version of BEST for the analysis of real components, an analysis of a commercial cooled turbine blade geometry was carried out. It is expected that the use of this analysis as a benchmark problem will be continued throughout the life of the Inelastic Methods program. This report discusses preliminary results for the elastic analysis of the blade.

The blade analyzed is a cooled high turbine blade presently in service. It is subject to mechanical loads (primarily centrifugal) and thermal loads. Of particular interest for this blade is the location and magnitude of the peak stress under the platform.

A BEST model was built for this problem. Both full and hidden line views of the model are shown in Figure 3.4-31. The model consists of five GMRs. The interfaces between GMRs are generally perpendicular to the radial direction. The characteristics of the model are summarized below.

GMR	Elements	Linear Source Points	Quadratic Source Points
1	60	61	180
2	86	85	256
3	107	98	303
4	106	96	298
5	80	76	232

The system equations for a fully linear analysis contain 1248 equations.

To date only a fully linear analysis for centrifugal loads has been carried out. Analysis of the results is still in a preliminary stage. The total centrifugal load at various spanwise stations on the blade has been compared with the design calculations for the blade (Figure 3.4-32). The agreement between the two totally independent calculations is excellent. The total centrifugal load for the blade is within 2% of the design calculation. The larger local error near the blade platform is believed to be due to the fact that the design calculation models the platform as a discontinuous addition of mass.

Extremely preliminary study of blade tip deflections, load distribution over the base of the blade neck and concentrated stresses indicates reasonable agreement with finite element results. Contour plots of principal stress contours have verified that the peak stress occurs in the correct location. It is clear, however, from the results of the verification problems that at least some use of quadratic variation will be required to achieve correct definition of critical stresses and strains.

A fully quadratic analysis of this problem would lead to a system of over 3800 equations. Analysis time, on the IBM 3081, would be approximately one hour, compared to about 16 minutes for the fully linear analysis. The results of the benchmark notch analysis clearly indicate that it should be possible to achieve acceptably accurate results at reasonable cost through the use of mixed variation. Present efforts are directed at identifying those areas of the model requiring quadratic variation and/or mesh modification.

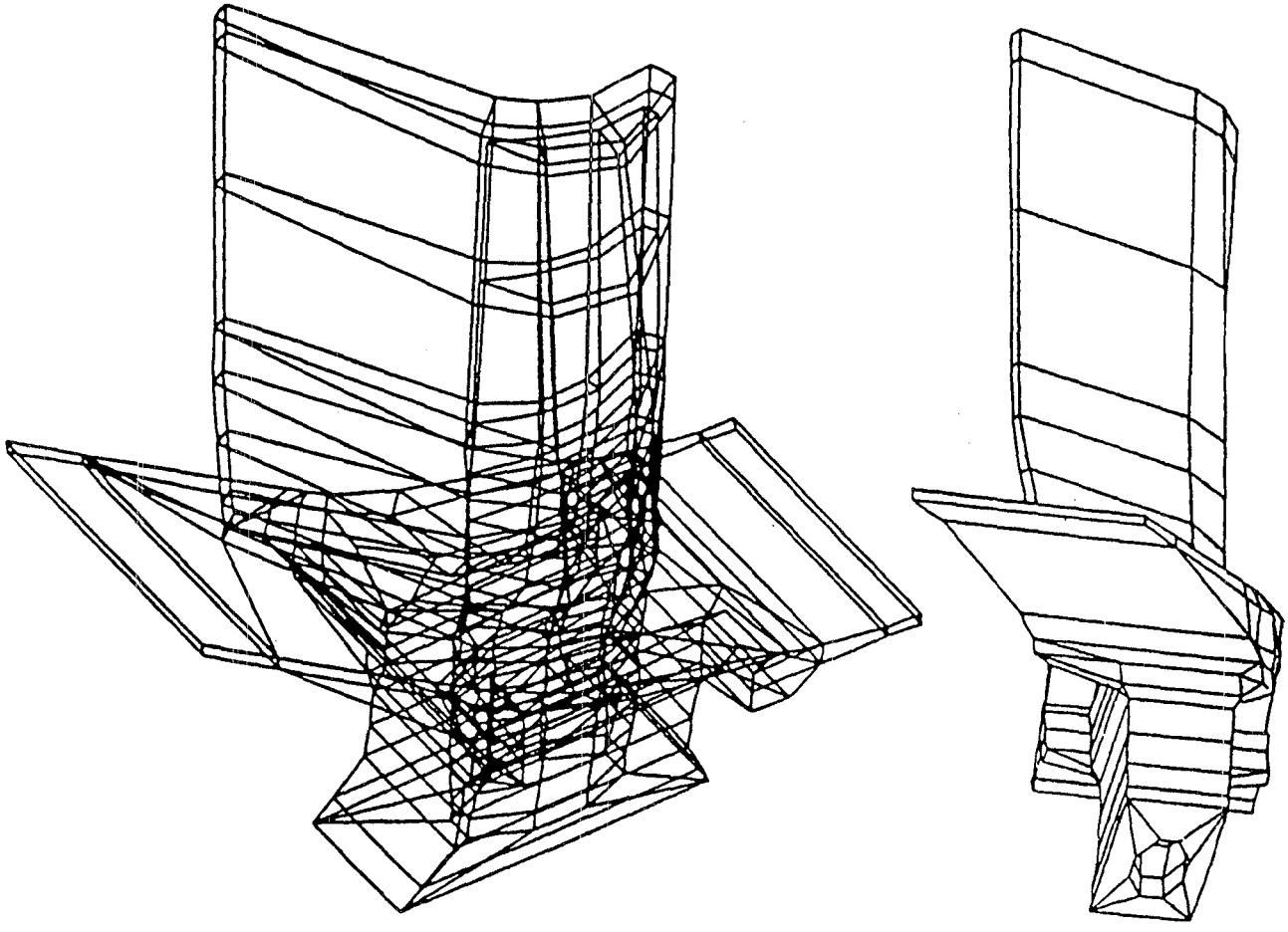

Figure 3.4-31 BEST Model of Cooled Turbine Blade

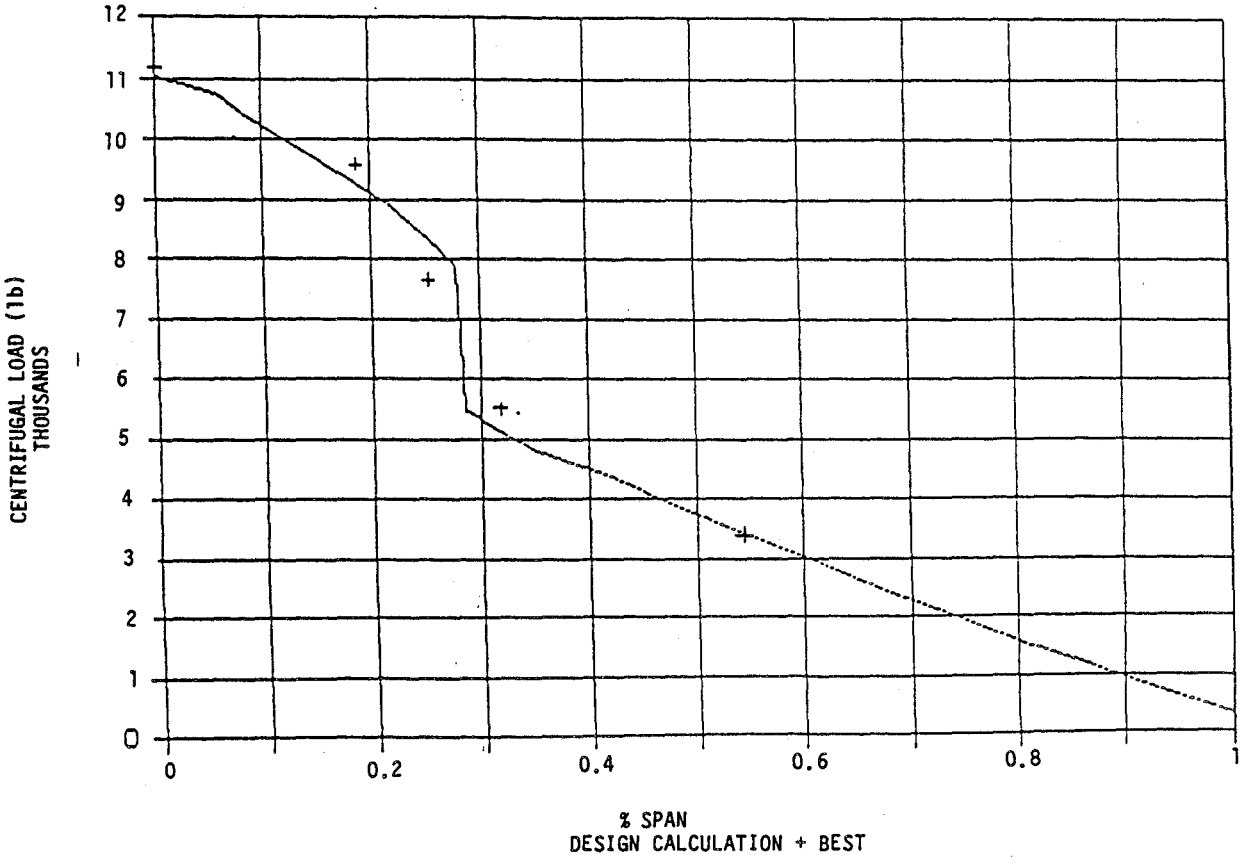

Figure 3.4-32 Centrifugal Load Distribution in a Cooled Turbine Blade

3.4.6 Boundary Element Stress Technology (BEST) Program U911 - Input Description

The input to U911 is divided into six sections as follows:

1. Case control (**CASE control)
2. Material properties (**MATErial property)
3. Generic modeling regions (**GMRegion)
4. Interfaces (**INTErface)
5. Boundary condition sets (**BCSEt)
6. Body forces (**BODY force).

A detailed description of each of these sections is provided in the following paragraphs. The interface and body force sections are optional; the other sections must be input at least once.

Input quantities may be either alphanumeric or numeric (integer, floating point, E, or D format) as specified and may be up to 16 characters. Individual entries on a card (both keyword and input) must be separated by at least one blank space. Input for certain keywords (as noted) may be continued onto more than one card by repeating the keyword on the new card(s).

Keywords may be input as shown; minimum input is the CAPITALIZED characters. Those keywords which are underscored must always be input. Keywords shown below are indented to indicate groups of cards to be input together. However, it is not necessary to indent the input in this manner.

Consistent units must be used. Angles are in degrees, speed is in revolutions per minute, and frequency is in radians per sound.

The current program limits include:

- 20 time points
- 10 generic modeling regions
- 15 surfaces per region
- 600 elements (416 quadratic elements in problems with body forces, 300 elements in problems having interior points)
- 11 infinite elements per region
- 2500 nodes (560 nodes per region)
- 1200 source points (600 source points in problems having interior points)
- 302 source points per region in a local coordinate system
- 99 interface and cyclic symmetry element pairs (total)
- 350 interface and cyclic symmetry node pairs (total)
- 20 boundary condition sets with cyclic symmetry
- 60 boundary condition sets with springs
- maximum element number of 9999
- maximum node number of 9999
- maximum of 24 entries per input card.

3.4.6.1 Case Control Input

The case control input section may be input only once.

Keyword	Type of Input	Input
**CASE control		
TITLe	Alphanumeric	Case title
CENTrifugal		
DYNAmic	Numeric	Frequency value, damping coefficient
INHOmogeneous		
THERmal		
PLASticity		
RESTart	Alphanumeric	READ or WRITE
TIMEs	Numeric	Output time value(s)
TRANsient	Numeric	Number of time intervals, time increment, damping coefficient

The analysis is assumed to be static, homogeneous, constant temperature, elastic, and time independent unless the appropriate optional keyword is input. The optional keywords need be included only if a particular option is to be turned on.

The case title should have a maximum of 72 characters.

Input on the TIMEs card may be continued on more than one card.

3.4.6.2 Material Property Input

The material property input section must be repeated for each separate material.

Keyword	Type of Input	Input
**MATErial property		
ID	Alphanumeric	Material name
ISOTropic		
TEMPerature	Numeric	Temperature value(s)
EMODulus	Numeric	Young's modulus value(s)
ALPHa	Numeric	Alpha value(s)
DENSity	Numeric	Mass density value
POISson	Numeric	Poisson's ratio value

Keyword	Type of Input	Input
ANISotropic		
TEMPerature	Numeric	Temperature value
ALPHa	Numeric	Alpha value
CONStants	Numeric	Elastic constant values
DS		
INELastic		
MONOtonic		
CYCLic		
ISOTropic		
TIME	Numeric	Time point identifier(s) for slow algorithm
YIELd	Numeric	Proportional limit value
CURVe	Numeric	Stress value, plastic strain value
TWO surface		
TIME	Numeric	Time point identifier(s) for slow algorithm
YIELd	Numeric	Inner proportional limit value, outer proportional limit value
HARD	Numeric	Inner hardening parameter, outer hardening parameter
WALKER		

If the material name is a material library designation, then the TEMPerature, EMODulus, ALPHa, DENSity, and POISson cards may be omitted. However, any of them may be included to override the material library data.

The Young's modulus and alpha values must be input in the same order as the temperature values.

A DS card (indicating a directionally solidified material) must be included in ANISotropic input. The constants to be input for a directionally solidified material are C_{11}, C_{13}, C_{33}, C_{44}, and C_{66}.

Either a MONOtonic card (indicating monotonic loading) or a CYCLic card (indicating cyclic loading) must be included in INELastic input. Either the ISOTropic model, or the TWO surface model, or the WALKer must be used in INELastic input.

The value of stress at zero plastic strain (i.e., proportional limit) need not be included in CURVe input. The stress and strain values input should start with the first nonzero value of plastic strain, A HARDening parameter is calculated and used if a single stress/strain pair is input. Otherwise, the multipoint stress/strain algorithm is used.

Input on the TEMPerature, EMODulus, ALPHa, CONStants, and YIELd cards may be continued on more than one card.

3.4.6.3 Generic Modeling Region Input

The generic modeling region section must be repeated for each region.

Keyword	Type of Input	Input
**GMR		
ID	Alphanumeric	Region name
INHOmogeneous		
THERmal		
PLASticity		
MAT	Alphanumeric	Material name
TREFerence	Numeric	Reference temperature value
POINts	Numeric	Node number, coordinate values (x,y,z)
SURFace	Alphanumeric	Surface name, (reference surface name)
TYPE	Alphanumeric	LINI or QUAD
ELEMents	Numeric	(I), element number, node numbers, (ref. node)
TRANslate	Numeric	Translation values (x,y,z)
REF	Numeric	Axis of rotation reference point (x,y,z)
DIR	Numeric	Axis of rotation direction (x,y,z)
ROT	Numeric	Axis of rotation angle (degrees)
NORMal	Alphanumeric	Element number, + or -
VOLUme		
POINts	Numeric	Point number, coordinate values (x,y,z)
TYPE	Alphanumeric	LINI or QUAD
CELLs	Numeric	Cell number, node numbers (nodes 1 to 10) Cell number, node numbers (nodes 11 to 20)

The SURFace input may be either of two forms:

- a TYPE card and an ELEMents card to define element connectivity
- a REF card, a DIR card, a ROT card, and/or a TRANslate card to define one surface with reference to another surface (translations are performed first, followed by rotations).

The TYPE designation in SURFace input specifies the traction or displacement variation on the element. A surface may contain only one TYPE card. Therefore, if mixed variation is required in a region, two surfaces must be defined.

Elements must have either 6 (triangles) or 8 (quadrilaterals) nodes. Element numbering is consecutive around the boundary.

Infinite elements are indicated by an I on the element card and may have 7 (triangles) or 9 (quadrilaterals) nodes, where the extra node is the reference node. If the reference node is not input, it is assumed to be at the origin.

The sign associated with the defining element on the NORMal card should be plus (+) if the element is numbered in a counterclockwise direction as seen from the outside of the model or minus (-) if it is numbered in a clockwise direction. Disjoint boundaries must have multiple element/sign pairs on the NORMal card.

The points which are input in the VOLUme input (both points and cell nodes) are treated as "interior" points. These points may be either nodal points, other surface points, or true interior points. The TYPE designation in VOLUme input specifies cell source points (i.e., 8 corner nodes or all 20 nodes).

Cells must have 20 nodes. Cell numbering is consecutive around the "front" face boundary, followed by the four midplane nodes, followed by the "back" face boundary.

3.4.6.4 Interface Input

The interface section must be repeated for each interface.

Keyword	Type of Input	Input
**INTErface		
GMR	Alphanumeric	Region name of first region
SURFace	Alphanumeric	Surface name in first region
ELEMents	Numeric	Element number(s) in first region
POINts	Numeric	Node number(s) in first region
GMR	Alphanumeric	Region name of second region
SURFace	Alphanumeric	Surface name in second region
ELEMents	Numeric	Element number(s) in second region
POINts	Numeric	Node number(s) in second region
SLIDing		

The interface is assumed to have complete displacement compatibility unless a SLIDing card is input, in which case only normal displacement compatibility is assumed.

The ELEMents card and/or the POINts card are included in SURFace input only to designate a subset of that surface.

Input on the ELEMents and POINts cards may be continued on more than one card.

3.4.6.5 Boundary Condition Set Input

The boundary condition set section must be repeated for each new boundary condition.

Keyword	Type of Input	Input
**BCSEt		
ID	Alphanumeric	Boundary condition set name
GMR	Alphanumeric	Region name
VALUe		
RELATion		
SURFace	Alphanumeric	Surface name
ELEMents	Numeric	Element number(s)
POINts	Numeric	Node number(s)
TIMEs	Numeric	Input time value(s)
LOCAl		
CYCLic		
GMR	Alphanumeric	Region name
SURFace	Alphanumeric	Surface name
ELEMents	Numeric	Element number(s)
POINts	Numeric	Node number(s)
ANGLe	Numeric	Axis of rotation angle (degrees)
DIR	Numeric	Axis of rotation direction (x,y,z)
DISPlacement	Numeric	Component value
SPLIst	Numeric	Source point value(s) or ALL or SAME
T	Numeric	Time point identifier, displacement value(s)
RIGId	Numeric	Component value
SPRIng	Numeric	Component value, spring value
TRACtion		
SPLIst	Numeric	Source point value(s) or ALL or SAME
T	Numeric	Time point identifier, traction value(s)

The ELEMents card and/or the POINts card are included in SURFace input only to designate a subset of that surface.

The TIMEs card must be omitted in a boundary condition set which contains a RIGId card. If the value(s) on the TIMEs card differ from those values in the case control input, the output is calculated by linear interpolation. In the case of time independence (i.e., the TIMEs card is omitted) the time point identifier on the T card must be 1 (one).

The LOCAl card designates input in the outward normal direction. The component value on the CYCLic, DISPlacement, RIGId, SPRIng, or TRACtion card must be 1 (one). Care must be taken not to mix global and local coordinate systems on a particular element. Care must also be taken not to input conflicting components on a particular node in a particular element.

The VALUe card should be included with the DISPlacement card, the RIGId card, or the TRACtion card. The RELAtion card should be included with the CYCLic card or the SPRIng card.

Either CYCLic input, or DISPlacement input, or RIGId input, or SPRIng input, or TRACtion input must be included in a boundary condition set. This input set may be included up to three times (once for each component) in a boundary condition set. However, different boundary condition types may not be mixed in a boundary condition set.

The cyclic symmetry direction (DIR card) defaults to the z-axis (0,0,1).

The SPLIst card indicates the order in which the values are to be input on the T cards. The input may be in either of three forms:

- nodal values
- ALL to indicate that a single constant value is to be input
- SAME to use the previous source point list within the current boundary condition set (this option may not be used for the first source point list in the current boundary condition set).

Input on the ELEMents, POINts, SPLIst, and TIMEs cards may be continued on more than one card. Input on the T card may be continued on more than one card, including the time point identifier on each card.

3.4.6.6 Body Force Input

The body force section is optional.

Keyword	Type of Input	Input
**BODY force		
CENTrifugal		
DIR	Numeric	Axis of rotation direction (x,y,z)
PT	Numeric	Axis of rotation reference point (x,y,z)
SPEEd	Numeric	Speed value(s)
TIMEs	Numeric	Time value(s)
THERmal		
TIMEs	Numeric	Time value(s)
TEMPeratures	Numeric	Node number, temperature value(s) at time(s)

The CENTrifugal card and the TIMEs card must be included in the case control section in order to input centrifugal body forces.

The direction (DIR card) defaults to the z-axis (0,0,1). The reference point (PT card) defaults to the origin (0,0,0).

Input on the SPEEd and TIMEs cards may be continued on more than one card.

3.4.7 Sample Output from BEST

3.4.7.1 Input Echo

```
**** INPUT ECHO ****

 LINE            INPUT
    1     **CASE
    2       TITLE       U911 TEST CASE - CUBE IN SIMPLE TENSION WITH PLASTICITY
    3       TIMES    1.00        2.00        3.00        4.00        5.00
    4       PLASTICITY
    5     **MATE
    6       ID MAT1
    7         TEMP     70.0000
    8         EMOD     100.000
    9         POIS     .250000
   10         DENS     1.00000
   11       INELASTIC
   12         YIELD    100.
   13         TIMES     4
   14         CURVE
   15           150.      1.
   16     **GMR
   17       ID GMR1
   18       PLASTICITY
   19       MAT MAT1
   20       TREF 70.
   21       POINTS
   22              1     .0              .0              .0
   23              2     .0              .0              .500000
   24              3     .0              .0              1.00000
   25             11     .0              .500000         .0
   26             13     .0              .500000         1.00000
   27             21     .0              1.00000         .0
   28             22     .0              1.00000         .500000
   29             23     .0              1.00000         1.00000
   30            101     .500000         .0              .0
   31            103     .500000         .0              1.00000
   32            121     .500000         1.00000         .0
   33            123     .500000         1.00000         1.00000
   34            201     1.00000         .0              .0
   35            202     1.00000         .0              .500000
   36            203     1.00000         .0              1.00000
   37            211     1.00000         .500000         .0
   38            213     1.00000         .500000         1.00000
   39            221     1.00000         1.00000         .0
   40            222     1.00000         1.00000         .500000
   41            223     1.00000         1.00000         1.00000
   42       SURFACE SURF11
   43         TYPE LINI
   44         ELEMENTS
   45                 1     1     2     3    13    23    22    21    11
   46                 2   201   202   203   213   223   222   221   211
   47                 3     1     2     3   103   203   202   201   101
   48                 4    21    22    23   123   223   222   221   121
   49                 5     1    11    21   121   221   211   201   101
   50                 6     3    13    23   123   223   213   203   103
   51       NORMAL       1 +
   52       VOLUME
   53         TYPE QUAD
   54         CELLS
```

3.4.7.2 Case Control Summary

```
          **** CASE CONTROL INPUT ****

 JOB TITLE        U911 TEST CASE - CUBE IN SIMPLE TENSION WITH PLASTICITY
     TIMES FOR SOLUTION:       1.00      2.00      3.00      4.00      5.00
     PLASTICITY FLAG     1                       THERMAL FLAG      0
     CENTRIFUGAL LOAD FLAG     0                 TRANSIENT FLAG      0
     DYNAMIC FLAG      0                         INTEGRATION EPSILON    0.0010
     INTEGRATION GRADING FACTOR    1.4142        RESTART FLAG      0


         **** MATERIAL INPUT ****

     MATERIAL NAME MAT1
     INELASTIC
     ISOTROPIC
     YIELD STRESS:        100.00

          STRESS          STRAIN
        0.10000E+03     0.0
        0.15000E+03     0.10000E+01

     DENSITY:    1.0000  POISSONS RATIO:    0.2500

          TEMP          ALPHA                  E
        0.70000E+02     0.0             0.10000E+03
```

3.4.7.3 Generic Modeling Region (GMR) Definition

```
      **** GMR INPUT ****

 REGION     1
 NAME GMR1              MATERIAL MAT1        REFERENCE TEMPERATURE    70.00
 NODES    20            ELEMENTS     6       SURFACES     1
 SOURCE POINTS     8    CELLS      1         INFINITE ELEMENTS    0

 COORDINATE LIST
   NODE      X         Y         Z                NODE      X         Y         Z

     1     0.0       0.0       0.0                 2     0.0       0.0       0.5000
     3     0.0       0.0       1.0000             11     0.0       0.5000    0.0
    13     0.0       0.5000    1.0000             21     0.0       1.0000    0.0
    22     0.0       1.0000    0.5000             23     0.0       1.0000    1.0000
   101     0.5000    0.0       0.0               103     0.5000    0.0       1.0000
   121     0.5000    1.0000    0.0               123     0.5000    1.0000    1.0000
   201     1.0000    0.0       0.0               202     1.0000    0.0       0.5000
   203     1.0000    0.0       1.0000            211     1.0000    0.5000    0.0
   213     1.0000    0.5000    1.0000            221     1.0000    1.0000    0.0
   222     1.0000    1.0000    0.5000            223     1.0000    1.0000    1.0000

 SURFACE SURF11         LINEAR VARIATION
         1          1     2     3    13    23    22    21    11
         2        201   211   221   222   223   213   203   202
         3          1   101   201   202   203   103     3     2
         4         21    22    23   123   223   222   221   121
         5          1    11    21   121   221   211   201   101
         6          3   103   203   213   223   123    23    13

 SOURCE POINT LIST
1     3    21    23   201   203   221   223

 CELL INPUT
1     3     2     1    11    21    22    23    13   103   101   121   123   203   202   201   211   221   222   223   213
```

3.4.7.4 Boundary Condition Definition

```
          **** BOUNDARY CONDITION INPUT ****

BOUNDARY CONDITION SET NAME TRAC11          TYPE: VALUE
GMR GMR1            SURFACE SURF11

ELEMENT LIST
    2

SOURCE POINT LIST
  201   203   223   221
LOCAL (NORMAL) COORDINATE SYSTEM

TIME VALUES:
  1.0000   2.0000   3.0000   4.0000   5.0000

COMPONENT      1 TRACTION INPUT

TIME =      1.00       DATA VALUES:
 0.10000E+03  0.10000E+03  0.10000E+03  0.10000E+03

TIME =      2.00       DATA VALUES:
 0.10500E+03  0.10500E+03  0.10500E+03  0.10500E+03

TIME =      3.00       DATA VALUES:
 0.12000E+03  0.12000E+03  0.12000E+03  0.12000E+03

TIME =      4.00       DATA VALUES:
 0.11250E+03  0.11250E+03  0.11250E+03  0.11250E+03

TIME =      5.00       DATA VALUES:
 0.67500E+02  0.67500E+02  0.67500E+02  0.67500E+02
```

3.4.7.5 Boundary Solution (Element Basis)

JOB TITLE: U911 TEST CASE - CUBE IN SIMPLE TENSION WITH PLASTICITY
BOUNDARY SOLUTION FOR TIME = 1.00

ELEMENT	NODE NO.	X DISPLACEMENT	Y DISPLACEMENT	Z DISPLACEMENT	X TRACTION	Y TRACTION	Z TRACTION
1	1	0.0	0.0	0.0	-0.10000D+03	0.0	0.0
1	3	0.0	0.0	-0.25001D+00	-0.10000D+03	0.0	0.0
1	23	0.0	-0.25002D+00	-0.25001D+00	-0.10000D+03	0.0	0.0
1	21	0.0	-0.25002D+00	0.0	-0.10000D+03	0.0	0.0
2	201	0.10000D+01	0.0	0.0	0.10000D+03	0.0	0.0
2	221	0.10000D+01	-0.25001D+00	0.0	0.10000D+03	0.0	0.0
2	223	0.10000D+01	-0.25002D+00	-0.25002D+00	0.10000D+03	0.0	0.0
2	203	0.10000D+01	0.0	-0.25002D+00	0.10000D+03	0.0	0.0
3	1	0.0	0.0	0.0	0.0	-0.42969D-05	0.0
3	201	0.10000D+01	0.0	0.0	0.0	0.14693D-04	0.0
3	203	0.10000D+01	0.0	-0.25002D+00	0.0	-0.11761D-04	0.0
3	3	0.0	0.0	-0.25001D+00	0.0	0.63212D-06	0.0
4	21	0.0	-0.25002D+00	0.0	0.0	0.0	0.0
4	23	0.0	-0.25002D+00	-0.25001D+00	0.0	0.0	0.0
4	223	0.10000D+01	-0.25002D+00	-0.25002D+00	0.0	0.0	0.0
4	221	0.10000D+01	-0.25001D+00	0.0	0.0	0.0	0.0
5	1	0.0	0.0	0.0	0.0	0.0	-0.20575D-04
5	21	0.0	-0.25002D+00	0.0	0.0	0.0	-0.27697D-04
5	221	0.10000D+01	-0.25001D+00	0.0	0.0	0.0	0.21839D-04
5	201	0.10000D+01	0.0	0.0	0.0	0.0	0.36241D-04
6	3	0.0	0.0	-0.25001D+00	0.0	0.0	0.0
6	203	0.10000D+01	0.0	-0.25002D+00	0.0	0.0	0.0
6	223	0.10000D+01	-0.25002D+00	-0.25002D+00	0.0	0.0	0.0
6	23	0.0	-0.25002D+00	-0.25001D+00	0.0	0.0	0.0

3.4.7.6 Boundary Solution (Nodal Basis)

JOB TITLE: U911 TEST CASE - CUBE IN SIMPLE TENSION WITH PLASTICITY
NODAL OUTPUT AT TIME = 1.00

NODE	DISPLACEMENT X/Y/Z	STRESS XX/YY/ZZ	STRESS XY/XZ/YZ	STRAIN XX/YY/ZZ	STRAIN XY/XZ/YZ
1	0.0	0.10000E+03	0.0	0.10000E+01	0.0
	0.0	-0.11716E-02	0.0	-0.25001E+00	0.0
	0.0	-0.11579E-02	0.0	-0.25001E+00	0.0
2	0.0	0.10000E+03	0.0	0.10000E+01	0.0
	0.0	-0.10033E-02	-0.23842E-05	-0.25001E+00	-0.29802E-07
	-0.12501E+00	-0.17395E-02	-0.23842E-05	-0.25001E+00	-0.29802E-07
3	0.0	0.10000E+03	0.0	0.10000E+01	0.0
	0.0	-0.11691E-02	-0.15895E-05	-0.25001E+00	-0.19868E-07
	-0.25001E+00	-0.11698E-02	0.0	-0.25001E+00	0.0
11	0.0	0.10000E+03	0.23842E-05	0.10000E+01	0.29802E-07
	-0.12501E+00	-0.17748E-02	0.0	-0.25001E+00	0.0
	0.0	-0.99501E-03	0.0	-0.25001E+00	0.0
13	0.0	0.10000E+03	0.0	0.10000E+01	0.0
	-0.12501E+00	-0.17519E-02	0.0	-0.25001E+00	0.0
	-0.25001E+00	-0.99945E-03	0.23842E-05	-0.25001E+00	0.29802E-07
21	0.0	0.10000E+03	0.31789E-05	0.10000E+01	0.39736E-07
	-0.25002E+00	-0.11924E-02	0.0	-0.25001E+00	0.0
	0.0	-0.11606E-02	0.15895E-05	-0.25001E+00	0.19868E-07
22	0.0	0.10000E+03	0.0	0.10000E+01	0.0
	-0.25002E+00	-0.10028E-02	-0.47684E-05	-0.25001E+00	-0.59605E-07
	-0.12501E+00	-0.17242E-02	0.23842E-05	-0.25001E+00	0.29802E-07
23	0.0	0.10000E+03	-0.15895E-05	0.10000E+01	-0.19868E-07
	-0.25002E+00	-0.11628E-02	-0.63578E-05	-0.25001E+00	-0.79473E-07
	-0.25001E+00	-0.11546E-02	0.31789E-05	-0.25001E+00	0.39736E-07
101	0.50000E+00	0.10000E+03	-0.28610E-04	0.10000E+01	-0.35763E-06
	0.0	-0.75028E-03	0.0	-0.25001E+00	0.0
	0.0	-0.75923E-03	0.0	-0.25001E+00	0.0
103	0.50000E+00	0.10000E+03	-0.95367E-05	0.10000E+01	-0.11921E-06
	0.0	-0.74490E-03	-0.47684E-05	-0.25001E+00	-0.59605E-07
	-0.25002E+00	-0.74768E-03	0.0	-0.25001E+00	0.0
121	0.50000E+00	0.10000E+03	0.11921E-04	0.10000E+01	0.14901E-06
	-0.25001E+00	-0.75531E-03	0.19073E-04	-0.25001E+00	0.23842E-06
	0.0	-0.76147E-03	0.0	-0.25001E+00	0.0
123	0.50000E+00	0.10000E+03	0.26226E-04	0.10000E+01	0.32783E-06
	-0.25002E+00	-0.74005E-03	0.11921E-04	-0.25001E+00	0.14901E-06
	-0.25002E+00	-0.74005E-03	0.0	-0.25001E+00	0.0
201	0.10000E+01	0.10000E+03	-0.50863E-04	0.10000E+01	-0.63578E-06
	0.0	-0.11649E-02	0.0	-0.25001E+00	0.0
	0.0	-0.11921E-02	0.0	-0.25001E+00	0.0

3.4.7.7 Cell Node Displacements

JOB TITLE: U911 TEST CASE - CUBE IN SIMPLE TENSION WITH PLASTICITY
INTERIOR DISPLACEMENT AT TIME = 1.00

NODE	X DISPLACEMENT	Y DISPLACEMENT	Z DISPLACEMENT
3	0.0	0.0	-0.250015D+00
2	0.298025D-07	-0.745103D-08	-0.125007D+00
1	0.0	0.0	0.0
11	0.298025D-07	-0.125008D+00	-0.745102D-08
21	0.0	-0.250015D+00	0.0
22	0.298025D-07	-0.250015D+00	-0.125007D+00
23	0.0	-0.250015D+00	-0.250015D+00
13	0.298025D-07	-0.125008D+00	-0.250015D+00
103	0.500002D+00	-0.745103D-08	-0.250015D+00
101	0.500002D+00	-0.745103D-08	-0.745103D-08
121	0.500002D+00	-0.250015D+00	-0.745103D-08
123	0.500002D+00	-0.250015D+00	-0.250015D+00
203	0.100000D+01	0.0	-0.250015D+00
202	0.100000D+01	-0.745103D-08	-0.125008D+00
201	0.100000D+01	0.0	0.0
211	0.100000D+01	-0.125008D+00	-0.745104D-08
221	0.100000D+01	-0.250015D+00	0.0
222	0.100000D+01	-0.250015D+00	-0.125008D+00
223	0.100000D+01	-0.250015D+00	-0.250015D+00
213	0.100000D+01	-0.125008D+00	-0.250015D+00

3.4.7.8 Cell Node Stresses

JOB TITLE: U911 TEST CASE - CUBE IN SIMPLE TENSION WITH PLASTICITY
INTERIOR STRESS AT TIME = 1.00

NODE	SIGMAXX	SIGMAYY	SIGMAZZ	TAUXY	TAUXZ	TAUYZ
3	0.100000D+03	-0.117113D-02	-0.116272D-02	0.0	-0.369847D-05	0.186150D-07
2	0.100000D+03	-0.101165D-02	-0.174628D-02	0.0	-0.277385D-05	0.139612D-07
1	0.100000D+03	-0.117198D-02	-0.116293D-02	0.0	0.0	0.0
11	0.100000D+03	-0.175666D-02	-0.998175D-03	0.707289D-06	0.0	-0.455990D-06
21	0.100000D+03	-0.117293D-02	-0.116126D-02	0.943053D-06	0.0	-0.607987D-06
22	0.100000D+03	-0.101269D-02	-0.174674D-02	0.0	-0.221812D-05	-0.898019D-06
23	0.100000D+03	-0.117098D-02	-0.116263D-02	-0.812824D-06	-0.295749D-05	-0.589372D-06
13	0.100000D+03	-0.175332D-02	-0.100615D-02	-0.609618D-06	0.0	-0.428068D-06
103	0.100000D+03	-0.745262D-03	-0.745801D-03	0.147083D-06	-0.179219D-06	0.0
101	0.100000D+03	-0.753163D-03	-0.758670D-03	-0.391312D-06	0.536849D-05	0.0
121	0.100000D+03	-0.749292D-03	-0.751388D-03	0.102327D-05	0.590688D-05	0.0
123	0.100000D+03	-0.747848D-03	-0.744976D-03	-0.107215D-05	0.147064D-05	0.0
203	0.100000D+03	-0.117299D-02	-0.118080D-02	0.196111D-06	0.345951D-05	0.759594D-06
202	0.100000D+03	-0.101920D-02	-0.177882D-02	0.0	0.796312D-05	0.569695D-06
201	0.100000D+03	-0.117799D-02	-0.119901D-02	-0.521750D-06	0.715798D-05	0.0
211	0.100000D+03	-0.176135D-02	-0.103718D-02	-0.753350D-07	0.0	-0.177290D-05
221	0.100000D+03	-0.117134D-02	-0.118888D-02	0.421303D-06	0.787584D-05	-0.236386D-05
222	0.100000D+03	-0.101771D-02	-0.177266D-02	0.0	0.959564D-05	-0.297610D-05
223	0.100000D+03	-0.117627D-02	-0.117792D-02	-0.616713D-06	0.491835D-05	-0.160427D-05
213	0.100000D+03	-0.176790D-02	-0.102502D-02	-0.315451D-06	0.0	-0.633508D-06

3.4.7.9 Cell Node Strains

JOB TITLE: U911 TEST CASE - CUBE IN SIMPLE TENSION WITH PLASTICITY
INTERIOR STRAIN AT TIME = 1.00

NODE	EPS XX	EPS YY	EPS ZZ	EPSXY	EPSXZ	EPSYZ
3	0.100001D+01	-0.250009D+00	-0.250009D+00	0.0	-0.462309D-07	0.232687D-09
2	0.100001D+01	-0.250006D+00	-0.250015D+00	0.0	-0.346731D-07	0.174515D-09
1	0.100001D+01	-0.250009D+00	-0.250009D+00	0.0	0.0	0.0
11	0.100001D+01	-0.250015D+00	-0.250005D+00	0.884112D-08	0.0	-0.569987D-08
21	0.100001D+01	-0.250009D+00	-0.250009D+00	0.117882D-07	0.0	-0.759983D-08
22	0.100001D+01	-0.250006D+00	-0.250015D+00	0.0	-0.277265D-07	-0.112252D-07
23	0.100001D+01	-0.250009D+00	-0.250009D+00	-0.101603D-07	-0.369686D-07	-0.736715D-08
13	0.100001D+01	-0.250015D+00	-0.250006D+00	-0.762022D-08	0.0	-0.535085D-08
103	0.100000D+01	-0.250006D+00	-0.250006D+00	0.183554D-08	-0.224023D-08	0.0
101	0.100000D+01	-0.250006D+00	-0.250006D+00	-0.489140D-08	0.671060D-07	0.0
121	0.100000D+01	-0.250006D+00	-0.250006D+00	0.127986D-07	0.738360D-07	0.0
123	0.100000D+01	-0.250006D+00	-0.250006D+00	-0.134019D-07	0.183831D-07	0.0
203	0.100001D+01	-0.250009D+00	-0.250009D+00	0.245139D-08	0.432439D-07	0.949492D-08
202	0.100001D+01	-0.250006D+00	-0.250015D+00	0.0	0.995390D-07	0.712118D-08
201	0.100001D+01	-0.250009D+00	-0.250009D+00	-0.652187D-08	0.894747D-07	0.0
211	0.100001D+01	-0.250015D+00	-0.250006D+00	-0.941687D-09	0.0	-0.221612D-07
221	0.100001D+01	-0.250009D+00	-0.250009D+00	0.526629D-08	0.984480D-07	-0.295483D-07
222	0.100001D+01	-0.250006D+00	-0.250015D+00	0.0	0.119946D-06	-0.372013D-07
223	0.100001D+01	-0.250009D+00	-0.250009D+00	-0.770891D-08	0.614793D-07	-0.200534D-07
213	0.100001D+01	-0.250015D+00	-0.250006D+00	-0.394313D-08	0.0	-0.791885D-08

3.4.8 List of Symbols

List of Symbols
Referenced Within Section 3.4

Symbol	Description	Page
x_j	Cartesian coordinates	3.4-6
ε_{ij}	Inelastic strain rate	3.4-6
λ, μ	Lamé constants	3.4-6
$\dot{u}_i$	Displacement rate	3.4-6
δ_{ij}	Kronecker delta	3.4-6
E	Young's modulus	3.4-6
α	Coefficient of thermal expansion	3.4-6
$\dot{T}$	Time derivative of temperature	3.4-6
$\dot{f}$	Time derivative of body forces	3.4-6
S	Boundary of body to be analyzed	3.4-7
ξ_0	Point on boundary S	3.4-7
x	Integration point	3.4-7
y_i	$= \lvert x_i - \xi_i \rvert$	3.4-7
r	$= \lvert y \rvert$	3.4-7
V	Interior of body to be analyzed	3.4-7
G_{ij}	Kelvin solution	3.4-7
T_{ijk}	Stresses derived from G_{ij}	3.4-7
F_{ij}	Tractions derived from T_{ijk} and surface normal	3.4-7
C_{ij}	1/2 δ_{ij} if S is smooth at ξ_j; otherwise depends on surface geometry at ξ	3.4-7

List of Symbols
Referenced Within Section 3.4 (continued)

Symbol	Description	Page
n_i	Surface normal	3.4-7
t_i	Tractions	3.4-8
$\dot{\sigma}_{jk}$	Stress rate	3.4-8
D_{ijk}, S_{ijk}, M_{ijk}	Higher order kernels derived from G_{ij} by differentiation and use of Hooke's Law	3.4-8
$\overline{\ }$	Placed over symbol, denotes use of a local axis system	3.4-8
$\underline{x}$	Vector of all unknown freedoms (displacements and tractions)	3.4-10
$\underline{y}$	Vector of all known freedoms (displacements and tractions)	3.4-10
ρ	Mass density	3.4-12
C_1	Dilatational wave speed	3.4-12
C_2	Distortional wave speed	3.4-12
$L(\cdot)$	Laplace transform	3.4-12
$\overline{\ }$	Denotes (in Section 3.4.3.3) the Laplace transform of a function	3.4-12
s	Transform parameter	3.4-12
ω	Frequency	3.4-14
$\overline{G}_{ij}$, $\overline{F}_{ij}$	Laplace transforms of the dynamic kernel functions	3.4-14
β	Damping ratio	3.4-17
η	Coefficient of viscosity	3.4-17

3.4.9 References

1. Jaswon, M. A. and A. R. Ponter, "An Integral Equation Solution of the Torsion Problem," Proc. Roy. Soc., Ser. A, 273, 1963, pp. 237-246.

2. Rizzo, F. J., "An Integral Equation Approach to Boundary Value Problems of Classical Elastostatics," Quart. Appl. Math., Vol. 25, 83-95, 1967.

3. Brebbia, C. A. and S. Walker, Boundary Element Techniques in Engineering, Newness-Butterworths, London, 1980.

4. Banerjee, P. K. and R. Butterfield, Boundary Element Methods in Engineering Science, McGraw-Hill, London, 1981.

5. Liggett, J. and P. Liu, Boundary Integral Equation for Porous Media Flow, Allen and Unwin, London, 1983.

6. Crouch, S. L. and A. M. Starfield, Boundary Element Methods in Solid Mechanics, Allen and Unwin, London, 1983.

7. Mukherjee, S., Boundary Element Methods in Creep and Fracture, Applied Science Publishers, London, 1982.

8. Banerjee, P. K. and R. Butterfield, Developments in Boundary Element Methods I, Applied Sci. Publishers, Barking, Essex, UK, 1979.

9. Banerjee, P. K. and R. P. Shaw, Developments in Boundary Element Methods - II, Applied Sci. Publishers, Barking, Essex, UK, 1982.

10. Banerjee, P. K. and S. Mukherjee, Developments in Boundary Element Methods - III, Applied Sci. Publishers, Barking, Essex, UK, 1984.

11. Cruse, T. A. and F. J. Rizzo, (eds.), Boundary-Integral Equation Method: Computational Applications in Applied Mechanics, AMD-Vol. 11, ASME, New York, 1975.

12. Mendelson, A., "Boundary-Integral Methods in Elasticity and Plasticity," NASA TN, D-7418, 1973.

13. Cruse, T. A., "Mathematical Foundations of the Boundary-Integral Equation Method in Solid Mechanics," AFOSR-TR-77-1002, PWA-5539, 1977.

14. Cruse, T. A., and R. B. Wilson, "Boundary-Integral Equation Methods for Elastic Fracture Mechanics Analysis," AFOSR-TR-78-0355, 1978.

15. Banerjee, P. K. and R. Butterfield, "Boundary Element Methods in Geomechanics," in Finite Elements in Geomechanics, ed. by G. Gudehus, John Wiley & Sons, London-New York, 1977, pp. 529-570.

16. Lachat, J. C. and J. O. Watson, "Effective Numerical Treatment of Boundary Integral Equations: A formulation for Three-Dimensional Elasto-statics," Int. J. Num. Meth. in Engng., 10, 1976, pp. 991-1005.

17. Watson, J. O., "Advanced Implementation of the Boundary Element Method for Two- and Three-Dimensional Elastostatics," in Banerjee, P. K. and R. Butterfield, Developments in Boundary Element Methods - I, Applied Science Publishers, London, 1976, pp. 31-64.

18. Banerjee, P. K., "Integral Equation Methods for Analysis of Piece-wise Non-homogeneous Three-Dimensional Elastic Solids of Arbitrary Shape," Int. J. Mech. Sci., 18, 1976, pp. 293-303.

19. Banerjee, P. K., "Foundations Within a Finite Elastic Layer - Application of the Integral Equation Method," Civ. Engng., 1971, pp. 1197-1202.

20. Butterfield, R. and P. K. Banerjee, "The Problem of Pile Cap, Pile Groups Interaction," Geotechq., 21(2), 1971, pp. 135-141.

21. Rizzo, F. J. and D. J. Shippy, "An Advanced Boundary Integral Equation Method for Three-dimensional Thermo-elasticity," Int. J. Num. Meth. in Engng., 11, 1977, pp. 1753-1768.

22. Rizzo, F. J. and D. J. Shippy, "Recent Advances of the Boundary Element Method in Thermoelasticity," in P. K. Banerjee and R. Butterfield, eds., Developments in Boundary Element Methods, Vol. I, Chapt. VI, Applied Science Publishers, London, 1979.

23. Cruse, T. A., "Two and Three-dimensional Problems of Fracture Mechanics," in P. K. Banerjee and R. Butterfield, eds., Developments in Boundary Element Methods, Vol. I, Chapt. V., Applied Science Publishers, London, 1979.

24. Cruse, T. A., "Numerical Solutions in Three-dimensional Elastostatics," Int. J. Solids and Struct., 5, 1969, pp. 1259-1274.

25. Cruse, T. A., "Application of the Boundary Integral Equation Method to Three-dimensional Stress Analysis," Int. J. Computer and Struct., 3, 1973, pp. 509-527.

26. Cruse, T. A., "An Improved Boundary Integral Equation Method for Three-dimensional Elastic Stress Analysis," Computer and Struct., 4, 1974, pp. 741-754.

27. Cruse, T. A., D. W. Snow and R. B. Wilson, "Numerical Solutions in Axisymmetric Elasticity," Computers and Struct., 7, 1977, pp. 445-451.

28. Snyder, M. D. and T. A. Cruse, "Boundary-Integral Equation Analysis of Cracked Anisotropic Plates," Int. J. Frac., 11, 1975, pp. 315-328.

29. Cruse, T. A. and G. J. Meyers, "Three Dimensional Fracture Mechanics Analysis," J. of the Struct. Div., ASCE, 103, 1977, pp. 309-320.

30. Cruse, T. A. and R. B. Wilson, "Advanced Applications of Boundary-Integral Equation Methods," Nuc. Engng. and Des., 46, 1977, pp. 223-234.

31. Alarcon, E., C. A. Brebbia and J. Dominquez, "The Boundary Element Method in Elasticity," Int. J. Mech. Sci., 20, 1978, pp. 625-639.

32. Wilson, R. B. and T. A. Cruse, "Efficient Inplementation of Anisotropic Three-dimensional Boundary Integral Equation Stress Analysis," Int. J. Num. Meth. Eng., Vol. 12, 1978, pp. 1383-1397.

33. Mayer, M., W. Drexler and G. Kuhn, "A Semi-analytical Boundary Integral Approach for Axisymmetric Elastic Bodies with Arbitrary Boundary Conditions," Int. J. Solids & Struct., 16, 1980, pp. 863-871.

34. Rizzo, F. J. and D. J. Shippy, "An Advanced Boundary Integral Equation Method for Three-Dimensional Thermoelasticity," Int. J. Num. Meth. Eng., 11, 1977, pp. 1753-1768.

35. Chaudouet, A. and G. Loubignac, "Boundary Integral Equations Used to Solve Thermoelastic Problems: Application to Standard and Incompressible Materials," in Numerical Methods in Heat Transfer, ed., by R. W. Lewis, K. Morgan and O. C. Zienkiewicz, John Wiley & Sons, London-New York, 1981, pp. 115-133.

36. Hansen, E. B., "Numerical Solution of Integro-Differential and Singular Integral Equations for Plate Bending Problems," J. Elasticity, 6, 1976, pp. 39-56.

37. Stern, M., "A General Boundary Integral Formulation for the Numerical Solution of Plate Bending Problems," Int. J. Solids & Struct., 15, 1979, pp. 769-782.

38. Bezine, G., "Boundary Integral Formulation for Plate Flexure with Arbitrary Boundary Conditions," Mech. Res. Comm., 5, 1978, pp. 197-206.

39. Bezine, G. and D. A. Gamby, "A New Integral Equation Formulation for Plate Bending Problems," in Recent Advances in Boundary Element Methods, ed. by C. A. Brebbia, Pentech Press, London, 1978, pp. 327-342.

40. Bezine, G., "Application of Similarity to Research of New Boundary Integral Equations for Plate Flexure Problems," Appl. Math. Modelling, 5, 1981, pp. 66-70.

41. Wu, B. C. and N. J. Altiero, "A New Numerical Method for the Analysis of Anisotropic Thin-Plate Bending Problems," Compt. Meth. Appl. Mech. & Eng., 25, 1981, pp. 343-353.

42. Cruse, T. A. and W. Van Buren, "Three Dimensional Elastic Stress Analysis of a Fracture Specimen with an Edge Crack," Int. J. Fract. Mech., 7, 1971, pp. 1-15.

43. Cruse, T. A., "Numerical Evaluation of Elastic Stress Intensity Factors by the Boundary-Integral Equation Method," in The Surface Crack: Physical Problems and Computational Solutions, ed. J. L. Swedlow, American Society of Mechanical Engineers, New York, 1972.

44. Rudolphi, T. J. and N. E. Ashbaugh, "An Integral-Equation Solution for a Bounded Elastic Body Containing a Crack: Mode I Deformation," Int. J. Frac., 14, 1978, pp. 527-541.

45. Tan, C. L. and R. T. Fenner, "Elastic Fracture Mechanics Analysis by the Boundary Integral Equation Method," Proc. Roy. Soc., Ser. A, 369, 1979, pp. 243-260.

46. Tan, C. L. and R. T. Fenner, "Stress Intensity Factors for Semi-Elliptical Surface Cracks in Pressurized Cylinders Using the Boundary Integral Equation Method," Int. J. Frac., 16, 1980, pp. 233-245.

47. Blandford, G. E., A. R. Ingraffea and J. A. Liggett, "Two-Dimensional Stress Intensity Factor Computations Using the Boundary Element Method," Int. J. Num. Meth. Eng., 17, 1981, pp. 387-404.

48. Banaugh, R. P. and W. Goldsmith, "Diffraction of Steady Elastic Waves by Surfaces of Arbitrary Shape," J. of Appl. Mech., Vol. 30, 1963, pp. 589-597.

49. Kobayashi, S., T. Fukui and N. Azuma, "An Analysis of Transient Stresses Produced Around a Tunnel by the Integral Equation Method," Proc. Symp. Earthquake Engng., Japan, 1975, pp. 631-638.

50. Niwa, Y., S. Kobayashi and T. Fukui, "Applications of Integral Equation Method to Some Geotechnical Problems," in C.S. Desai, Edit., Numerical Methods in Geomechanics, ASCE, N.Y., 1976, pp. 120-131.

51. Doyle, J. M., "Integration of the Laplace Transformed Equations of Classical Elastostatics," Jour. Math. Analy. Appl., 13, 1966, pp. 118-131.

52. Cruse, T. A. and F. J. Rizzo, "A Direct Formulation and Numerical Solution of the General Transient Elastodynamic Problem I," J. Math. Anal. & Applic., 1968, pp. 244-259.

53. Cruse, T. A., "A Direct Formulation and Numerical Solution of the General Elastodynamic Problem II," J. Math. Anal. & Applic., 22, 1968, pp. 341-355.

54. Manolis, G. D. and D. E. Beskos, "Dynamic Stress Concentration Studies by Boundary Integrals and Laplace Transform," Int. J. Num. Meth. Eng., 17, 1981, pp. 573-599.

55. Niwa, Y., S. Kobayashi, T. Fukui and N. Azuma, "Transient Stresses Around Inclusions During the Passage of Traveling Waves Analyzed by the Integral Equation Method," Proc. Japan Soc. Civil Engrs., No. 248, 1976, pp. 41-53, in Japanese.

56. Cole, D. M., D. D. Kosloff and J. B. Minster, "A Numerical Boundary Integral Equation Method for Elastodynamics I," Bull. Seismological Soc. Amer., 68, 1978, pp. 1331-1357.

57. Manolis, G. D., "A Comparative Study on Three Boundary Element Method Approaches to Problems in Elastodynamics," Int. J. of Num. Meth. Engng., Vol. 19, 1983, pp. 71-93.

58. Swedlow, J. L. and T. A. Cruse, "Formulation of Boundary Integral Equations for Three-Dimensional Elastoplastic Flow," Int. J. Solids & Struct., 7, 1971, pp. 1673-1684.

59. Rzasnicki, W., A. Mendelson, L. U. Albers and D. D. Raftopoulos, "Application of Boundary Integral Method to Elastoplastic Analysis of V-Notched Beams," NASA TN, D-7637, 1974.

60. Tells, J. C. F. and C. A. Brebbia, "The Boundary Element Method in Plasticity," Appl. Math. Modeling, 5, 1981, pp. 275-281.

61. Tells, J. C. F. and C. A. Brebbia, "Boundary Elements: New Developments in Elastoplastic Analysis," Appl. Math. Modeling, 5, 1981, pp. 376-382.

62. Mukherjee, S., "Corrected Boundary-Integral Equations in Planar Thermoelastoplasticity," Int. J. Solids & Struct., 13, 1977, pp. 331-335.

63. Bui, H. D., "Some Remarks About the Formulation of Three-Dimensional Thermoelastoplastic Problems by Integral Equations," Int. J. Solids & Struct., 14, 1978, pp. 935-939.

64. Mukheree, S. and V. Kumar, "Numerical Analysis of Time-Dependent Inelastic Deformation in Metallic Media Using the Boundary-Integral Equation Method," ASME J. Appl. Mech., 45, 1978, pp. 785-790.

65. Morjaria, M. and S. Mukherjee, "Inelastic Analysis of Transverse Deflection of Plates by Boundary Element Method," ASME J. Appl. Mech., 47, 1980.

66. Mukherjee, S. and M. Morjaria, "A Boundary Element Formulation for Planar Time-Dependent Inelastic Deformation of Plates with Cutouts," Int. J. Solids & Struct., 17, 1981, pp. 115-126.

67. Morjaria, M. and S. Mukherjee, "Numerical Analysis of Planar, Time-Dependent Inelastic Deformation of Plates with Cracks by the Boundary Element Method," Int. J. Solids & Struct., 17, 1981, pp. 127-143.

68. Banerjee, P. K. and G. Mustoe, "Boundary Element Methods in Two-Dimensional Elastoplasticity," Proc. of Int. Conf. on Recent Developments of Boundary Element Methods, Southampton University, Pentec Press, London, 1978, pp. 283-300.

69. Banerjee, P. K., D. N. Cathie and T. G. Davies, "Two- and Three-Dimensional Problems of Elastoplasticity," in Developments in Boundary Element Methods - I, eds. P. K. Banerjee and R. Butterfield, Applied Sci. Publishers, 1979, pp. 65-95.

70. Banerjee, P. K. and D. N. Cathie, "A Direct Formulation and Numerical Implementation of the Boundary Element Method for Two-Dimensional Problems of Elastoplasticity," Int. J. Mech. Sci., 22, 1980, pp. 233-245.

71. Cathie, D. N. and P. K. Banerjee, "Boundary Element Methods in Axisymmetric Plasticity," Innovative Numerical Analysis for the Applied Engineering Sciences, ed. R. P. Shaw et al, University of Virginia Press, 1980.

72. Cathie, D. N. and P. K. Banerjee, "Boundary Element Methods for Plasticity and Creep Including a Viscoplastic Approach," Res. Mechanica, Vol. 4, 1982, pp. 3-22.

73. Kobayashi, S. and N. Nishimura, "Elastoplastic Analysis by the Integral Equation Method," Mem. Fac. Eng., Kyoto Univ., 43, 1980, pp. 324-334.

74. Kumar, V. and S. Mukherjee, "A Boundary-Integral Equation Formulation for Time-Dependent Inelastic Deformation in Metals," Int. J. Mech. Sci., 19, 1977, pp. 713-724.

75. Banerjee, P. K. and T. G. Davies, "Advanced Implementation of Boundary Element Methods for Three-Dimensional Problems of Elastoplasticity and Viscoplasticity," Chapter 1 in Developments in Boundary Element Methods - III, Applied Science Publishers, London, 1984.

76. Mukherjee, S. and A. Chandra, "Boundary Element Formulations for Large Strain - Large Deformation Problems of Plasticity and Viscoplasticity," Chapter 2 in Developments in Boundary Element Methods - III, Applied Science Publishers, London, 1984.

77. Mukherjee, S. and A. Chandra, Private Communications, 1983.

78. Durbin, F., "Numerical Inversion of Laplace Transforms: An Efficient Improvement to Dubner and Abate's Method," Computer, J., Vol. 17, 1974, pp. 371-376.

79. Dubner, R. and J. Abate, "Numerical Inversion of Laplace Transforms by Relating Them to the Finite Fourier Cosine Transforms," J. Assoc. Comp. Mach., Vol. 15, 1968, pp. 115-123.

80. Cooley, J. W. and J. W. Tukey, "An Algorithm for Machine Calculation of Complex Fourier Series," Math. Comp., Vol. 19, 1965, pp. 297-310.

81. Stroud, A. H. and D. Secrest, Gaussian Quadrature Formulas, Prentice Hall, New York, 1966.

82. Dongarra, J. J., et al, Linpack Users' Guide, SIAM, Philadelphia, PA, 1979.

83. Domas, P. A., et al, "Benchmark Notch Test for Life Prediction," NASA CR-165571, June, 1982.

DISTRIBUTION LIST - FIRST ANNUAL STATUS REPORT

3-D INELASTIC ANALYSIS METHODS FOR
HOT SECTION COMPONENTS (BASE PROGRAM)
CONTRACT NAS3-23697

NASA Lewis Research Center
Attn: Contracting Officer, MS 500-312
21000 Brookpark Road
Cleveland, OH 44135

NASA Lewis Research Center
Attn: Technical Report Control
Officer, MS 5-5
21000 Brookpark Road
Cleveland, OH 44135

NASA Lewis Research Center
Attn: Technical Utilization Office
MS 3-16
21000 Brookpark Road
Cleveland, OH 44135

NASA Lewis Research Center
Attn: AFSC Liaison Office, MS 501-3
21000 Brookpark Road
Cleveland, OH 44135

NASA Lewis Research Center
Attn: S&MT Division Contract
File, MS 49-6 (2 copies)
21000 Brookpark Road
Cleveland, OH 44135

NASA Lewis Research Center
Attn: Library, MS 60-3
21000 Brookpark Road
Cleveland, OH 44135

NASA Lewis Research Center
Attn: L. Berke, MS 49-6
21000 Brookpark Road
Cleveland, OH 44135

NASA Lewis Research Center
Attn: R. H. Johns, MS 49-6
21000 Brookpark Road
Cleveland, OH 44135

NASA Lewis Research Center
Attn: D. A. Hopkins, MS 49-6
21000 Brookpark Road
Cleveland, OH 44135

NASA Lewis Research Center
Attn: C. C. Chamis, MS 49-6
(4 copies)
21000 Brookpark Road
Cleveland, OH 44135

NASA Lewis Research Center
Attn: M. S. Hirschbein, MS 49-6
21000 Brookpark Road
Cleveland, OH 44135

NASA Lewis Research Center
Attn: J. A. Ziemianski, MS 49-6
21000 Brookpark Road
Cleveland, OH 44135

NASA Lewis Research Center
Attn: G. R. Halford, MS 49-7
21000 Brookpark Road
Cleveland, OH 44135

NASA Lewis Research Center
Attn: D. J. Gauntner, MS 23-2
21000 Brookpark Road
Cleveland, OH 44135

NASA Lewis Research Center
Attn: A. Kaufman, MS 49-7
21000 Brookpark Road
Cleveland, OH 44135

NASA Lewis Research Center
Attn: R. C. Bill, MS 49-7
21000 Brookpark Road
Cleveland, OH 44135

NASA Lewis Research Center
Attn: T. J. Miller, MS 49-1
21000 Brookpark Road
Cleveland, OH 44135

NASA Lewis Research Center
Attn: D. E. Sokolowski, MS 49-1
21000 Brookpark Road
Cleveland, OH 44135

National Aeronautics & Space Admin.
Attn: NHS-22/Library
Washington, DC 20546

National Aeronautics & Space Admin.
Attn: RTM-6/M. A. Greenfield
Washington, DC 20546

NASA-Ames Research Center
Attn: Library, MS 202-3
Moffett Field, CA 94035

NASA-Goddard Space Flight Center
Attn: 252/Library
Greenbelt, MD 20771

NASA-John F. Kennedy Space Center
Attn: Library, MS AD-CSO-1
Kennedy Space Center, FL 32931

NASA-Langley Research Center
Attn: Library, MS 185
Hampton, VA 23665

NASA-Langley Research Center
Attn: M. F. Card, MS 244
Hampton, VA 23665

NASA-Langley Research Center
Attn: J. Starnes
Hampton, VA 23665

NASA-Lyndon B. Johnson Space Center
Attn: JM6 Library
Houston, TX 77001

NASA-George C. Marshall
Space Flight Center
Attn: AS61/Library
Marshall Space Flt. Center, AL 35812

Jet Propulsion Laboratory
Attn: Library
4800 Oak Grove Drive
Pasadena, CA 91103

Jet Propulsion Laboratory
Attn: B. Wada
4800 Oak Grove Drive
Pasadena, CA 91103

NASA S&T Information Facility
Attn: Acquisition Division
(10 copies)
P. O. Box 8757
Baltimore-Washington
Int. Airport, MD 21240

Air Force Aeronautical Prop. Lab.
Attn: Z. Gershon
Wright-Patterson AFB, OH 45433

Air Force Aeronautical Prop. Lab.
Attn: E. Bailey
Wright-Patterson AFB, OH 45433

Air Force Systems Command
Attn: Library
Aeronautical Systems Division
Wright-Patterson AFB, OH 45433

Air Force Systems Command
Attn: C. W. Cowie
Aeronautical Systems Division
Wright-Patterson AFB, OH 45433

Air Force Systems Command
Attn: R. J. Hill
Aeronautical Systems Division
Wright-Patterson AFB, OH 45433

Aerospace Corporation
Attn: Library-Documents
2400 E. El Segundo Blvd.
Los Angeles, CA 90045

Air Force Office of Sci. Res.
Attn: A. K. Amos
Washington, DC 20333

Department of the Army
Attn: AMCRD-RC
U. S. Army Material Command
Washington, DC 20315

U. S. Army Ballistics Res. Lab.
Attn: Dr. Donald F. Haskell, DRXBR-BM
Aberdeen Proving Ground, MD 21005

Mechanics Research Laboratory
Attn: Dr. E. M. Lenoe
Army Materials & Mechanics Res. Center
Watertown, MA 02172

U. S. Army Missile Command
Attn: Document Section
Redstone Scientific Info. Center
Redstone Arsenal, AL 35808

Commanding Officer
U. S. Army Research Office (Durham)
Attn: Library
Box CM, Duke Station
Durham, NC 27706

Bureau of Naval Weapons
Attn: RRRE-6
Department of Navy
Washington, DC 20360

Commander
U. S. Naval Ordinance Laboratory
White Oak
Attn: Library
Silver Springs, MD 20910

Director, Code 6180
Attn: Library
U. S. Naval Research Laboratory
Washington, DC 20390

Denver Federal Center
Attn: P. M. Lorenz
U. S. Bureau of Reclamation
P. O. Box 25007
Denver, CO 80225

Naval Air Propulsion Test Center
Attn: Mr. James Salvino
Aeronautical Engine Department
Trenton, NJ 08628

Federal Aviation Administration
Code ANE-214, Propulsion Section
Attn: Mr. Robert Berman
12 New England Executive Park
Burlington, MA 01803

Federal Aviation Admin. DOT
Office of Aviation Safety, FOB 10A
Attn: Mr. John H. Enders
800 Independence Ave., S.W.
Washington, DC 20591

FAA, ARD-520
Attn: Commander John J. Shea
2100 2nd Street, S.W.
Washington, DC 20591

National Trans. Safety Board
Attn: Mr. Edward P. Wizniak, TE-20
800 Independence Avenue, S.W.
Washington, DC 20594

Northwestern University
Dept. of Civil Engineering
Attn: S. Nemat-Nasser
Evanston, IL 60201

Northwestern University
Dept. of Civil Engineering
Attn: T. Belytschco
Evanston, IL 60201

Rockwell International Corporation
Attn: Mr. Joseph Gausselin
D 422/402 AB71
Los Angeles International Airport
Los Angeles, CA 90009

Rensselaer Polytechnic Institute
Attn: R. Loewy
Troy, NY 12181

Rensselaer Polytechnic Institute
Attn: E. Krempl
Troy, NY 12181

Cleveland State University
Department of Civil Engineering
Attn: Dr. P. Bellini
Cleveland, OH 44115

Massachusetts Institute of Technology
Attn: K. Bathe
77 Massachusetts Avenue
Cambridge, MA 02139

Massachusetts Institute of Technology
Dept. of Aeronautics & Astronautics
Building 33-307
Attn: Prof. J. W. Mar
77 Massachusetts Avenue
Cambridge, MA 02139

Massachusetts Institute of Technology
Attn: E. A. Witmer
77 Massachusetts Avenue
Cambridge, MA 02139

Massachusetts Institute of Technology
Attn: T. H. Pian
77 Massachusetts Avenue
Cambridge, MA 02139

Univ. of Illinois at Chicago Circle
Department of Materials Engineering
Attn: Dr. Robert L. Spilker
Box 4348
Chicago, IL 60680

Detroit Diesel Allison
General Motors Corporation
Attn: Mr. William Springer
Speed Code T3, Box 894
Indianapolis, IN 46206

Detroit Diesel Allison
General Motors Corporation
Attn: Mr. J. Byrd
Speed Code T3, Box 894
Indianapolis, IN 46206

Detroit Diesel Allison
General Motors Corporation
Attn: Mr. L. Snyder
Speed Code T3, Box 894
Indianapolis, IN 46206

General Motors Corporation
Attn: R. J. Trippet
Warren, MI 48090

Arthur D. Little
Acorn Park
Attn: P. D. Hilton
Cambridge, MA 02140

AVCO Lycoming Division
Attn: Mr. Herbert Kaehler
550 South Main Street
Stratford, CT 06497

Beech Aircraft Corp., Plant 1
Attn: Mr. M. K. O'Connor
Wichita, KA 67201

Bell Aerospace
Attn: R. A. Gallatly
P. O. Box 1
Buffalo, NY 14240

Bell Aerospace
Attn: S. Gellin
P. O. Box 1
Buffalo, NY 14240

Boeing Aerospace Company
Impact Mechanics Lab
Attn: Dr. R. J. Bristow
P. O. Box 3999
Seattle, WA 98124

Boeing Commercial Airplane Company
Attn: Dr. Ralph B. McCormick
P. O. Box 3707
Seattle, WA 98124

Boeing Commercial Airplane Company
Attn: Dr. David T. Powell, 73-01
P. O. Box 3707
Seattle, WA 98124

Boeing Commercial Airplane Company
Attn: Dr. John H. Gerstle
P. O. Box 3707
Seattle, WA 98124

Boeing Company
Attn: Mr. C. F. Tiffany
Wichita, KA

McDonnell Douglas Aircraft Corporation
Attn: Library
P. O. Box 516
Lambert Field, MO 63166

Douglas Aircraft Company
Attn: Mr. M. A. O'Connor, Jr., 36-41
3855 Lakewood Blvd.
Long Beach, CA 90846

Garrett AiResearch Manufacturing Co.
Attn: L. A. Matsch
111 S. 34th Street
P. O. Box 5217
Phoenix, AZ 85010

General Dynamics
Attn: Library
P. O. Box 748
Fort Worth, TX 76101

General Dynamics/Convair Aerospace
Attn: Library
P. O. Box 1128
San Diego, CA 92112

General Electric Company
Attn: Dr. L. Beitch, K221
Interstate 75, Bldg. 500
Cincinnati, OH 45215

General Electric Company
Attn: Dr. M. Roberts, K221
Interstate 75, Bldg. 500
Cincinnati, OH 45215

General Electric Company
Attn: Dr. R. L. McKnight, K221
Interstate 75, Bldg. 500
Cincinnati, OH 45215

General Electric Company
Aircraft Engine Group
Attn: Mr. Herbert Garten
Lynn, MA 01902

Grumman Aircraft Eng. Corp.
Attn: Library
Bethpage, Long Island, NY 11714

Grumman Aircraft Eng. Corp.
Attn: H. A. Armen
Bethpage, Long Island, NY 11714

IIT Research Institute
Technology Center
Attn: Library
Chicago, IL 60616

Lockheed California Company
Attn: Mr. D. T. Pland
P. O. Box 551
Dept. 73-31, Bldg. 90, PL. A-1
Burbank, CA 91520

Lockheed California Company
Attn: Mr. Jack E. Wignot
P. O. Box 551
Dept. 73-31, Bldg. 90, PL. A-1
Burbank, CA 91520

Northrop Space Laboratories
Attn: Library
3401 West Broadway
Hawthorne, CA 90250

North American Rockwell, Inc.
Rocketdyne Division
Attn: K. R. Rajagopal
6633 Canoga Avenue
Canoga Park, CA 91304

North American Rockwell, Inc.
Rocketdyne Division
Attn: F. Nitz
6633 Canoga Avenue
Canoga Park, CA 91304

North American Rockwell, Inc.
Space & Information Systems Div.
Attn: Library
12214 Lakewood Blvd.
Downey, CA 90241

Norton Company
Attn: Mr. George E. Buron
Industrial Ceramics Division
Armore & Spectramic Products
Worcester, MA 01606

Norton Company
Attn: Mr. Paul B. Gardner
1 New Bond Street
Industrial Ceramics Division
Worcester, MA 01606

United Technologies Corporation
Pratt & Whitney
Government Products Division
Attn: Library
P. O. Box B2691
West Palm Beach, FL 33402

United Technologies Corporation
Pratt & Whitney
Government Products Division
Attn: R. A. Marmol
P. O. Box B2691
West Palm Beach, FL 33402

United Technologies Corporation
Pratt & Whitney
Attn: Library
400 Main Street
East Hartford, CT 06108

United Technologies Corporation
Pratt & Whitney
Attn:#E. S. Todd, MS 163-09
400 Main Street
East Hartford, CT 06108

United Technologies Corporation
Hamilton Standard
Attn: Dr. R. A. Cornell
Windsor Locks, CT 06096

Aeronautical Research Association
of Princeton, Inc.
Attn: Dr. Thomas McDonough
P. O. Box 2229
Princeton, NJ 08540

Republic Aviation
Attn: Library
Fairchild Hiller Corporation
Farmington, Long Island, NY

Rohr Industries
Attn: Mr. John Meaney
Foot of H Street
Chula Vista, CA 92010

TWA, Inc.
Attn: Mr. John J. Morelli
Kansas City International Airport
P. O. Box 20126
Kansas City, MO 64195

State University of New York
at Buffalo
Attn: R. Shaw
Dept. of Civil Engineering
Buffalo, NY 14214

Solar Turbine Inc.
Attn: G. L. Padgett
P. O. Box 80966
San Diego, CA 92138

Southwest Research Institute
Attn: T. A. Cruse
6220 Culebra Road
San Antonio, TX 78284

Lockheed Palo Alto Research Labs
Attn: D. Bushnell
Palo Alto, CA 94304

Lockheed Palo Alto Research Labs
Attn: R. F. Hurtung
Palo Alto, CA 94304

Lockheed Missiles & Space Company
Huntsville Res. & Eng. Center
Attn: H. B. Shirley
P. O. Box 1103
Huntsville, AL 18908

Lockheed Missiles & Space Company
Huntsville Res. & Eng. Center
Attn: W. Armstrong
P. O. Box 1103
Huntsville, AL 18908

MacNeal-Schwendler Corporation
Attn: R. H. MacNeal
7442 North Figueroa Street
Los Angeles, CA 90041

MARC Analysis Research Corporation
Attn: P. V. Marcel
260 Sheridan Avenue, Suite 314
Palo Alto, CA 94306

United Technologies Research Center
Attn: Dr. A. Dennis, MS 18
East Hartford, CT 06108

Georgia Institute of Technology
School of Civil Engineering
Attn: S. N. Atluri
Atlanta, GA 30332

Georgia Institute of Technology
Attn: G. J. Semetsis
225 North Avenue
Atlanta, GA 30332

Georgia Institute of Technology
Attn: R. L. Calson
225 North Avenue
Atlanta, GA 30332

Lawrence Livermore Laboratory
Attn: M. L. Wilkins
P. O. Box 808, L-421
Livermore, CA 94550

Leigh University Institute of
Fracture and Solid Mechanics
Attn: G. T. McAllister
Bethlehem, PA 18015

National Bureau of Standards
Engineering Mechanics Section
Attn: R. Mitchell
Washington, DC 20234

Purdue University
School of Aeronautics & Astronautics
Attn: C. T. Sun
West Lafayette, IN 47907

Stanford University
Applied Mechanics, Durand Bldg.
Attn: T. J. R. Hughes
Stanford, CT 94305

University of Dayton
Research Institute
Attn: F. K. Bogner
Dayton, OH 45409

The University of Akron
Attn: D. G. Fertis
302 E. Buchtel Avenue
Akron, OH 44325

The University of Akron
Attn: T. Y. Chang
302 E. Buchtel Avenue
Akron, OH 44325

The University of Akron
Attn: J. Padovan
302 E. Buchtel Avenue
Akron, OH 44325

Texas A&M University
Aerospace Engineering Dept.
Attn: W. E. Haisler
College Station, TX 77943

Texas A&M University
Aerospace Engineering Dept.
Attn: D. Allen
College Station, TX 77943

V.P.I. and State University
Department of Engineering Mechanics
Attn: R. H. Heller
Blacksburg, VA 24061

University of Arizona
College of Engineering
Attn: H. Kamel
Tucson, AZ 87521

University of Arizona
College of Engineering
Attn: P. H. Wirsching
Tucson, AZ 87521

University of California
Department of Civil Engineering
Attn: E. Wilson
Berkeley, CA 94720

University of Kansas
School of Engineering
Attn: R. H. Dodds
Lawrence, KS 66045

University of Texas at Austin
Dept. of Aerospace Engineering
& Engineering Mechanics
Attn: J. T. Oden
Austin, TX 78712

Westinghouse R&D Center
Attn: N. E. Dowling
1310 Beulah Road
Pittsburgh, PA 15235

Westinghouse Adv. Energy Sys. Div.
Attn: P. T. Falk
Waltz Mill
P. O. Box 158
Madison, PA 15663

End of Document